DETECTION OF THE METASTATIC POTENTIAL OF BREAST CANCER CELL LINES TO SPECIFIC TARGET TISSUES

A Thesis Submitted to
the Graduate School of Engineering and Sciences of
İzmir Institute of Technology
in Partial Fulfillment of the Requirements for the Degree of

DOCTOR OF PHILOSOPHY

in Molecular Biology and Genetics

by
Burcu FIRATLIGİL YILDIRIR

March 2021
İZMİR

ACKNOWLEDGEMENT

I would like to express my deepest gratitude to my supervisor Assoc. Prof. Dr. Özden Yalçın Özuysal for her continuous guidance, support, encouragement and understanding throughout my PhD journey.

I am also grateful to Assoc. Prof. Dr. Nonappa Nonappa from Tampere University, Finland, who accepted me as a short-term fellow and shared all of his valuable experiences and advices with me. Special thanks to Assoc. Prof. Dr. Susanna Fagerholm from Helsinki University, Finland who provided me every kind of support for using all of the instruments and facilities in her lab. Dr. Carla Guenther and Dr. Imrul Faisal deserve special thanks for their extreme help in the laboratory work and for the amazing accompany during my stay in Finland. I am also grateful to Prof. Dr. Devrim Pesen Okvur and her research group for providing lab-on-a-chip (LOC) platforms for my PhD work.

I would also like to thank to my dissertation committee members Prof. Dr. Devrim Pesen Okvur, Assoc. Prof Dr. Nur Başak Sürmeli Eraltuğ, Assoc. Prof. Dr. Şerif Şentürk and Assist Prof. Dr. Yavuz Oktay.

I am especially grateful to Assoc. Prof. Dr. Gülistan Meşe and Assoc. Prof. Dr. Engin Özçivici for their valuable advices during lab meetings and to my research group members Zehra Elif Günyüz, Eda Efe, Hülya Doğan and Kübra Telli. I would like to thank to Dr. Aslı Kısım and Dr. Gizem Batı Ayaz for sharing their experiences and discussions about experiments. I would like to express my special thanks to Ceren Tabak Buru and Dr. Özge Karadaş, who always motivated and supported me throughout my PhD studies.

I would like to thank warmly my husband Cevdet Cem Yıldırır, who supported me in every aspect and suffers all of my whims.

The biggest thanks are for my family. My parents Nagihan and Fuat Ergin Fıratlıgil were always by my side throughout my life and I felt their support every single day. I would like to thank to my brother Fahri Burçin Fıratlıgil as well for all the moments we share.

Finally, I would like to thank to TUBITAK for supporting my PhD project, which was the part of a 1003 project with the grant number of 115E057.

ABSTRACT

DETECTION OF THE METASTATIC POTENTIAL OF BREAST CANCER CELL LINES TO SPECIFIC TARGET TISSUES

Breast cancer is one of the most frequently diagnosed cancer types and the second leading cause of cancer-associated deaths in women. Breast cancer begins as a local disease which can then metastasize to distant sites specifically to bone, lung and liver. The increasing rate of the metastasis-related deaths asserts the need to develop *in vitro* diagnostic strategies representing *in vivo* properties better. In this study, two different lab-on-a-chip (LOC) platforms, IC- and EX-chips, were used to detect the invasion and extravasation potentials, respectively, of breast cancer cells to 3D *in vitro* generated bone, lung, liver and breast microenvironments. The metastatic MDAMB231, but not non-metastatic MCF7 breast cancer cells showed higher invasion and extravasation potentials towards lung and liver microenvironments than breast microenvironment. Lung-specific but not bone-specific metastatic subclonal cells invaded significantly towards lung microenvironment. On the other hand, an intensive invasion was observed in bone-specific but not lung-specific metastatic subclonal cells towards bone microenvironment demonstrating different *in vivo* metastatic behaviors of breast cancer cells. Overall, the tissue-specific invasion and extravasation capacities of breast cancer cells were demonstrated with IC- and EX-chips where the physiologically more relevant bone, lung, liver and breast homing target sites were generated by a specific emphasis on ECM components, stromal cells and secreted factors. This study is important in providing a basis for the development of diagnostic tools and precision therapeutics for breast cancer metastasis.

ÖZET

MEME KANSERİ HÜCRE HATLARININ BELİRLİ HEDEF DOKULARA METASTAZ POTANSİYELLERİNİN TESPİT EDİLMESİ

Meme kanseri, en sık teşhis edilen kanser türlerinden biridir ve kadınlarda kansere bağlı ölümlerin ikinci önce gelen nedenidir. Lokal bir hastalık olarak başlayan meme kanseri, daha sonra uzak bölgelere, özellikle kemik, akciğer ve karaciğere metastaz yapabilir. Metastaza bağlı ölümlerin artan oranı, *in vivo* özellikleri daha iyi temsil eden *in vitro* tanı stratejileri geliştirme ihtiyacını ortaya koymaktadır. Bu çalışmada, meme kanseri hücrelerinin 3B *in vitro* olarak oluşturulmuş kemik, akciğer, karaciğer ve meme mikroortamlarına olan invazyon ve ekstravazasyon potansiyellerinin tespiti için IC-çip ve EX-çip olmak üzere iki farklı lab-on-a-chip (LOC) platformu kullanılmıştır. Metastatik MDAMB231 meme kanseri hücreleri, akciğer ve karaciğer mikroortamlarına meme mikroortamına göre daha yüksek invazyon ve extravazasyon potansiyelleri gösterirken, metastatik olmayan MCF7 meme kanseri hücrelerinde bu yönelimler görülmemiştir. Akciğere özgü metastaz yapan meme kanseri hücrelerinin akciğer mikro ortamına doğru önemli ölçüde invazyon yapması, kemiğe özgü metastaz yapan meme kanseri hücrelerinin ise kemik mikro ortamına yoğun invazyon göstermesiyle, meme kanseri hücrelerinin farklı *in vivo* metastatik davranışları ortaya konulmuştur. Genel olarak, IC- ve EX- çipleri sayesinde, meme kanseri hücrelerinin dokuya özgü invazyon ve ekstravazasyon kapasiteleri özellikle matriks bileşenlerinin, stromal hücrelerinin ve salgılanan faktörlerin önemi vurgulanarak gösterilmiştir. Bu çalışma, meme kanseri metastazı için teşhis kitleri ve hassas terapötiklerin geliştirilmesi için bir temel oluşturması açısından önemlidir.

Dedicated to my family...

TABLE OF CONTENTS

LIST OF FIGURES

Figure **Page**

Figure **Page**

LIST OF TABLES

Table **Page**

CHAPTER 1

INTRODUCTION

1.1. Breast Cancer

Breast cancer is one of most malignant and frequent cancer types among women. It is considered as the second leading cause of cancer-related deaths due to the metastasis. The global breast cancer incidence and mortality statistics for 2018 reported by GLOBOCAN (Global Cancer Observatory) revealed that breast cancer was the most common cancer type in 154 of 185 countries and that nearly 2.1 million women were diagnosed with breast cancer, which contributes to around 12% of the total cancer incidence (Bray et al., 2018; Ferlay et al., 2019).

Breast cancer is known to start at different parts within the breast, but the vast majority of cases initiate in the glands and ducts of the tissue. These sites are related to milk production and transportation of the produced milk from glands to nipples, respectively (Javed & Lteif, 2013). The two main histological subtypes of breast cancer are in situ carcinoma and invasive (infiltrating) carcinoma (Makki, 2015). In situ carcinoma, the non-invasive breast cancer, is then classified as either ductal or lobular based on the site they are originated from. The ductal carcinomas are the ones that are originated from the ducts while lobular carcinomas are originated from the lobules of the breast tissue (Makki, 2015; Malhotra, Zhao, Band, & Band, 2010). Invasive carcinoma types include infiltrating ductal, ductal/lobular, invasive lobular, tubular, colloid, medullary and papillary carcinoma. Infiltrating ductal carcinoma (IDC) constitutes aroud 70-80% of diagnosed breast cancer cases that is the most common invasive breast cancer subtype (Malhotra et al., 2010).

The gene expression profile approaches have revealed several intrinsic molecular subtypes of breast cancer whose classification provides effective treatment approaches. These molecular markers include estrogen receptor (ER), progesterone receptor (PR), the cell proliferation marker (Ki67) and human epidermal growth factor receptor 2 (HER2) (W. Chen, Hoffmann, Liu, & Liu, 2018). The intrinsic molecular subtypes of breast cancer are categorized as Luminal A (ER+/PR+/HER2- and Ki67

low) and B (ER+/PR+/HER2-/+ and Ki67 high), HER2-enriched (ER-/PR-/HER2+) and Triple Negative/Basal-like (ER-/PR-/HER2-) (Dai, Cheng, Bai, & Li, 2017; Malhotra et al., 2010). Another intrinsic subtype of breast cancer called as claudin-low, was currently identified that show similar characteristics with basal-like subtype. Together with basal-like molecular subtype, they form the vast majority of the aggressive subtype, triple negative breast cancer (TNBC) (Pommier et al., 2020).

1.2. Breast Cancer Metastasis

Metastasis is a multi-step process, which is responsible for more than 90% of cancer-associated deaths. The development of metastases is initiated by migration and local invasion of cancer cells to the surrounding stroma that is followed by their intravasation into the vascular system. Once they are in circulation, some cancer cells adhere to blood vessel walls and extravasate into new cellular surroundings in the target organ site (Fares, Fares, Khachfe, Salhab, & Fares, 2020). In the secondary site, cancer cells adapt to and ultimately succeed in the foreign environmental conditions to form metastatic colonization (Figure 1.1).

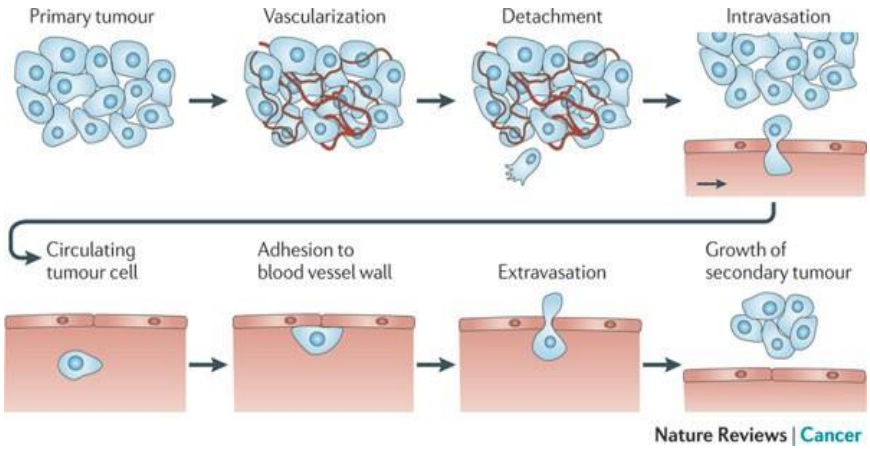

Figure 1.1. Schematic representation of cancer cell metastasis (Wirtz, Konstantopoulos, & Searson, 2011)

Cancer cells must first undergo invasion through the basement membrane and the surrounding extracellular matrix (ECM) to perform the metastasis process. Therefore, the invasion of cancer cells requires the degradation of ECM which is related to the upregulation of ECM degrading proteases such as matrix metalloproteases (MMPs) (Fares et al., 2020). Following their successful survival in blood circulation, cancer cells interact with endothelial cells in the endothelial layer of the target site to penetrate into the target site stroma as the extravasation step of the metastasis process.

Breast cancer is a disease which starts locally but it can metastasize to the lymph nodes and to various distant organs. The metastasis process is a non-random distribution to certain target organs which is known as metastatic organotropism or organ-specific metastasis. This process is mediated by several factors such as tumor-intrinsic factors, the connection between tumor cells and target site microenvironment and organ-specific niches (Gao et al., 2019). It was reported by several studies that the most common metastatic sites of breast cancer are bone (50-65%) and lung (21-32%) followed by liver (15%) and brain (4-10%) (Kimbung, Loman, & Hedenfalk, 2015; Lu & Kang, 2007; Yousefi et al., 2018).

Invasive ductal adenocarcinoma (IDC) mainly prefers to metastasize to the lungs and lymph nodes, while invasive lobular adenocarcinoma (ILC) has a tendency to metastasize to ovaries and gastrointestinal tract (W. Chen et al., 2018). Furthermore, it was revealed that different molecular subtypes of breast cancer are associated with different sites of distant metastasis. It was revealed by SEER-based analysis that TNBC subtype patients show more lung metastasis (32.09%), while HER2-enriched subtype patients have a high probability of brain and liver metastasis (31,72%) compared to luminal A and B subtype patients (Kennecke et al., 2010; Wu et al., 2017).

The metastatic organotropism process of breast cancer cells is closely associated with the microenvironment of their specific target sites. This microenvironment, called the pre-metastatic niche, is a well-organized site for the colonization of tumor cells and spread of them to distant target sites. This environment includes ECM, host stromal cells, immune cells, secreted factors and proteins such as growth factors and cytokines (Monteiro, Custódio, & Mano, 2019) making this region inevitable for tumor progression and metastasis. Once tumor cells metastasize to their distant target organs, they come across this complex microenvironment whose composition and structure are different than that of the primary tumor site. Therefore, the survival of tumor cells and

formation of metastatic tumors at the distant sites are highly dependent on sufficient interactions between tumor cells and the pre-metastatic niches.

1.3. Breast Cancer Metastasis to Lung

The lungs are the most common metastatic site for breast cancer cells especially for those of TNBC subtype (Wu et al., 2017). The breast cancer metastasis to the lungs is associated with the poor prognosis and high patient mortality and morbidity. Therefore, as the earlier diagnosis seems to be the best approach to prevent lung metastasis of breast cancer cells, the development of more effective methods for early detection is of paramount importance.

Dissemination and colonization of breast cancer cells to the lungs are mainly mediated by the crosstalk between the cells residing in the tumor microenvironment and the lung stroma. Breast cancer cells invade the local vasculature, are carried through the venous circulation to the heart and then transmitted to the lungs. In the lungs, some of these cancer cells can be mechanically arrested in the capillary beds and the specific lung-derived signals affect the successive growth and colonization of them within the lungs (Piaseczny & Allan, 2014).

Growing evidence reveals that chemokines, a family of chemotactic cytokines secreted by the cells, are correlated with the lung-specific dissemination of breast cancer cells (Esquivel-Velázquez et al., 2015). In this study, three cytokines, CXCL12, CCL5, IGF-1, that are mainly implicated in lung metastasis were focused on.

The expression of CXCR4 chemokine receptor on the surface of the breast cancer cells is important in cell migration and tissue invasion (Müller et al., 2001). CXCL12 is the ligand of CXCR4 and preferentially expressed in the lungs. CXCL12-CXCR4 interaction regulates breast cancer metastasis to the lungs implying the importance of receptor-ligand interactions in breast cancer metastasis organotropism. The effects of CXCL12 on cancer cells boil down two main mechanisms. The first one is the direct autocrine signaling, which promotes growth and metastasis of cancer cells. The second one is indirectly facilitating the recruitment of CXCR4 positive cancer cells to the site where CXCL12 is expressed to initiate metastasis (Chatterjee, Azad, & Nimmagadda, 2014; Guo et al., 2016).

Besides interaction with its ligand CXCL12, CXCR4 also interacts with various growth factors contributing to normal or pathological responses. Insulin growth factor-1 (IGF-1) cytokine was demonstrated to transactivate CXCR4 signaling in MDAMB231 cell lines, together with IGF-1R activation that induces cell migration (Akekawatchai, Holland, Kochetkova, Wallace, & McColl, 2005; X. Sun et al., 2010). This activation was not observed in non-metastatic MCF7 cell lines although they are positive for both CXCR4 and IGF-1R. Altogether, the complex formation between CXCR4 and IGF-1R receptors in MDAMB231 cells was confirmed through which IGF-1 activates migration signaling pathways (Akekawatchai et al., 2005).

Furthermore, CCL5 (CC chemokine ligand 5) has been also shown to strongly mediate carcinogenesis, which was secreted by both cancer cells and/or stromal cells. CCL5 acts through three different G-protein coupled receptors known as CCR1, CCR3 and CCR5 (Sarvaiya, Guo, Ulasov, Gabikian, & Lesniak, 2013), the latest being investigated as the main receptor in MDAMB231 cell lines (Karnoub et al., 2007). In recent studies, the overexpression of CCL5 in breast cancer cells was shown to increase lung metastasis, while the inhibition of CCR5 receptor expression in MDAMB231 cells inhibited their metastatic potential and weakened the tumor progressive roles of the cells regulated by CCL5-CCR5 loop (Karnoub & Weinberg, 2007).

WI38 cell line, which was used as a stromal cell for lung microenvironment generation throughout this study, is a human-derived embryonic lung fibroblast. The secretion of CXCL12 and CCL5 chemokines was previously detected in these cells and they were shown to promote the metastatic potential of MDAMB231 cells towards their sites (Karnoub et al., 2007; Ohira et al., 2006).

1.4. Breast Cancer Metastasis to Bone

Bones are the most frequent metastatic organs for breast cancer cells with more than 50% of breast cancer patients showing bone metastases (Yin, Pollock, & Kelly, 2005).

The communication between metastatic breast cancer cells and the bone marrow is mainly promoted by the interaction between the chemokine CXCL12 and its receptors CXCR4 and CXCR7. CXCL12 is an effective regulator of homing between

bone marrow and blood for hematopoietic progenitors (Broxmeyer et al., 2005) and thus, breast cancer cells simulate this process by expressing CXCR4 or/and CXCR7. This receptor expression helps metastatic breast cancer cells to react to chemoattractive gradients of CXCL12 and they imitate the vascular exit mechanism of hematopoietic progenitors turning back to the bone marrow from blood circulation (Patel, Camacho, Shiozawa, Pienta, & Taichman, 2011).

Another bone-derived factor, insulin growth factor-1 (IGF-1) is released from bone stromal cells during bone remodeling and regulates osteoblastogenesis by activation of mTOR signaling (Xian et al., 2012). In terms of cancer cell dissemination, bone-derived IGF-1 promotes anchorage-independent growth of bone-specific metastatic breast cancer cells by interacting with IGF-1R receptor that is overexpressed in breast cancer cells. It was shown that this receptor-ligand interaction increases the cellular proliferation and survival of breast cancer cells in bone metastases through the activation of Akt/NFκB signaling (Hiraga et al., 2012).

HS5 cell line, which is used as a stromal cell for bone microenvironment generation, is a human-derived bone marrow fibroblast cell line. The secretion of CCL5 and CXCL12 chemokines was detected in these cells, downregulation of which inhibited the invasion of several cancer types (Bai et al., 2014). Bone tissue is a dynamic system that undergoes bone remodeling continuously in which bone-forming osteoblasts and bone-resorbing osteoclasts are the key components. The balance between osteoblasts and osteoclasts is essential for normal skeletal functions and bone homeostasis (Park, Eber, Widner, & Shiozawa, 2018). Therefore, both cellular milieu and chemical and mechanical stimuli including tensile stiffness and topography of the bone microenvironment should be considered together when remodeling the bone tissue.

1.5. Breast Cancer Metastasis to Liver

The liver is the essential organ where the insulin-mediated metabolism, glucose and lipid homeostasis are regulated by growth factors such as insulin-like growth factor 1 and 2 (IGF-1 and IGF-2). The roles of IGF in tumor invasion were revealed in several studies. IGF-1R, which is the receptor of IGF-1 was shown to promote MMP-2 synthesis, thereby facilitate tumor cell invasion. The modulation of IGF-1R expression

changed the expression levels of MMP-2, which then altered the invasion and metastasis in a lung carcinoma model (Samani, Yakar, LeRoith, & Brodt, 2007; Donglei Zhang, Bar-Eli, Meloche, & Brodt, 2004). *In vitro* studies revealed that the IGF system, basically IGF-1 growth factor promotes motility and invasion of breast cancer cell lines such as T47D, MDAMB435 and MDAMB231 (Sachdev, Hartell, Lee, Zhang, & Yee, 2004).

Besides lung and bone metastasis, CXCR4 chemokine receptor expressed in breast cancer cells also contributes to the liver metastasis of breast cancer cells. The expression of CXCL12, which is the ligand of CXCR4 receptor, is observed in the liver demonstrating the role of CXCR4/CXCL12 interaction on liver metastasis. It was also reported that this interaction contributed to breast cancer to liver metastasis through the modulation of integrin-adhesion-receptor signaling (R. Ma et al., 2015; Müller et al., 2001).

The role of CCL5 on liver metastasis of breast cancer was also indicated in several studies. The secretion of CCL5 by the cells within tumor microenvironment was shown to promote the dissemination of breast cancer cells to the liver, which was also confirmed by the reduced capacity of breast cancer cells to spread to the liver when tumor-derived CCL5 was inhibited (Soria & Ben-Baruch, 2008; Stormes, Lemken, Lepre, Marinucci, & Kurt, 2005).

BRL3A cell line, which was used as a stromal cell for liver microenvironment generation, is a rat-derived liver epithelial cell line. Expression profiles of CXCL12, CCL5 and IGF-1 chemokines in BRL3A were not reported and no relation between this cell line and breast cancer was shown.

1.6. Lab-on-a-Chip Systems

As the clinical importance of metastasis increases, the development of *in vitro* diagnostic strategies mimicking the *in vivo* physicochemical properties of tissues, becomes crucial for a deeper understanding of metastasis process to increase metastasis related cancer survival rates.

Traditional assays such as boyden chamber and wound- healing assays, have been commonly used for cell migration and invasion studies since they provide a simple

and high through-put screening method with several experimental samples subjected to a testing simultaneously. However, the complex cell-cell and cell-matrix interactions can not be analyzed accurately with these techniques and also they do not provide complete control of local microenvironment since they are highly simplifed and do not allow the application of continuous gradients.

Lab-on-a-chip platforms address these limitations and they provide a useful model system to investigate complex metastasis process with a tight control of the biophysical and biochemical microenvironments (Bersini et al., 2014; Jeon, Zervantonakis, Chung, Kamm, & Charest, 2013). Therefore, there are several lab-on-a-chip platforms developed to allow the investigation of critical points involved tumor metastasis including local invasion, intravasation (Truong et al., 2016), angiogenesis (Vickerman & Kamm, 2012) and extravasation. Truong et al., analyzed the interactions between cancer cells and chemotactic factors to investigate the role of EGF on the invasion of SUM-159 breast cancer cells. The LOC platform used in the study allowed visualization and quantification of breast cancer cell invasion towards EGF-stimulated site, but it did not allow for investigation of 3D microenvironmental factors of homing target sites.

Zervantonakis et al., investigated the endothelial barrier function on the intravasation of fibrosarcoma cells. The endothelial permeability was shown to be related to TNF- α stimulation or macrophages leading to enhanced intravasation rate (Zervantonakis et al., 2012). However, the roles of different blood cells such as neutrophils and platelets or cancer-secreted factors such as exosomes were not shown in the study.

Overall, although each steps of metastasis are commonly investigated by LOC platforms, there are limited research indicating the roles of ECM components, cellular milieu, receptor-ligand interactions together with shear stress on the invasion and extravasation potentials of breast cancer cells towards *in vitro* generated microenvironments.

CHAPTER 2

AIM OF THE PROJECT

The emerging role of the organization of 3D cell-laden artificial scaffolds to mimic the physiological complexity of the homing sites to study breast cancer metastasis has been recently emphasized, yet there are still some gaps to be filled for modeling homing tissues, considering the importance of ECM components, cellular density and milieu as well as the receptor-ligand interactions. Most of the studies were mainly focused on the roles of secreted factors from stromal cells but not considered the contribution of different ECM components and cell types on the metastatic potentials of breast cancer cells. More importantly, the potency of 3D generated *in vitro* homing tissues was not commonly confirmed by organ-specific metastatic clones which is essential to demonstrate the *in vivo* behaviors of metastatic cancer cells towards generated microenvironments.

The aim of the thesis was to investigate the invasion and extravasation potentials of metastatic breast cancer cell line, MDAMB231; its tissue-specific metastatic subclones, bone-specific MDAMB231 BoM 1833 and lung-specific MDAMB231 LM2; and non-metastatic breast cancer cell line, MCF7 towards 3D *in vitro* generated bone, lung, liver and breast homing sites by using lab-on-a-chip (LOC) platforms. Therefore, it was aimed to elucidate the contribution of extracellular matrix (ECM) components, stromal cells and secreted chemokines on the invasiveness and homing site preferences of breast cancer cells within LOC platforms by a particular emphasis on the generation of more native-like target tissue microenvironments.

CHAPTER 3

METHODS

3.1. Cell Lines

Human breast cancer cell lines, basal type triple negative breast cancer cell line (MDAMB231) and luminal type breast cancer cell line (MCF-7), human normal mammary epithelial cell line (MCF10A), human normal breast fibroblast cell line (Hs 578Bst), human normal lung fibroblast cell line (WI38), rat normal liver cell line (BRL3A), human normal bone marrow fibroblast cell line (HS-5), human umbilical vein endothelial cell line (HUVEC-C) were obtained from ATCC; human embryonic kidney cell line (HEK293T) and mouse embryonic fibroblast cell line (NIH3T3) were provided by Prof. Cathrin Brisken Laboratory (EPFL, ISREC); human bone-marrow mesenchymal stem cells (hBM-MSC) were provided by Assoc. Prof. Nonappa NONAPPA; human fetal osteoblast cell line (hFOB 1.19), human osteosarcoma bone fibroblast cell line (SaOs-2), mouse bone marrow mesenchymal stem cells (D1 ORL UVA) were provided by Assoc. Prof. Engin ÖZÇİVİCİ and human histiocytic lymphoma monocytes (U937) were provided by Assoc. Prof. Hüseyin Cumhur TEKİN. Organ-specific metastatic clones of MDAMB231, lung specific metastatic clone (MDAMB231 LM2) and bone specific metastatic clone (MDAMB231 1833-BoM), were gifts from the Joan Massagué Lab in Memorial Sloan Kettering Cancer Center. The general information about the cell lines including their ATCC number and growth media, tissue and organisms they are originated from and diseases they are belonging to, is represented in Table 3.1.

Table 3.1. The selected cell lines for modeling homing microenvironments, breast cancer cells and endothelial monolayer

Cell Lines	ATCC Number	Growth Media	Tissue/ Organism	Disease
MDAMB231	HTB-26™	DMEM	Breast/Human	Invasive adenocarcinoma
MDAMB231 LM2	-	DMEM	Breast/Human	Lung invasive adenocarcinoma
MDAMB231 BoM 1833	-	DMEM	Breast/Human	Bone invasive adenocarcinoma
MCF-7	HTB-22	DMEM	Breast/Human	Non-invasive adenocarcinoma
MCF10A	CRL-10317	DMEM-F12	Breast/Human	Normal
Hs578Bst	HTB-125™	Hybri-Care	Breast/Human	Normal
WI38	CCL-75™	MEM-α	Lung/Human	Normal
BRL3A	CRL-1442™	MEM-α	Liver/Rat	Normal
HS-5	CRL-11882™	DMEM	Bone Marrow/ Human	Normal
hFOB 1.19	CRL-11372™	DMEM-F12	Bone Marrow/ Human	Normal
U937	CRL-1593.2™	DMEM	Pleura/Human	Histiocytic lymphoma
hBM-MSC	PCS-500-012™	DMEM	Bone Marrow/ Human	Normal
HUVEC-C	CRL-1730™	DMEM-F12K	Umbilical Vein/ Human	Normal
HEK 293T	CRL-3216™	DMEM	Kidney/Human	Normal
NIH3T3	CRL-1658™	DMEM	Embryo/Mouse	Normal
D1 ORL UVA	CRL-12424™	DMEM	Bone Marrow/ Mouse	Normal
SaOs-2	HTB-85™	DMEM	Bone/Human	Osteosarcoma

MDAMB231, its derivatives, MCF-7, HS-5, HEK293T, SaOs-2, D1 ORL UVA, hBM-MSC and U937 were cultured in DMEM high glucose (11965092, Gibco) with Fetal Bovine Serum (FBS, A3840001, Gibco, 10%) and Penicillin/Streptomycin (15070063, Gibco, 1%); MCF-10A was cultured in DMEM-F12 high glucose (11330057, Gibco) with Horse Serum (04-004-1A, Biological Industries, 5%), Insulin (I9278, Sigma, 10 μg/mL), Cholera Toxin (C8052, Sigma, 100 ng/mL), EGF (E9644, Sigma, 20 ng/mL), Hydrocortisone (H0888, Sigma, 0.5 μg/mL) and Penicillin/Streptomycin (1%); Hs578Bst was cultured in Hybri-Care medium (46-X, ATCC) which was reconstituted in 1L ultrapure autoclaved H_2O with sodium bicarbonate (S6014, Sigma 1.5 g/L), EGF (E9644, Sigma, 30 ng/mL), Fetal Bovine Serum (FBS, 10%) and Penicillin/Streptomycin (1%); NIH3T3 was cultured in DMEM high glucose with New Born Calf Serum (NBCS, 04-1021A, Biological Industries, 10%) and Penicillin/Streptomycin (1%); WI38 and BRL3A were cultured in high glucose MEM-α (01-042-1A, Biological Industries) with Fetal Bovine Serum (FBS, 10%) and Penicillin/Streptomycin (1%); HUVEC-C cell line was cultured in DMEM-F12K high glucose (01-095-1A, Biological Industries) with Fetal Bovine Serum (FBS, 10%), Heparin (H3393, Sigma, 0.1 mg/mL), endothelial cell growth supplement (EGCS, 0.05 mg/mL) (354006, Sigma) and Penicillin/Streptomycin (1%); hFOB 1.19 cell line was cultured in DMEM-F12 high glucose (11330057, Gibco) with Fetal Bovine Serum (FBS, 10%) and Penicillin/Streptomycin (1%). All cell lines were cultured at 37°C in a humidified incubator with 5% CO_2.

3.2. 3D Cell Culture

Growth Factor Reduced (GFR) Matrigel (GFR-Matrigel, 354230, Corning), collagen type I (C3867, Sigma), agarose (A9539, Sigma) and/or chitosan (448877, Sigma) were used for 3D culturing of stromal cells and generation of 3D environments. WI38, BRL3A, MCF10A, HS5, hFOB 1.19 and U937 cell lines were seeded into GFR-matrigel solution of 4mg/ml, collagen I solution of 3mg/ml, agarose solution of 2.5mg/ml and chitosan solution of 10mg/ml as a final concentration.

For GFR-Matrigel experiments, the cells were prepared at a concentration two times more than the final concentration in serum free media and placed on ice.

Meanwhile matrigel aliquot was thawed on ice and once thawed, it was mixed with the cell solution in 1:1 ratio to have final concentration of cells in 4mg/ml final matrigel concentration. Plates or LOCs were kept on ice and loaded with matrigel/cell mixture on ice.

Table 3.2. The required volumes of collagen type I, 10X PBS or medium, 1N NaOH and dH_2O for neutralization of collagen type I. (V:total volume, S:stock concentration of collagen type I, F:final concentration of collagen type I)

Reagent	**Volume Required**
Collagen Type I	(F.V)/S
PBS or medium	V/10
1N NaOH	((F.V)/S).0,023
dH_2O	Complete to V

Collagen I working solution was prepared according to the Table 3.2. First, the calculated volume of 10X PBS, 1N NaOH and dH_2O were mixed in an eppendorf tube on ice and then collagen I stock solution was added (Table 3.2). Cells were prepared at two times the final concentration in serum-free media. Then, the cells were mixed with collagen I working solution in 1:1 ratio to obtain the required concentration of cells in 2 mg/ml, 3mg/ml or 4mg/ml final collagen I concentration.

Agarose was dissolved in 1X PBS and heated until the gel became homogenous. Once a homogenous solution was formed, 2-3 minutes were waited to have the agarose solution around 37^0C before mixing it with cells and collagen I that were prepared at a concentration of two times more than the final concentration. Different concentrations of agarose (10mg/ml, 5mg/ml and 2.5mg/ml) were used to optimize the condition for the cells.

Chitosan was dissolved in 1% acetic acid solution and stirred continuously at RT overnight. Following the incubation, NaOH solution was added until pH was in between

7.2–7.5. Meanwhile collagen I solution was prepared as explained in Table..Once the neutral pH was reached for chitosan solution, collagen I and the cells prepared at a concentration three times more than the final concentration, were added to the solution. A final chitosan concentration of 10mg/ml was used throughout the experiments.

The cell-laden matrigel, collagen I, agarose and/or chitosan hydrogels were loaded into HMC of LOC system or onto plates and the polymerization of the hydrogels was performed for 30 minutes at RT or 37°C in a humidified incubator with 5% CO_2. Following the polymerization, serum-free culture media was added to the MCs of LOC system or over the hydrogels within plates and the cells were visualized using 3D imaging by confocal microscopy.

The stiffnesses of different hydrogels were measured with oscillatory rheology at 37^0C. 2.5mg/ml of agarose with (HS5: $1x10^6$ cells/ml) or without cells, 3 mg/ml collagen I with (HS5: $1x10^6$ cells/ml) or without cells and 2.5mg/ml agarose + 3 mg/ml collagen I with (HS5: $1x10^6$ cells/ml) or without cells were prepared 2 days before the measurement. Rheological measurements were carried out using TA Instruments AR2000 stress-controlled rheometer equipped with a Peltier heated plate and 20 mm smooth steel parallel plate.

3.3. Lab-on-a-chip Platform Fabrication and Surface Modification

Two different lab-on-a-chip (LOC) platforms which are IC-chip for invasion and EX-chip for extravasation experiments were used throughout the thesis project (Figure 3.1). Each LOC platform consists of three channels that are media channel 1 (MC1), homing matrix channel (HMC) and media channel 2 (MC2) for IC-chip and endothelial monolayer channel (EMC), homing matrix channel (HMC) and media channel (MC) for EX-chip. The dimensions of each channel for both IC-chip and EX-chip are given in Table 3.3.

Table 3.3. The dimensions of (a) Invasion chip (IC-chip) and (b) Extravasation chip (EX-chip) channels

a IC-Chip Channels	Dimensions
Medium Channel 1 (MC1)	3 mm width x 10 mm length x 200 µm height
Homing Matrix Channel (HMC)	3 mm width x 12 mm length x 200 µm height
Medium Channel 2 (MC2)	3 mm width x 10 mm length x 200 µm height

b EX-Chip Channels	Dimensions
Endothelial Monolayer Channel (EMC)	3 mm width x 20 mm length x 200 µm height
Homing Matrix Channel (HMC)	3 mm width x 15 mm length x 200 µm height
Medium Channel (MC)	3 mm width x 10 mm length x 200 µm height

LOC platforms were either generated by soft lithography or provided by Initio Biomedical Engineering (Turkey). Briefly, in soft lithography fabrication, SU-8 negative photoresist polymer was spin-coated on silicon wafers. UV light was then exposed on SU-8 polymer through a mask to develop SU-8 patterns. Polydimethylsiloxane (PDMS) solution was poured on the wafer after the uncrosslinked SU-8 polymer was removed. Following PDMS polymerization, PDMS was peeled from the wafer, its inlets and outlets were punched, bonded to microscope slides and sterilized with UV-light for further use. LOC platforms were generated, optimized and provided by Prof. Devrim Pesen Okvur's research group.

The surface of EX-chips was modified with APTES and coated with laminin (L2020, Sigma Aldrich, 0.0125 mg/mL). Briefly, APTES was diluted in acetone to have 2% solution and then loaded to channels of the EX-chips. After 15 minutes of incubation at RT in laminar flow cabin, channels were washed with 1X PBS thrice. Meanwhile, laminin dilution was performed with 1X universal buffer (UB) containing 5mM Tris-HCl, 150 mM NaCl and 0,1% sodium-azide. Protein solution was then loaded to the channels and EX-chips were incubated at 37°C in a 5% CO_2 incubator for 1 hour. EX-chips were washed first with 1X UB buffer once and then with ultra-pure autoclaved H_2O thrice. The coated EX-chips were kept in vacuum desiccators at least one day before their use.

There were no surface modifications or coating for IC-chips.

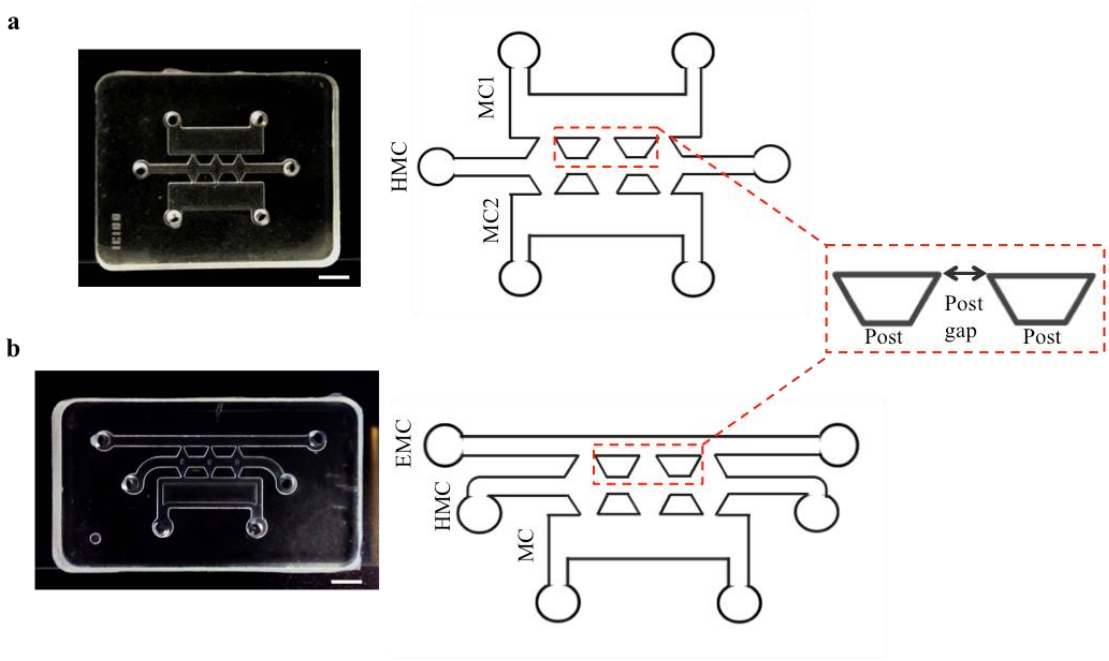

Figure 3.1. Lab-on-a-chip (LOC) platforms. (a) IC-chip for invasion and (b) EX-chip for extravasation assays. MC1: media channel 1, HMC: homing matrix channel, MC2: media channel 2, EMC: endothelial monolayer channel, MC: media channel. Scale bar: 5 mm.

3.4. Labeling of Cell Lines

MDAMB231, metastatic clones of MDAMB231 (LM2 and 1833-BoM) and MCF-7 cancer cell lines were stably labeled with a red fluorescent protein (DsRed), while WI-38, BRL3A, HS-5, MCF10A and HUVEC cell lines were stably labeled with a green fluorescent protein (eGFP). MSCV retroviruses expressing both DsRed or eGFP and puromycin resistance genes were used for infection. For the production of these viruses, HEK293T cells were seeded onto 10 cm cell culture plate with a concentration of $3x10^6$ cells/plate one day before the transfection. On the day of transfection, 2 µg of retroviral plasmid (DsRed or eGFP), 2 µg of packaging vector (Pcl10A) and 12 µl of Fugene HD (E2311, Promega) were mixed with serum-free culture media to the 500 µl final volume per plate. Following the incubation at RT for 30 minutes, the mixture was added over the seeded HEK293T cells drop by drop. 24 hours after transfection, the medium of the cells was refreshed. 48 and 72 hours after transfection, the medium

containing produced retroviruses was collected into 15 ml falcon tubes and stored at -80^{0}C until further use.

The produced retroviruses were then used for stable labeling of cell lines. Each cell line was seeded into 6-well plates one day before the infection with their optimized cell number (WI38: 2.5x10^5 cells/well, BRL3A: 2x10^5 cells/well, HS-5: 2x10^5 cells/well, MDAMB231, MDAMB231 LM2 and MDAMB231 BoM 1833: 3x10^5 cells/well, MCF10A: 2.5x10^5 cells/well, MCF7 cell line: 2.5x10^5 cells/well, Hs 578Bst: 1x10^5 cells/well, HUVEC: 1x10^5 cells/well). On the day of infection, 4ml of virus suspension supplemented with 8μg/ml polybrene (107689, Sigma Aldrich) which is added to virus suspension to enhance the transduction efficiency of viruses to the cells, was added to each cell after their growth media was discarded. Growth media without virus but with polybrene was used for the cells as a negative (mock) control. Following the addition of virus suspensions, the cells were centrifuged at 2500 rpm, at 32^{0}C for 2 hours. After centrifugation, virus suspensions were aspirated and fresh cell culture media was added to the cells. 48 hours after infection, fluorescent signal of the cells was observed with fluorescence microscopy and 2 μg/mL puromycin (P8833, Sigma) containing culture media was added for selection. Selection continued until all mock infected cells died.

Since HUVEC-C cells started to grow slowly after being stably labeled with retroviruses, labeling was performed transiently by using Green Cell Tracker CMFDA (C2925, Invitrogen). The tracker was first dissolved in DMSO to obtain a stock solution of 25 mM which was then diluted with DMEM-F12K media to obtain a working concentration of 5 μM. Cells, when they reached >70% confluency, were washed with warm 1X PBS once, and then adequate volume of tracker-medium solution to cover the plate surface, was added over the cells drop by drop. After 30 minutes of incubation at 37°C, the media was removed, cells were washed with warm 1X PBS once and then complete HUVEC-C growth media was added. Labeling was performed 30 minutes before the experimental set-up.

3.5. Cell Viability Assays

3.5.1. MTT and WST-8 (CCK-8) Assays

MTT (3-(4,Diphenyltetrazolium Bromide, 20395.03, Serva) assay was performed to detect the viability of cell lines seeded with different cell culture media. WI38, BRL-3A and MCF-10A cell lines were seeded to 48-well plate with total number of $2x10^4$ cells/well, $5x10^3$ cells/well and $2x10^4$ cells/well, respectively. Cells were cultured in complete DMEM media or in their own cell culture media (MEM-α high glucose or DMEM-F12 high glucose) and MTT assay was conducted at Day 1, Day 3 and Day 7 after the first seeding. On the indicated days, the culture media was changed with 200µl cell culture media containing 10% (v/v) MTT and the cells were incubated at 37°C in a humidified incubator with 5% CO_2 for 4 hours. Following incubation, tetrazolium salts produced by living cells were dissolved in 100µl DMSO (Sigma, D2650), and the absorbances of each condition were measured at 570 nm (the optimal wavelength for tetrazolium salts) and 650 nm (the reference wavelength to eliminate nonspecific background values) wavelengths through spectrophotometer (Thermo Fisher Scientific, Multiscan Spectrum, USA). DMSO only solution was used as a blank. The average values from triplicate measurements at both wavelengths were determined and the average values for the blank and 650 nm wavelength readings were substracted from 570 nm wavelength readings.

WST-8 (CCK8) (96992, Sigma) assay was used for cells seeded within 3D matrices for 4 days. hFOB, hBM-MSC and HS-5 cells were seeded within 10 mg/ml and 20 mg/ml of agarose hydrogels with a density of $1x10^5$ cells/ml, $5x10^4$ cells/ml and $5x10^4$ cells/ml, respectively. 10% CCK-8 solution was prepared freshly with cell culture media. For each measurement, the media from the cells was removed and 100µl of CCK-8 solution was added. After 3 hours of incubation at 37°C in a humidified incubator with 5% CO_2, the absorbances were measured at 450nm wavelength. CCK-8 only solution was used as the blank and cells plated on petri dishes without gel were used as control groups. The average values from triplicate readings were calculated for each day and the average value for the blank was substracted.

3.5.2. Live – Dead Assay

The viability of cells within different 3D hydrogels was determined by ReadyProbes Cell Viability Imaging Kit (R37609, Invitrogen). hFOB and U937 cell lines with concentrations of $1x10^5$ cells/ml and $5x10^4$ cells/ml, respectively, were seeded into collagen I only (3mg/ml), collagen I-chitosan (3mg/ml-10mg/ml) and collagen I-agarose (3mg/ml-2.5mg/ml) hydrogel. 2 drops of NucGreen® Dead reagent and NucBlue® Live reagent were added per ml of cell culture media and put over each hydrogel condition three days after the seeding. Following at least 15 minutes of incubation at 37°C in a humidified incubator with 5% CO_2, the cells were imaged in 3D using a Leica SP8 confocal microscope and total cells and dead cells were counted. The average values for both total and dead cells were determined from three different images, the value for the number of dead cells was substracted from the number of total cells to obtain the number of viable cells. The viability was then calculated as the percentage of viable cells among total cells.

3.6. Total RNA Isolation and Semi-quantitative Real-time PCR

Total RNA was isolated from homing cells seeded to cell culture plate (2D) or hydrogels (3D) using PureLink RNA Mini Kit (12183018, ThermoFisher Scientific). For 2D experiments, WI38, BRL3A, MCF10A and hFOB cell lines were seeded to 6 cm cell culture plates with their optimized concentrations (WI38: $4x10^4$ cells/plate; BRL3A: $1x10^4$ cells/plate; MCF10A: $4x10^4$ cells/plate, hFOB: $8x10^4$ cells/plate). The cells were grown both on DMEM or their own cell culture media (MEM-α or DMEM-F12) separately. On Day 1 and Day 3, the culture media was aspirated and plates were washed with 1X PBS once. Following the aspiration of 1X PBS, the cells were flash frozen in liquid nitrogen and stored at -80^0C until RNA isolation.

For 3D experiments, to optimize the cell number for 3D matrices, 500µl of GFP-labeled WI38, BRL3A, HS-5 and hFOB cell lines were seeded into GFR-Matrigel or collagen I in 48-well plate with serum-free cell culture media with different concentration for each cell line (HS5: $3x10^6$ cells/ml, $5x10^6$ cells/ml; WI38: $2.5x10^6$

cells/ml, $5x10^6$ cells/ml; BRL3A: $1x10^7$ cells/ml, $2x10^7$ cells/ml and hFOB: $5x10^6$ cells/ml, $6x10^6$ cells/ml) for Day 2.

The cells were harvested from GFR-Matrigel or from collagen I at Day 1 and Day 3 prior to RNA isolation. For the recovery of cells from matrigel, matrices were washed with cold PBS thrice and 1 ml of Cell Recovery Solution (354253, Corning) was added to each condition. The matrices were then scraped and taken into the ice-cold falcon tubes. Each well was then rinsed with an additional 1 ml Cell Recovery Solution and then the solution was added on top of the scraped matrices in the cold falcon tubes. Following 1-hour incubation on ice, the samples were centrifuged at 1000xg and 4^0C and for 1 minute and cell pellets were washed with cold PBS twice. Then total RNA isolation was done using PureLink RNA Mini Kit.

For the recovery from collagen I matrices, the media was removed and the matrix was detached from the plate by a scraper. The gel was then transferred to an eppendorf tube and centrifuged at 1000xg for 1 minute at 4^0C to spin down the collagen I matrix. The supernatant was carefully removed and lysis buffer which was prepared by adding 1 µl β-mercaptoethanol to every 100 µl lysis buffer of PureLink RNA Mini Kit was added. The gel was then homogenized by a tissue grinder (078.19.001, Isolab) on ice to prevent the heating of the samples and denaturation of RNA. The process was performed for a minute with a break after 30 seconds. The homogenized gel was then passed through an insulin needle several times. Following a quick centrifugation at 1000xg and 4^0C for 30 seconds, supernatant was collected and RNA isolation process by following the protocol of PureLink RNA Mini Kit was performed. The samples can be stored at -80^0C before the homogenization step if needed.

The same protocol was used for the recovery of the cells within collagen I/chitosan scaffolds as it is done for cell-laden collagen scaffolds.

cDNAs were synthesized from 1 µg total RNAs by RevertAid First Strand cDNA Synthesis Kit (K1622, ThermoFisher Scientific, USA). mRNA levels were analyzed with semi-quantitative real time reverse transcriptase PCR (RT-qPCR) using FastStart Essential DNA Green Master Kit (06402712001, Roche) on Light Cycler® 96 Instrument. The relative expression levels of each gene were calculated by ΔΔCt method by using human or rat TATA-box binding (TBP) protein or mouse GAPDH as the housekeeping gene. Non-template controls were included in each condition and p-values were calculated by two-tailed t-test. The primer pairs used in RT-qPCR reactions are shown in Table 3.4;

Table 3.4. The sequences of forward and reverse primers used for RT-qPCR reactions.

Gene	Forward Primer	Reverse Primer
CXCL12	5'CAACACTCCAAACTGTGCCC	5'TGTAAGGGTTCCTCAGGCGT
CCL5	5' TGCTGCTTTGCCTACATTGC	5' CTTGTTCAGCCGGGAGTCAT
rCCL5	5' GCAGTCGTCTTTGTCACTCG	5'GGAGTAGGGGGTTGCTCAGT
IGF1	5' TCAGCAGTCTTCCAACCCAA	5'GAGATGCGAGGAGGACATGG
ALP	5'TTTAGTACTGGCCATCGGCA	5'ATTGCCCTGAGTGGTGTTGCA
OCN	5'CTGACAAAGCCTTCATGTCCAA	5'GCGCCGGAGTCTGTTCACTA
TBP	5' TAGAAGGCCTTGTGCTCACC	5'TCTGCTCTGACTTTAGCACCTG
rTBP	5'TGCACAGGAGCCAAGAGTGA	5'CACATCACAGCTCCCCACCA
GAPDH	5'GACATGCCGCCTGGAGAAAC	5'AGCCCAGGATGCCCTTTAGT

3.7. Invasion Assay

3.7.1. Cell-free Assays

4mg/ml GFR-Matrigel was prepared in serum-free media as explained in section 3.2 and loaded into HMC of IC-chips. Following the polymerization of GFR-Matrigel at 37°C in a humidified incubator with 5% CO_2 for 30 minutes, serum-free or serum containing media was loaded to MC1 and MC2 (Figure 3.2a) and chips were incubated overnight. The next day, media within media channels was removed, channels were washed with serum-free media and serum-free or 10% serum-containing media was loaded to MC2 (Figure 3.2b). DsRed-MDAMB231 cells with a concentration of $1x10^6$ cells/ml in serum-free media were added to MC1 and the chips were incubated vertically for 3 days (Figure 3.2c). The invasion of MDAMB231 cells was visualized every 24 hours by 3D imaging using a Leica SP8 confocal microscope.

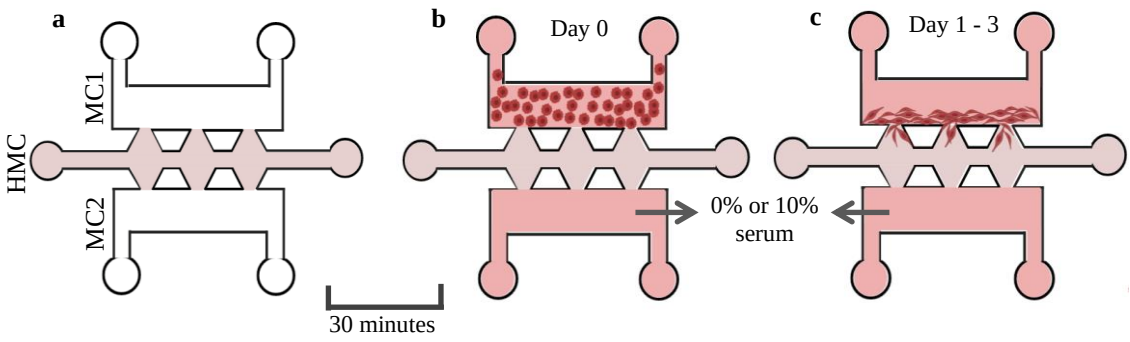

Figure 3.2. Schematic representation of cell-free invasion assay steps. (a) Loading of GFR-Matrigel into HMC, (b) loading of serum-free or serum-containing media into MC2, loading of DsRed-labeled MDAMB231 cells into MC2 (Day 0) and (b) observation of invasion (Day 1, Day 2, Day 3) from MC1 to HMC.

3.7.2. Serum vs. Serum-free Assays

BRL3A cells with the concentration of $1x10^7$cells/ml were loaded to HMC channel of IC-chips in GFR-Matrigel as explained in section 3.2. Overnight incubation was then performed with cell culture media with (2% and 10%) or without serum loaded into two media channels. The next day, serum-free media was loaded into media channel 2 after washing it with serum-free media. DsRed-MDAMB231 cells with a concentration of $1x10^6$ cells/ml in serum-free media were added to media channel 1 and the chips were incubated vertically for 3 days. The invasion of MDAMB231 cells was visualized every 24 hours by 3D imaging using a Leica SP8 confocal microscope.

3.7.3. Invasion of Cancer Cells

Lung, liver, breast and bone homing microenvironments were modeled by WI38, BRL3A, MCF10A, HS5 and hFOB-U937-HS-5 cells respectively. WI38, BRL3A and MCF10A cell lines were loaded in GFR-Matrigel, while hFOB, U937 and HS-5 cell lines were loaded in chitosan-collagen I into HMC of IC-chips at the

optimized cell concentrations (WI38:5x10^{6}cells/ml; BRL3A:1x10^{7}cells/ml; MCF10A: 4.4x10^{6}cells/ml; HS5 individually:5x10^{6}cells/ml; HS5 in combination with hFOB and U937:2x10^{6}cells/ml; hFOB individually: 5x10^{6}cells/ml, hFOB in combination with HS5 and U937:2x10^{6}cells/ml, U937:1x10^{6}cells/ml). Overnight incubation was performed with serum-free media at both media channels (MC1 and MC2). The next day, fresh serum-free media was added to MC2 of the chips. DsRed-labeled MDAMB231, lung specific metastatic clone (MDAMB231 LM2) and bone specific metastatic clone (MDAMB231 1833-BoM) or MCF7 cell lines seeded into the MC1 at the concentration of 1x10^6 cells/ml in serum-free medium (Figure 3.3). The chips were incubated vertically for 3 days. The invasion of each cancer cell line was visualized every 24 hours by 3D imaging using a Leica SP8 confocal microscope.

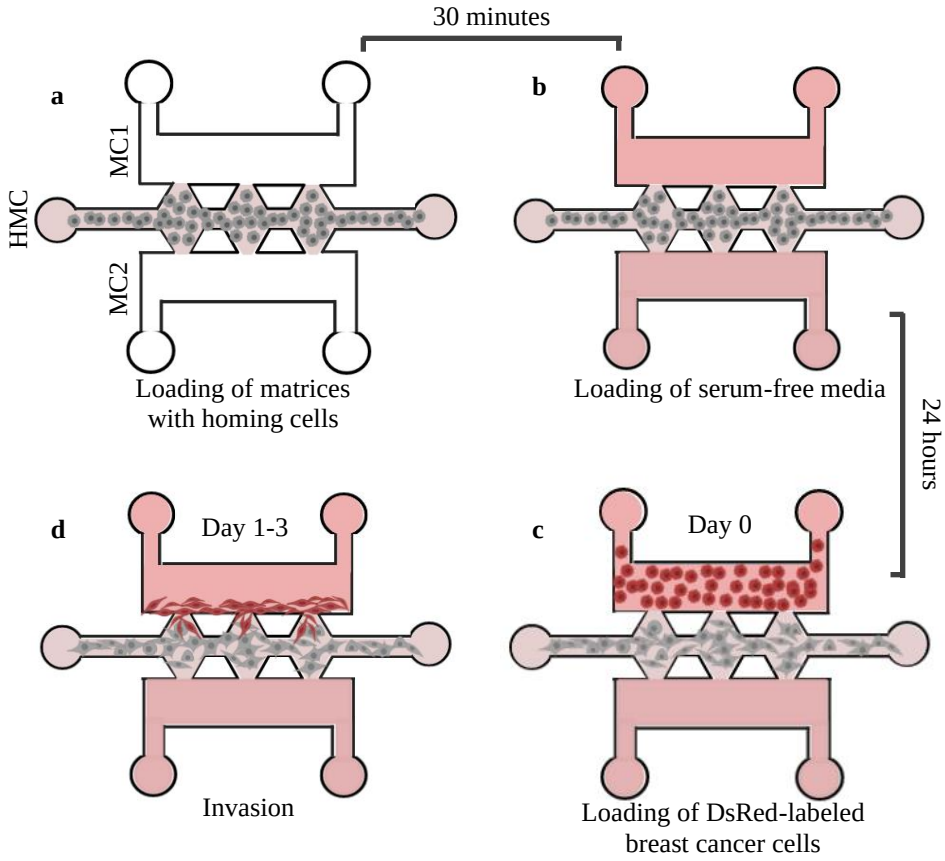

Figure 3.3. Schematic representation of the steps of breast cancer cell invasion assay. (a) Loading of matrices with homing cells to HMC, (b) loading of serum-free media to both MC1 and MC2, (c) loading of DsRed-labeled breast cancer cells to MC1 (Day 0) and (d) observation of invasion (Day 1, Day 2, Day 3) from MC1 to HMC.

3.7.4. Quantification of Invasion Assay

Z-stack images of IC-chips for each condition were obtained each day from Day 0 to Day 3 with a 10X objective and by scanning thoughout the hydrogel for 500 μm with a Z-step size of 7.52 μm. The sum projection of z-stacks of all conditions for each day (Figure 3.4) was prepared and then the same threshold value was applied to all images (Figure 3.4c). The distance of each bright pixel to the starting line (Figure 3.4c blue vertical line) defining the border of hydrogel was calculated by a program written in Python (Ilhan et al., 2020). The distribution of the distances were normalized to Day 1 for each dataset and then shown by box plots drawn on Rstudio.

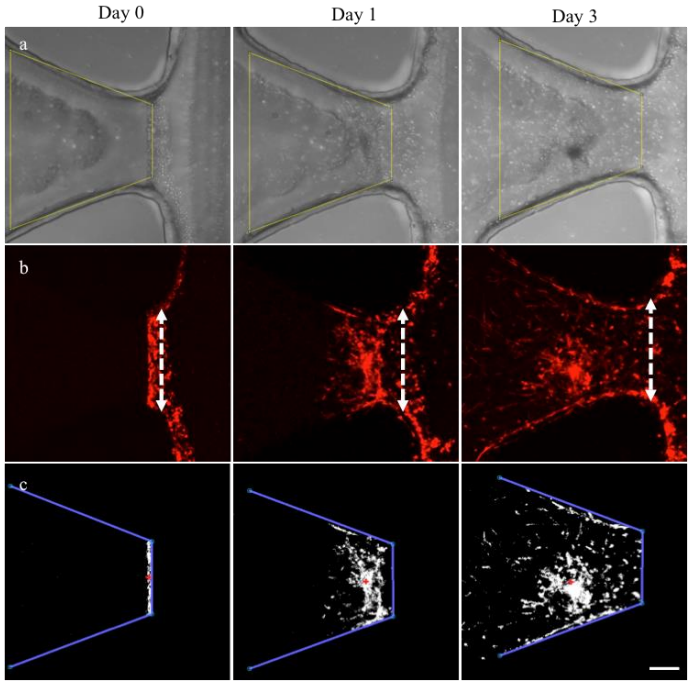

Figure 3.4. A representative post gap (b, two-sided white and dashed arrow) where WI38 cells were used as homing cells was shown. Both phase-contrast and fluorescence images obtained with a Z-step size of 7.52 μm, were collected as a single Z-stack image by ImageJ image processing program for each condition, day and post gaps. (a) Region of interests (ROI) (yellow-edged closed shape) were selected and the same ROI was applied on different days of the same post gaps, (b) the fluorescence images of different days (c) selected ROIs were assigned to fluorescence images (blue lines) by the Python program and the distance of each bright pixel to the starting line was calculated ("+"indicates the center of gravity). Scale bar: 100 μm.

3.8. Extravasation Assay

3.8.1. Formation of Endothelial Monolayer

The HUVEC-C endothelial cells labeled with Green Cell Tracker CMFDA and collected from cell culture plates, were resuspended in DMEM-F12K media containing 8% 450-650 kDa dextran (31392, Sigma Aldrich). The cells with the concentration of $3.85x10^6$ cell/ml were then loaded into EMC of APTES-Lam coated EX-chips in which homing microenvironments were generated with as explained in section 3.7.3. Following the overnight incubation of EX-chips vertically at 37°C in a humidified incubator with 5% CO_2, endothelial monolayer formation was confirmed by 3D imaging using a Leica SP8 confocal microscope.

Formation of intact endothelial monolayer was also confirmed by actin staining. The endothelial monolayer was formed as explained above in the EX-chips loaded with empty matrigel as explained in section 3.7.1. Following the overnight incubation of the HUVEC-C cells, cell culture media was removed from EMC and MC and 4% paraformaldehyde solution was loaded to both channels. After an additional overnight incubation at 4^0C, EMC and MC channels were washed with 1X PBS thrice. Then, permeabilization solution (PBS with 5% BSA and 0,1% Triton-X-100) was loaded to both channels and the EX-chip was incubated at RT for 15 minutes. EMC and MC channels were then washed with 1X PBS thrice and Phalloidin (1:40, Alexa Fluor™ 647) (A22287, Invitrogen) and DAPI (1:500) diluted in PBS were loaded into them. Following the incubation at RT for an hour in the dark, EMC and MC channels were washed with PBS and anti-fading mounting media (90% Glycerol, 10% PBS 10X, 0.1M or 2% (w/v) n-propyl gallate) was loaded to both channels. The chip was kept at +4°C and the next day, images were obtained by a Leica SP8 confocal microscope.

3.8.2. Extravasation Assay without Flow

Lung, liver, breast and bone homing microenvironments were modeled for extravasation assays as explained in section 3.7.3. Once the endothelial monolayer was formed by HUVEC-C cells in EMC of EX-chips as explained in section 3.8.1, DsRed-labeled MDAMB231 cells, lung metastatic (LM2) and bone metastatic (BoM 1833) clones were seeded into EMC at the concentration of $1x10^6$ cells/ml in serum-free media (Figure 3.5c). The chips were then incubated vertically throughout the extravasation process. The assay was only proceeded when the integrity of endothelial monolayer was confirmed shortly after addition of cancer cells (Figure 3.5c). The extravasation of breast cancer cells to the generated lung, liver, breast and bone homing sites was visualized by 3D imaging using a Leica SP8 confocal microscope at 10x magnification and with a z-step size of 7.52 µm for 3 days (Figure 3.5d).

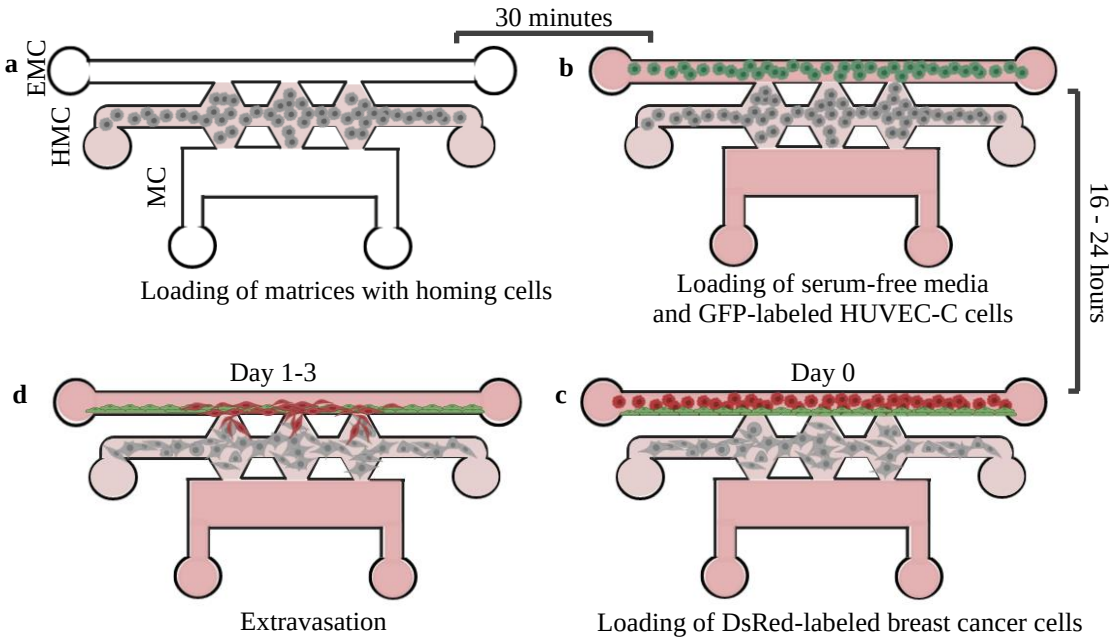

Figure 3.5. Schematic representation of cancer cell extravasation assay without flow. (a) Loading of matrices with homing cells into HMC, (b) loading of serum-free media into MC and HUVEC-C cells into EMC, (c) loading of DsRed-labeled breast cancer cells into EMC (Day 0) and (d) observation of extravasation (Day 1, Day 2, Day 3) from EMC to HMC.

3.8.3. Extravasation Assay under Flow Conditions

3.8.3.1. Viability of Cells with Flow

Different concentrations of MDAMB231 cells ($5x10^4$ cells/ml and $7.5x10^4$ cells/ml) were subject to flow at different shear stresses (0.85 dyne/cm^2 and 0.75 dyne/cm^2) in a closed system containing peristaltic pump for the application of shear stress, marprenes, silicon hoses for circulation of cancer cells within the system and bubble trap for continous application of cancer cells to the system (Figure 3.6) for 2 days. The viability of cells was checked with either MTT assay in each day or EVE automated cell counter machine in 24 hours with 4-hour intervals.

In addition to that, colony formation assay was performed. Cell suspensions collected from bubble trap (Figure 3.6b) when they were taken for MTT assay, were seeded to 6cm cell culture plates and their ability to form colonies was determined by crystal violet (0.5% crystal violet in 25% methanol) staining after 10 days of the first seeding.

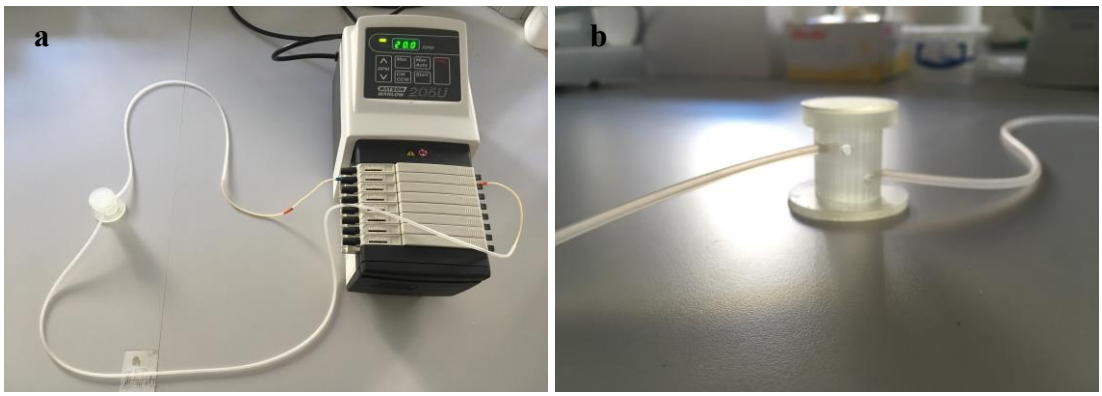

Figure 3.6. Experimental set-up for extravasation assay under flow conditions. (a) Set up and (b) bubble trap.

Two different approaches were applied for extravasation of breast cancer cells under flow conditions. The homing microenvironments were generated in EX-chips with the same protocol performed as explained in section 3.7.3. Following the confirmation of endothelial monolayer formation in EMC of the chips, MDAMB231 cells at a density of $1x10^6$ cells/ml were placed in bubble trap and connected to flow for 4 hours at 0,76 dyne/cm^2 (20 rpm) in peristaltic pump (Figure 3.6a). After 4 hours of circulation, MDAMB231 cells were collected from bubble trap and loaded to the EMC channel where the intact endothelial monolayer was formed. The chips were incubated vertically for 3 days. Secondly, following the generation of homing microenvironments in HMC and endothelial monolayer in EMC of EX-chips, $1x10^6$ cells/ml of MDAMB231 cells were loaded to bubble trap and both trap and EX-chip, from inlet and outlet of EMC channel, were connected to a shear stress of 0,76 dyne/cm^2 (20 rpm) for 4 hours in peristaltic pump. After 4 hours of circulation, the chips were disconnected and incubated vertically for 3 days at 37°C in a humidified incubator with 5% CO_2.

In both conditions, the extravasation of breast cancer cells to the generated lung, liver, breast and bone homing sites was visualized by 3D imaging using a Leica SP8 confocal microscope at 10x magnification and with a z-step size of 7.52 μm for 3 days.

3.8.4. Quantification of Extravasation Assay

Breast cancer cells were described as extravasated when they passed through the endothelial monolayer while they were defined as associated if they stayed connected to the endothelial monolayer (Figure 3.7). Region of interests (ROIs) were selected for each post gaps of each condition and ROIs were only included in the analysis where the formation of intact endothelial monolayer was confirmed. The extravasated and associated cells were then counted from every side of each 3D image and the extravasation capacity of breast cancer cells was determined.

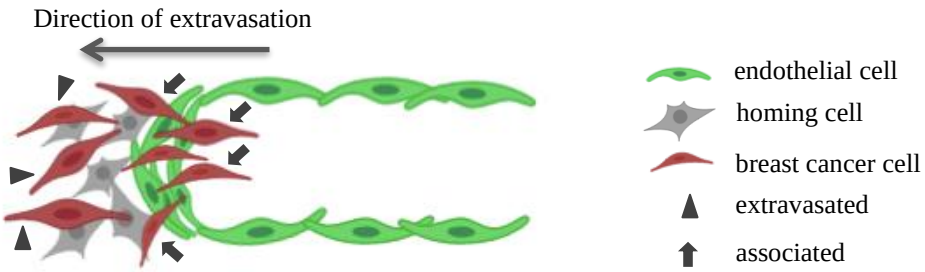

Figure 3.7. Schematic illustration of breast cancer cell (red) extravasation across endothelial monolayer (green) into homing cell microenvironment (gray) showing extravasated (arrow head) and associated (arrow) cancer cells.

CHAPTER 4

RESULTS

4.1. Generation of Stably Labeled Cell Lines

Cell lines were infected with MSCV retroviruses expressing red fluorescent protein (DsRed) or green fluorescent protein (eGFP) and puromycin resistance genes to be visualized within 3D hydrogels and LOC system without any further staining throughout the study.

Metastatic breast cancer cell lines, MDAMB231 and its clones, Lung metastatic MDAMB231 LM2 and bone metastatic MDAMB231 BoM 1833, non-metastatic breast cancer cell line, MCF7, and normal breast cell line, MCF10A, were stably labeled with DsRed protein, while normal cell lines, WI38, BRL3A, HS5 and MCF10A used for modeling homing microenvironments and HUVEC-C cell line used for endothelial monolayer formation, were stably labeled with eGFP protein. Fluorescence microscope images of infected cells revealed that cell lines stably labeled with DsRed (Figure 4.1) and eGFP (Figure 4.2) were successfully generated after puromycin antibiotic selection.

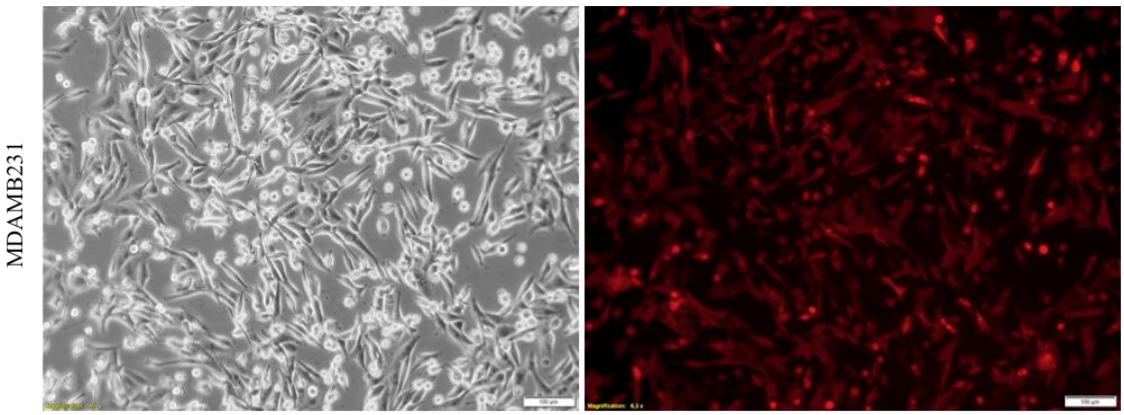

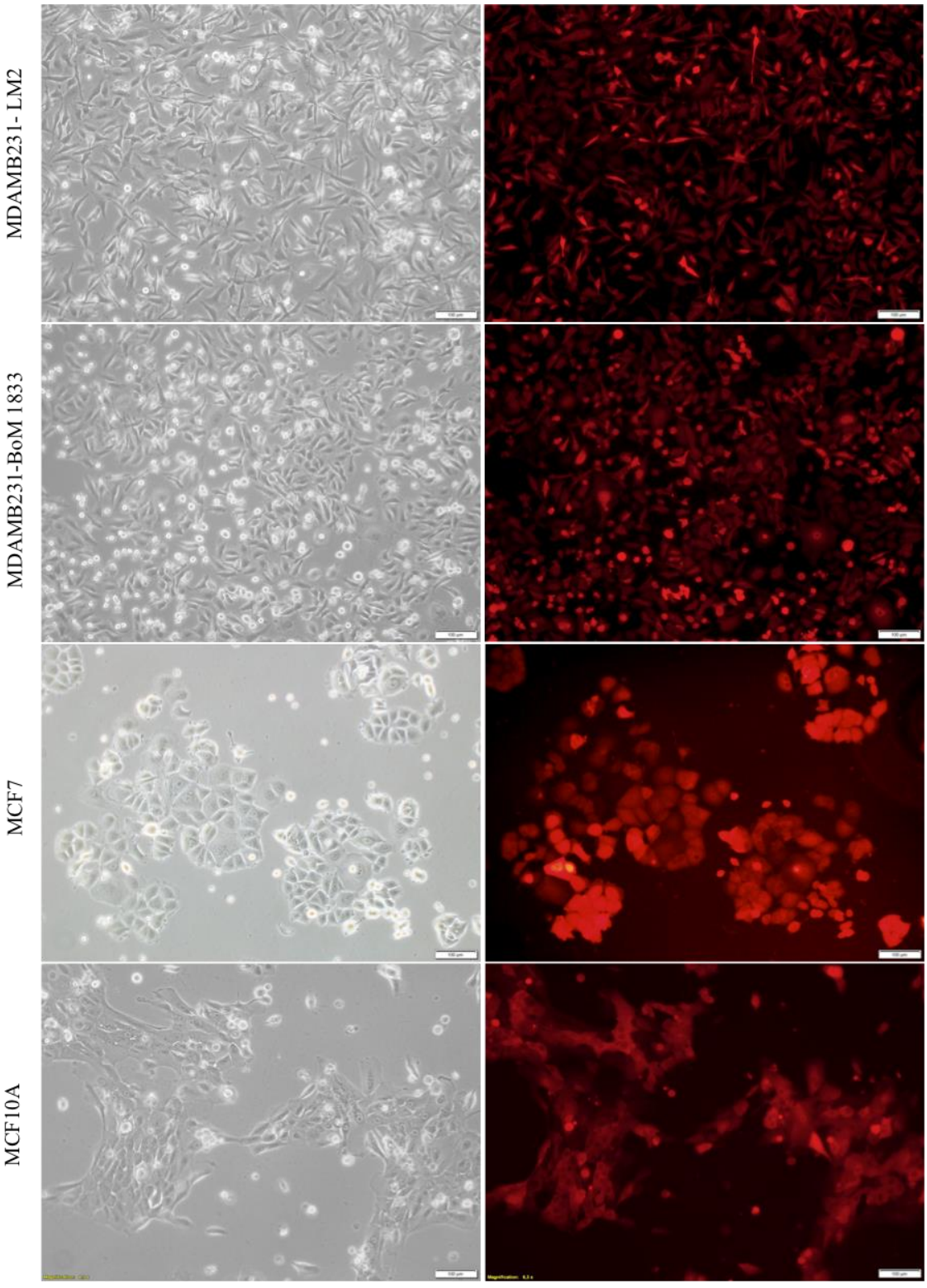

Figure 4.1. Fluorescence microscope images showing stable labeling of metastatic (MDAMB231, MDAMB231 LM2 and MDAMB231 BoM 1833), non-metastatic (MCF7) breast cancer cell lines and normal breast cell line (MCF10A) with DsRed fluorescent protein. Scale bar 100 μm.

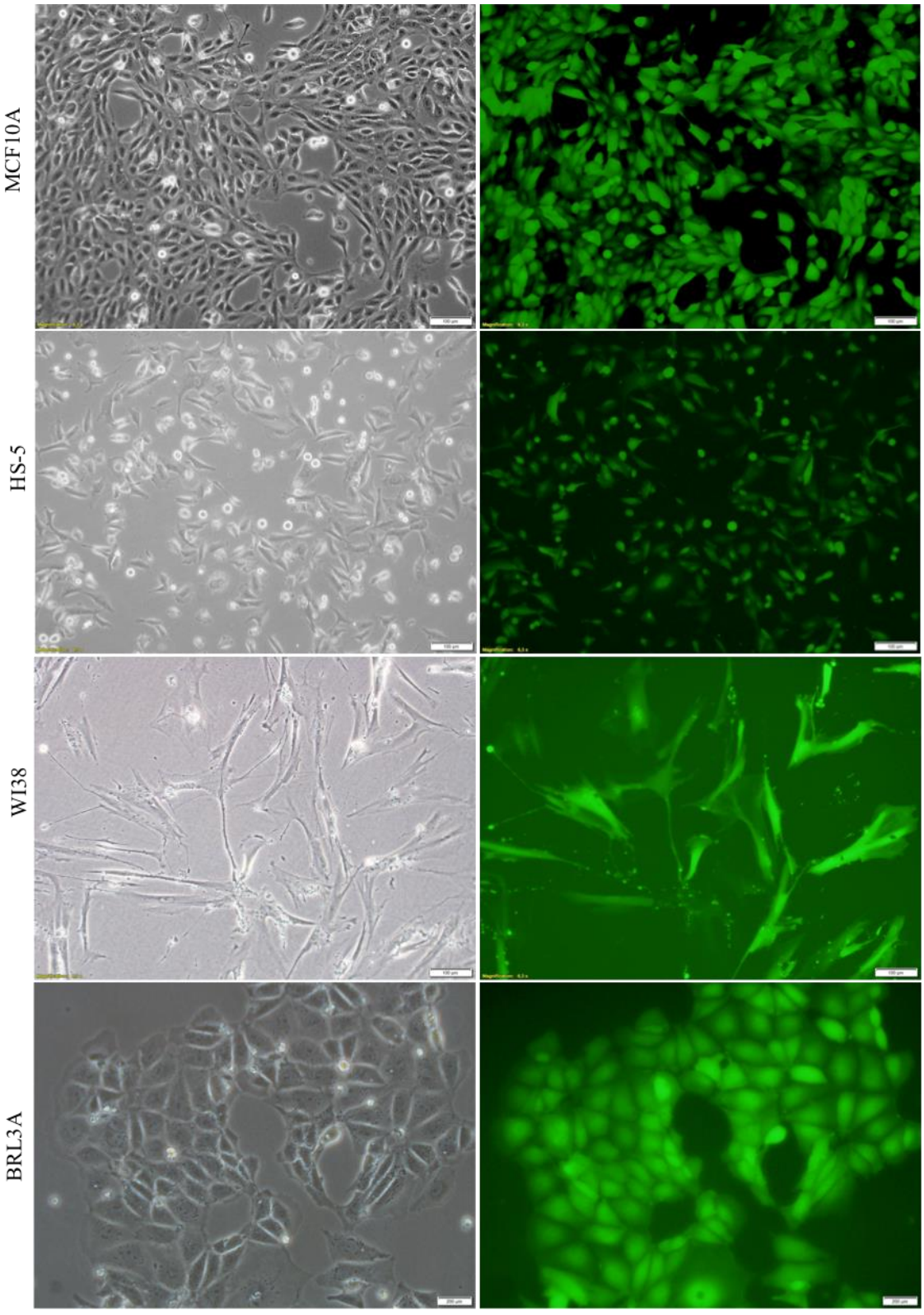
MCF10A
HS-5
WI38
BRL3A

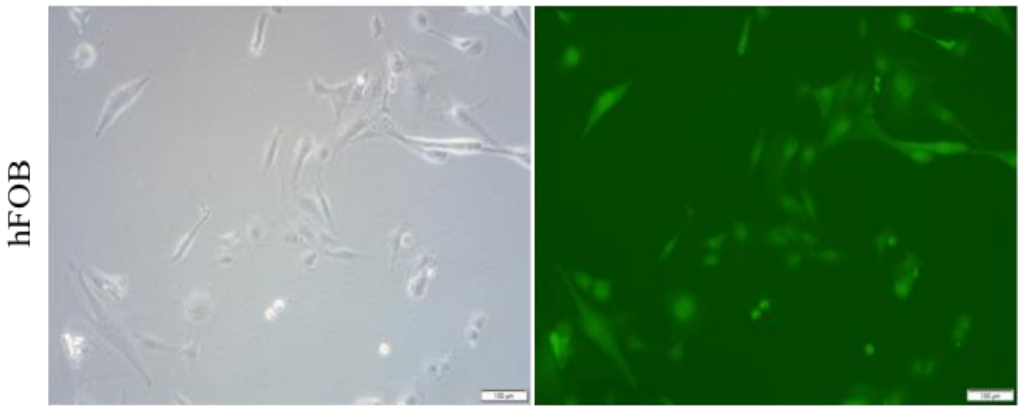

Figure 4.2. Fluorescence microscope images showing stable labeling of normal stromal cell lines; breast epithelial cell line (MCF10A), bone marrow fibroblast cell line (HS-5), lung fibroblast cell line (WI38), liver epithelial cell line (BRL3A) and fetal osteoblast cell line (hFOB) with eGFP fluorescent protein. Scale bar 100 μm.

HUVEC-C cell lines were successfully labeled with eGFP (Figure 4.3), however they started to grow slowly after being stably labelled with retroviruses. Thus Green Cell Tracker CMFDA was used to label the cells transiently. This transient labeling was performed prior to experimental set-up and did not affect the growth rate of HUVEC-C cells. Therefore, Green Cell Tracker CMFDA labeling was performed for all the experiments where HUVEC-C cells were used.

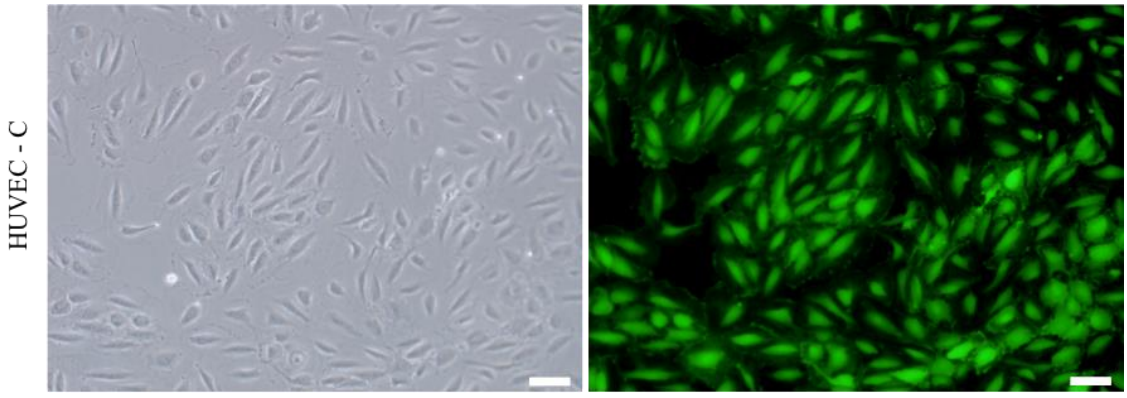

Figure 4.3. Fluorescence microscope images showing stable labeling of HUVEC-C endothelial cells with eGFP fluorescent protein. Scale bar 100 μm.

4.2. Cell Culture Medium Optimization

Stromal cells used for mimicking target microenvironments, require different cell culture media although their growth conditions are similar (Table 3.1). Thus, to avoid any effect on the invasiveness of breast cancer cells due to media differences, stromal cells were grown in the same cell culture medium. The medium of MDAMB231 cell line (DMEM with 10% FBS and 1% P/S) was chosen as the common cell culture medium and its effects on viability and expression of chemokines that are critical for breast cancer invasion were identified in stromal cells.

4.2.1. Determination of Cell Viability

The cellular viability of stromal cells seeded either with DMEM or their own cell culture media (MEM-alpha or DMEM-F12) was determined by MTT assay in which the metabolic activity of living cells is assessed, at day 1, 3 and 7. When the growth curves of WI38, BRL3A, MCF10A and hFOB cell lines were compared, it was observed that each cell line showed similar growth trend in both media (Figure 4.4). However, although there was no significant difference between the number of MCF10A and hFOB cells on the 3rd day in both culture media, around 1.2 and 1.4 fold, respectively, increase was detected on the 7th day when they were cultured in their own medium (DMEM-F12) (Figure 4.4c,d). The increase in the growth rate of MCF10A and hFOB cell lines might be linked to the rich and complex content of DMEM-F12 medium (Arora, 2013) supporting the growth of cells more than that of DMEM-based medium. On the other hand, considering that MCF10A and hFOB cell lines showed a continual increase in their cell number from day 1 to day 7, albeit slower and the LOC-based experiments were completed within 3 days, it was concluded that DMEM medium was suitable for culturing the stromal cells.

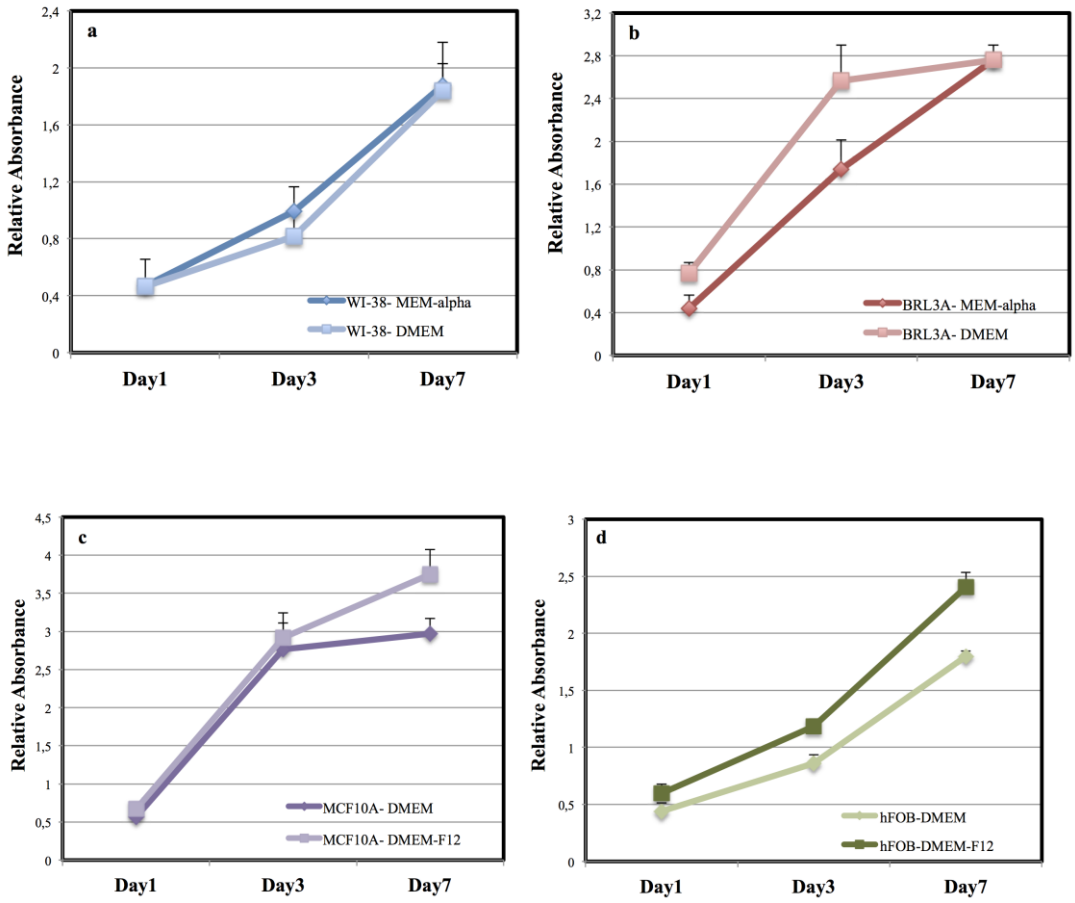

Figure 4.4. MTT assay for the viability of stromal cells in DMEM-based or their own cell culture media. Cellular viability of a) WI38 cell lines, b) BRL3A cell lines, c) MCF10A cell lines and d) hFOB cell lines at Day 1, Day 3 and Day 7.

4.2.2. Determination of 2D Gene Expression Levels

The reciprocal interaction between cancer cells and the local stroma at the metastatic site play crucial roles in promoting cancer cell migration, invasion and dissemination (Chow & Luster, 2014; Esquivel-Velázquez et al., 2015). The contribution of chemokines that are secreted from stromal cells at the metastatic target site, to the tumor progression has been well established. In the literature, various studies have revealed the secretion of CXCL12 from normal lung and bone fibroblasts, and CCL5 and IGF1 from normal osteoblasts and bone fibroblasts as explained in section 1.

Therefore, to investigate whether culturing of stromal cells with DMEM-based medium can affect the expression of chemokines, RT-qPCR was performed. The expression patterns of each chemokine were analyzed in the stromal cells cultured either in DMEM-based or their own growth medium by using chemokine specific primers at Day 1 and Day 3.

The mRNA expression of CXCL12 and IGF1 chemokines was observed in WI38 cell line in both cell culture conditions. The mRNA level for CXCL12 gene was lower in DMEM compared to MEM-alpha conditions both at Day 1 and Day 3 (Figure 4.5a). IGF1 mRNA expression increased in MEM-alpha while a slight fall was observed in DMEM conditions from Day 1 to Day 3 (Figure 4.5b). In BRL3A cell lines, the mRNA expression of both CXCL12 and CCL5 genes was detected in both conditions.

Overall, the expression patterns of each chemokine were similar in both cell culture conditions. A modest decrease was observed in the expression of CXCL12 gene, whereas a slight rise was determined in CCL5 expression at Day 3 in both culture conditions in BRL3A cells (Figure 4.5c,d). In hFOB cells, IGF1 expression was identified when they were cultured either with DMEM or DMEM-F12 while CXCL12 and CCL5 expressions were not detectable. The expression patterns of IGF1 showed a similar increasing trend in both conditions from Day 1 to Day 3 (Figure 4.5e). In the other bone-related cell line, HS-5, growth medium of which is DMEM-based, the mRNA expressions of CXCL12 and CCL5 but no expression of IGF1 were observed unlike hFOB cells (Figure 4.5f,g). There was no expression of CXCL12, CCL5 and IGF1 chemokines in MCF10A cells cultured either in DMEM or DMEM-F12.

Overall, DMEM medium was determined to use as a common medium, considering both the viability of stromal cells and expression patterns of chemokines.

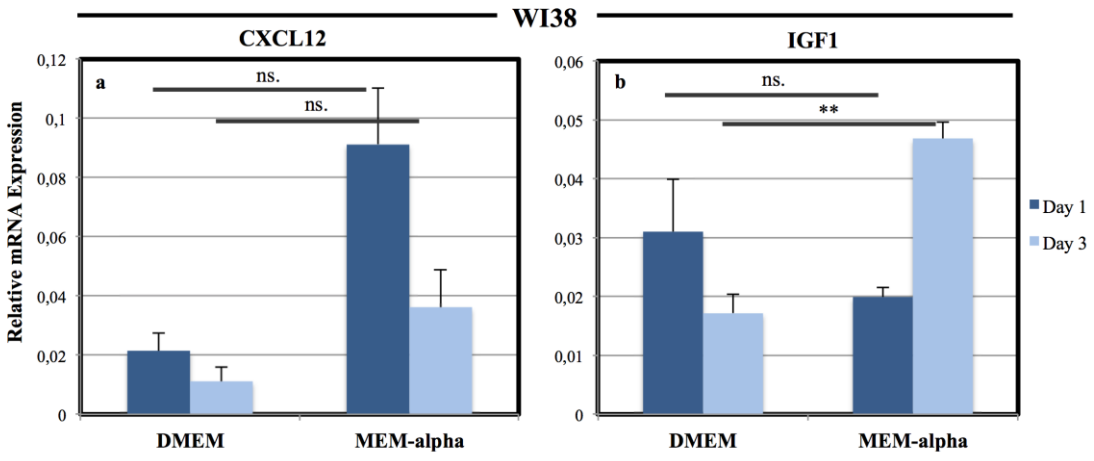

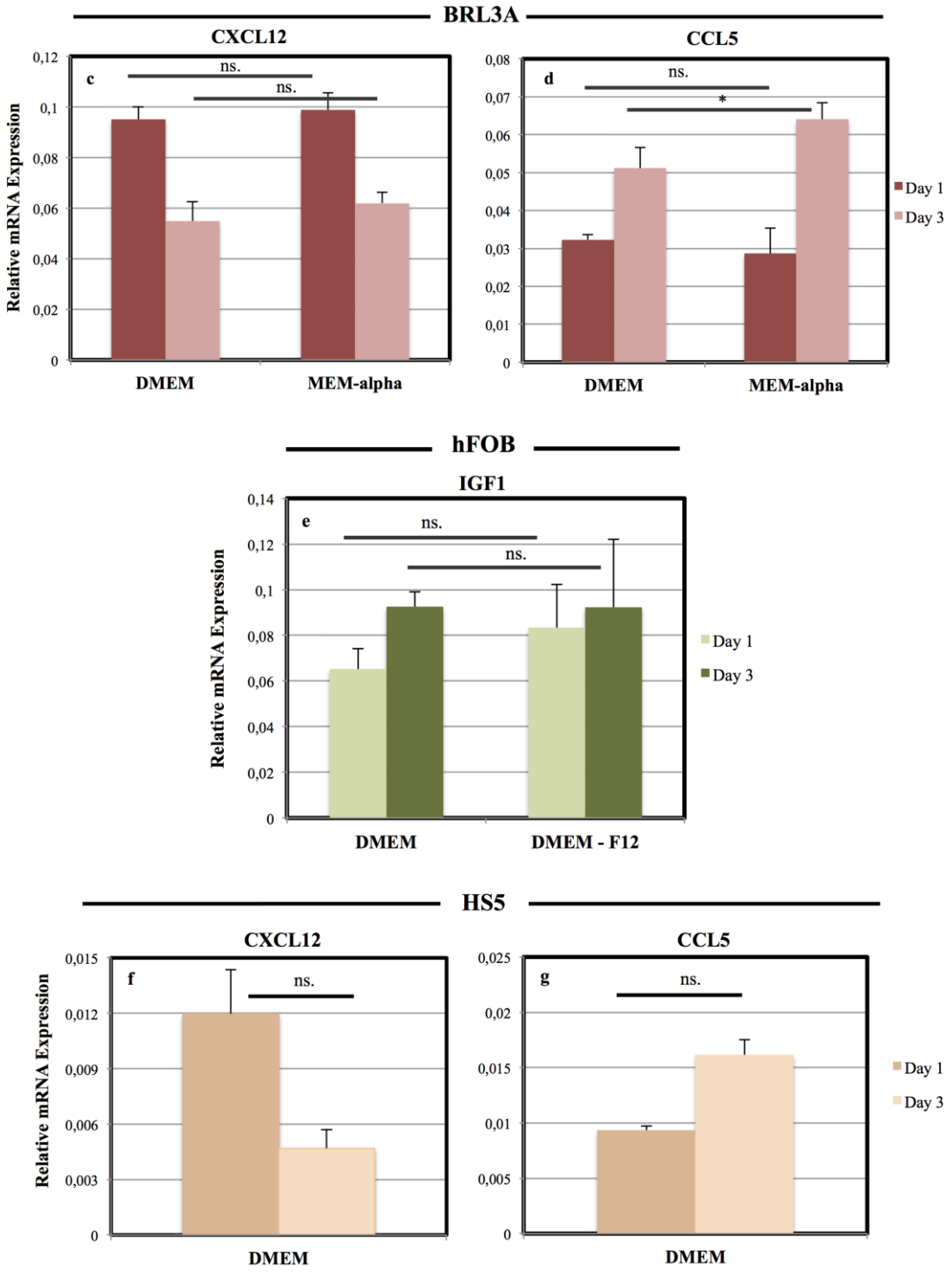

Figure 4.5. The effects of different growth media on the expression of chemokines secreted from stromal cells. The mRNA expression patterns of CXCL12, CCL5 and IGF1 in a, b) WI38 cell line, c, d) BRL3A cell line, e) hFOB cell line and f,g) HS-5 cell line. The relative expression levels show the mean ± standard deviation for three independent experiments. *$p \leq 0.05$; **$p \leq 0.01$.

4.3. Optimization of Cell Number for Lab-on-a-chip Platform

The cell density within 3D cell-laden hydrogels has a crucial role in cell-cell signaling and one of the key regulators of cellular differentiation. The optimal cell seeding density relies primarily on the components of 3D matrix and the type of seeded cells (Maia, Lourenço, Granja, Gonçalves, & Barrias, 2014). The impacts of the initial cell seeding density in 3D hydrogels were investigated in recent years. The high seeding densities were shown to promote the formation of multicellular clusters, which then increased cell-to-cell interactions and stimulated cellular differentiation and morphological changes (J. Zhang et al., 2020). Therefore, as cell-to-cell and cell-to-matrix interactions are essential to mimic the 3D environment of stromal cells, higher initial cell seeding densities were used to optimize the cellular concentrations within LOC systems.

The homing sites were modeled within LOC systems by growing stromal cells in 3D environment. Two different matrix components, Growth Factor Reduced (GFR)-Matrigel and Collagen type I, were tested to generate 3D homing microenvironments.

GFR-Matrigel provides a biologically relevant environment and so it is widely used in several applications including native-like 3D microenvironment generation and it is a rich matrix containing laminin, collagen type IV, entactin and heparan sulfate proteoglycan (Hughes, Postovit, & Lajoie, 2010). GFR-Matrigel was chosen to eliminate the influences of growth factors on the invasiveness of the breast cancer cells and to evaluate the impacts of secreted factors from stromal cells on breast cancer dissemination.

Collagen type I is the most abundant collagen type in stroma and the main component of the connective tissues (Weber, Kirsch, Müller, & Krieg, 1984). Therefore, it is commonly used for the modeling biological 3D matrices by providing *in vivo* like conditions.

Therefore, the optimal cell seeding densities for each stromal cell into each ECM component were determined by evaluating the morphology of the cells and the mRNA expression levels of CXCL12, CCL5 and IGF1 genes.

4.3.1. 3D Gene Expression Levels

The seeding density of the cells in 3D cultures can affect the expression profiles of the genes (Heng et al., 2011; Maia et al., 2014). Therefore, to investigate the optimal cell seeding density, the expression levels of CXCL12, CCL5 and IGF1 chemokines were examined in the stromal cells with different initial seeding densities.

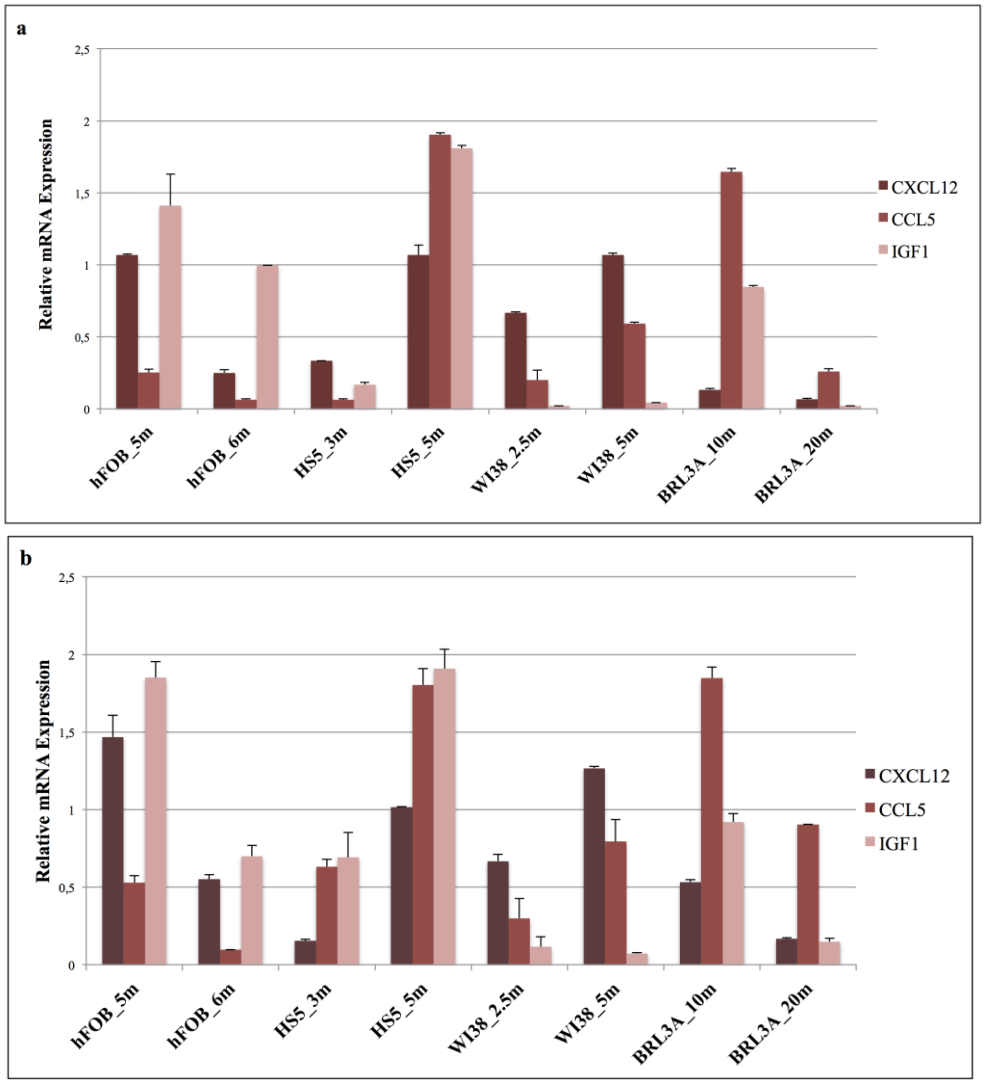

Figure 4.6. The effects of different initial seeding densities on the expression of chemokines secreted from stromal cells in a) GFR-Matrigel and b) Collagen I hydrogels. The mRNA expression patterns of CXCL12, CCL5 and IGF1 in hFOB, HS5, WI38 and BRL3A cell line on Day 2. The relative expression levels show the mean ± standard deviation.

Different concentrations, $5x10^6$ cells/ml and $6x10^6$ cells/ml for hFOB; $3x10^6$ cells/ml and $5x10^6$ cells/ml for HS5; $2.5x10^6$ cells/ml and $5x10^6$ cells/ml for WI38 and $1x10^7$ cells/ml and $2x10^7$ cells/ml for BRL3A cells were seeded into GFR-Matrigel or collagen type I and the change in the expression patterns of CXCL12, CCL5 and IGF1 chemokines due to different initial seeding densities was examined. It was shown in Figure 4.6 that all three chemokines were highly expressed in hFOB cells with $5x10^6$ cells/ml, HS5 cell with $5x10^6$ cells/ml, WI38 cells with $5x10^6$ cells/ml and BRL3A cells with $1x10^7$ cells/ml in both hydrogel conditions. Therefore, these concentrations for each cell line were used for evaluating the morphology of the cells with 3D environments.

MCF10A cells were seeded into both GFR-Matrigel and collagen I hydrogels with the concentration of $4.5x10^6$ cells/ml according to the literature (Baenke, 2013). However, there was no chemokine expression in each condition and the sufficiency of the concentration was only evaluated through the morphology of MCF10A cells seeded either into GFR-Matrigel or collagen I hydrogels.

4.3.2. Morphology

GFP-labeled stromal cells, WI38, HS5, BRL3A and MCF10A, were seeded into HMC (Figure 3.2) of IC-chips either with 4mg/ml GFR-Matrigel or 2mg/ml collagen type I as explained in section 3.2. Lung fibroblast cell line, WI38 and bone fibroblast cell line, HS5 were seeded at a density of $5x10^6$ cells/ml, while liver epithelial cell line, BRL3A and breast epithelial cell line, MCF10A were seeded at densities of $1x10^7$ cells/ml and $4.5x10^6$ cells/ml, respectively, into both GFR-Matrigel and collagen I hydrogels.

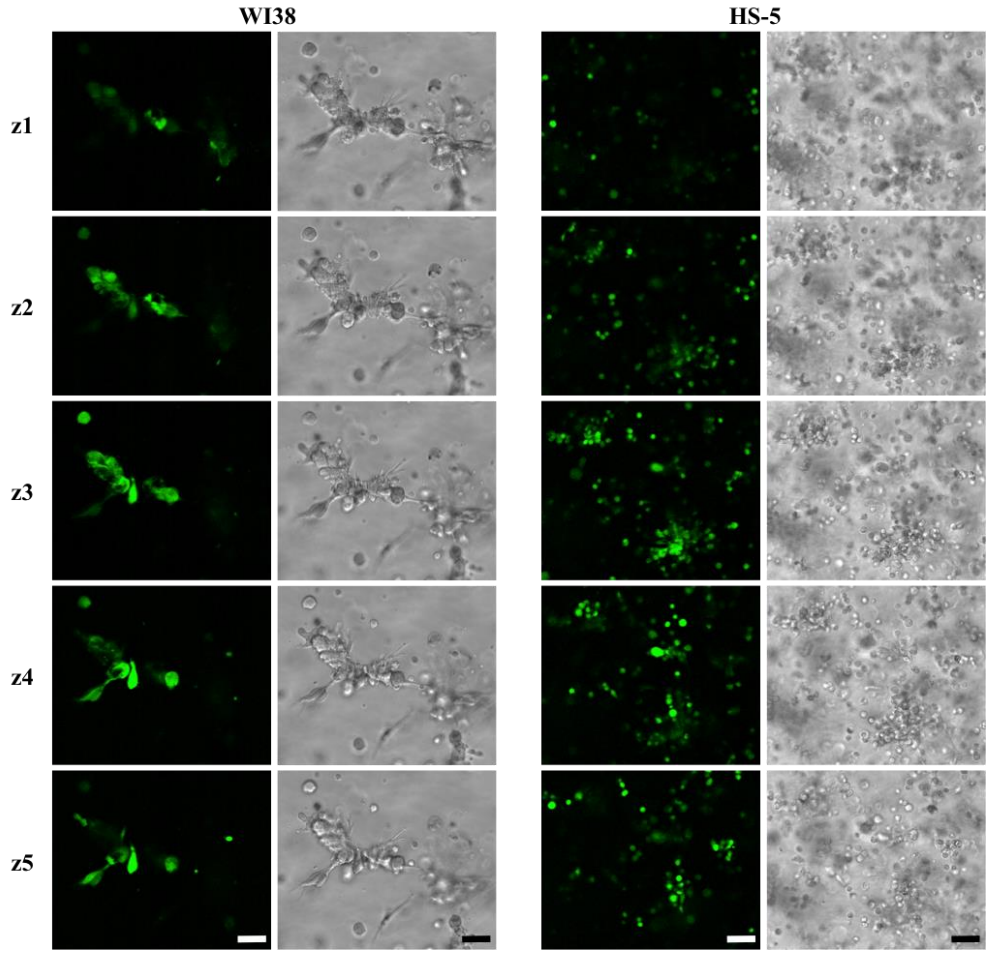

Figure 4.7. Stromal cells grown in GFR-Matrigel. Different z-planes (z1-z5) of fluorescence and phase-contrast images of WI38 and HS-5 cells seeded into 4 mg/ml of GFR-Matrigel at Day 2. Scale bar: 100 μm, distance between adjecent z-planes: 30 μm.

The morphological differences as well as the structures formed by the cells were visualized by confocal microscope by scanning an area of approximately 1 mm in depth. It was observed that all stromal cells could grow in different axes forming 3D structures in the GFR-Matrigel (Figure 4.7 and 4.8). WI38 (Figure 4.7) and BRL3A cells (Figure 4.8) formed multicellular structures while HS5 and MCF10A cells revealed more uniform distribution within GFR-Matrigel hydrogels (Figure 4.7 and 4.8).

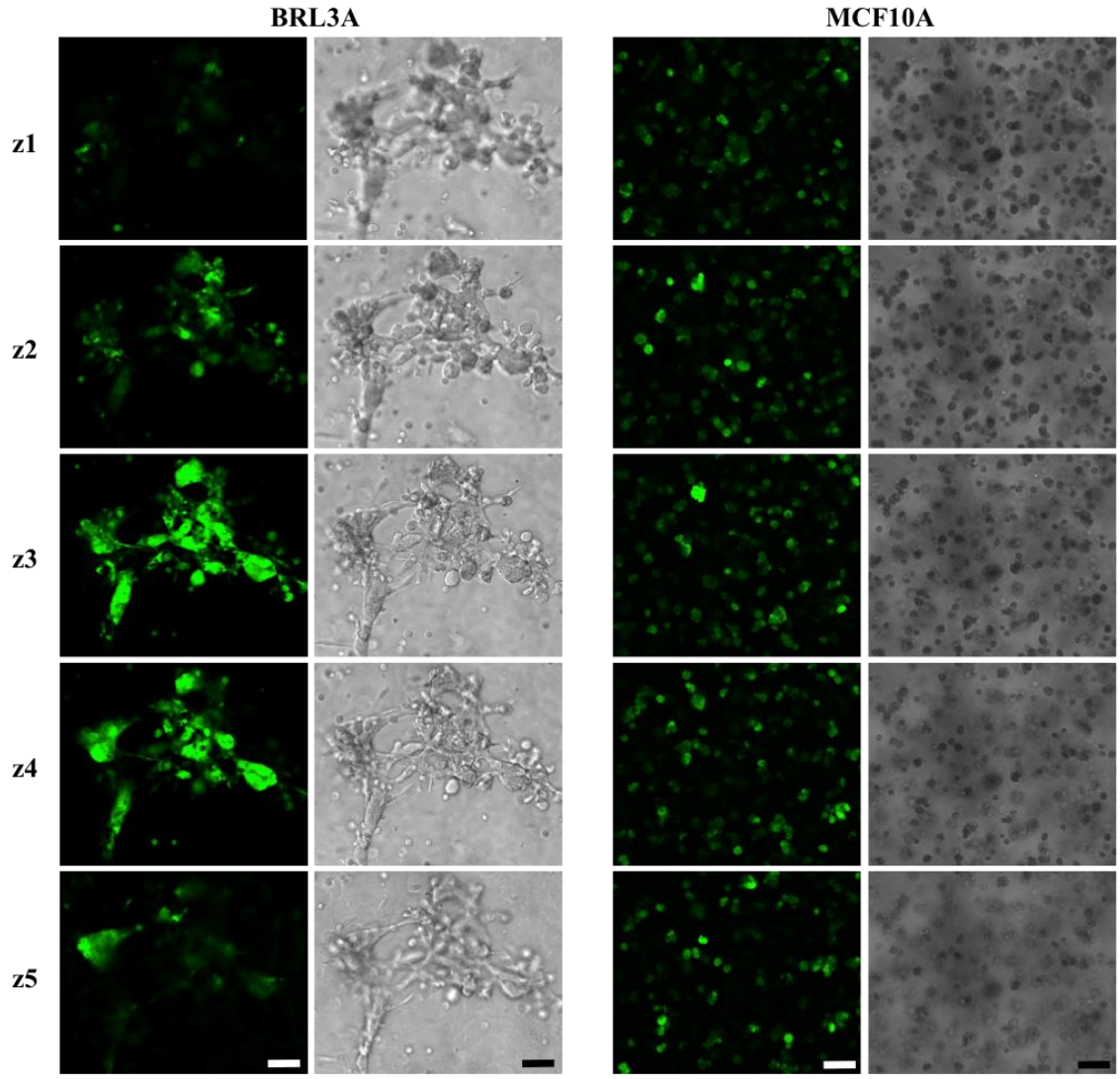

Figure 4.8. Stromal cells grown in GFR-Matrigel. Different z-planes (z1-z5) of fluorescence and phase-contrast images of BRL3A and MCF10A cells seeded into 4 mg/ml of GFR-Matrigel at Day 2. Scale bar: 100 μm, distance between adjecent z-planes: 30 μm.

The stromal cells growing in collagen I hydrogels were more homogeneously distributed in the matrix than those in GFR-Matrigel (Figure 4.9 and 4.10). They showed more fibroblast-like morphology, which were more apparent in bone fibroblast cell line, HS-5 (Figure 4.9).

The multicellular structures formed by stromal cells when seeded with GFR-Matrigel were important to promote their cell-to-cell communication and to activate both intra- and intercellular signaling (D. Sun, Lu, Chen, Yu, & Li, 2014) leading to

formation of more native-like environments. Therefore, GFR-Matrigel was determined to use as the common ECM component for generation of homing microenvironments.

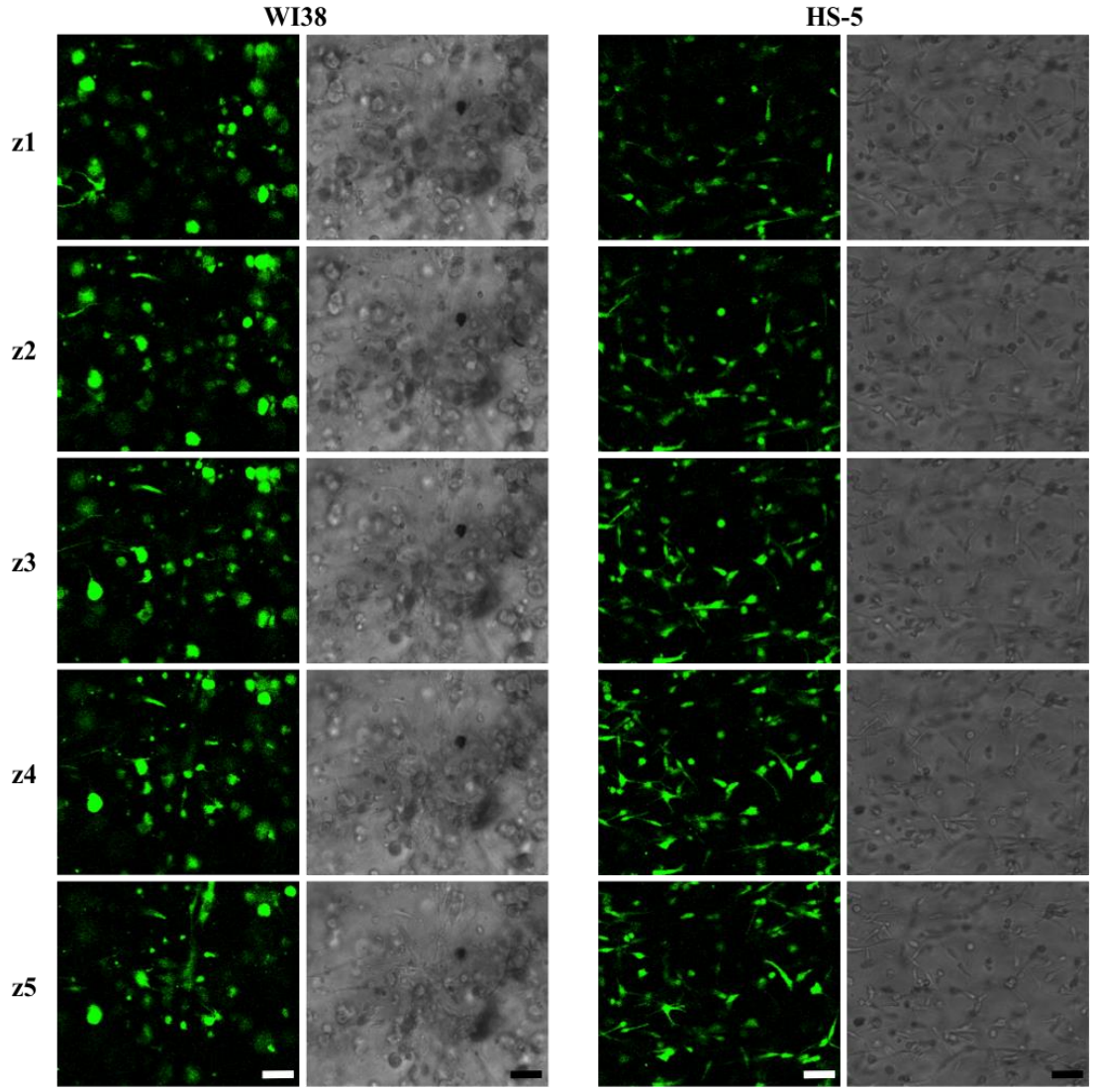

Figure 4.9. Stromal cells grown in type I Collagen. Different z-planes (z1-z5) of fluorescence and phase-contrast images of WI38 and HS-5 and cells seeded into 2 mg/ml of GFR-matrigel at Day 2. Scale bar: 100 μm, distance between adjecent between z-planes: 30 μm.

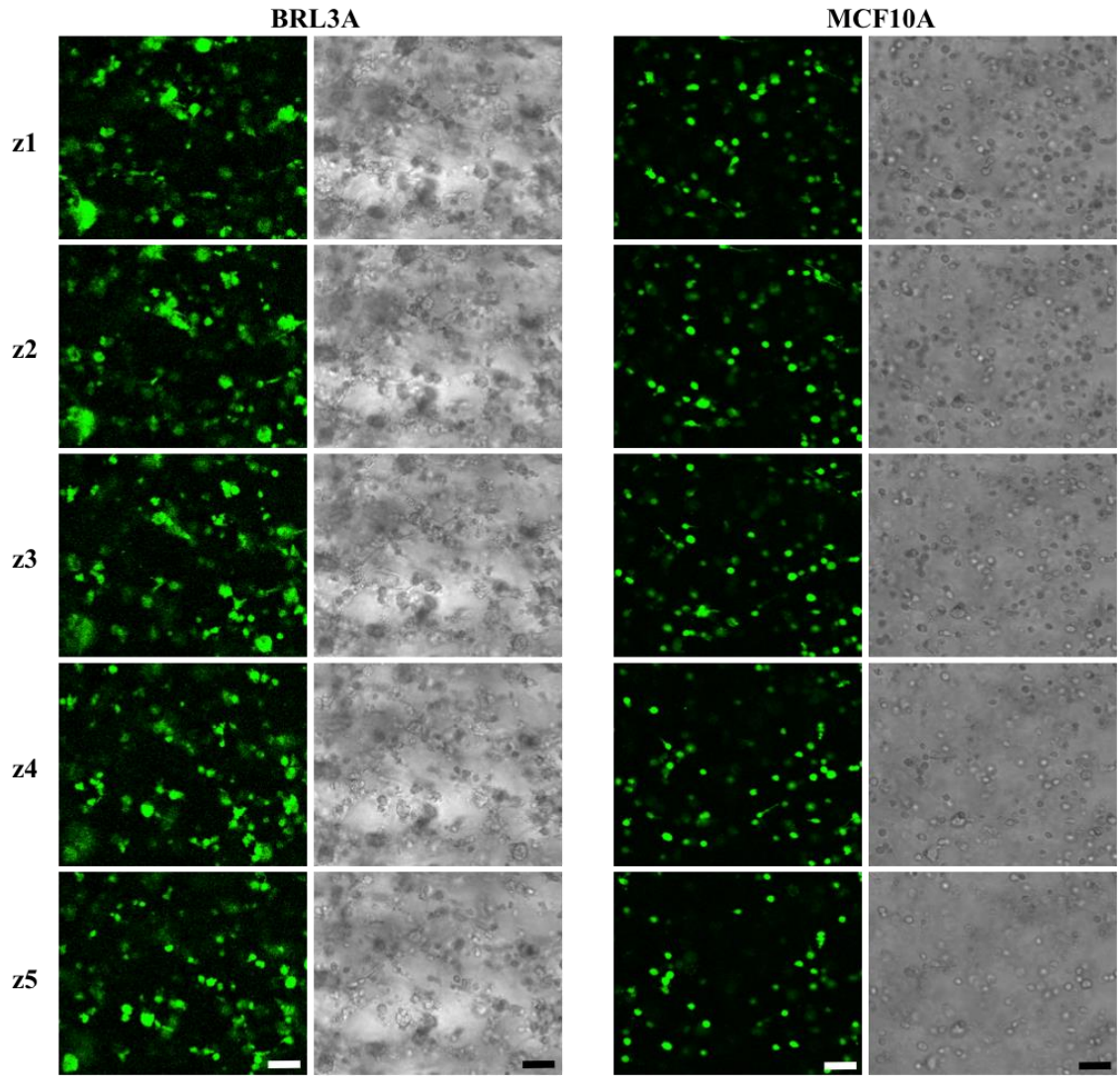

Figure 4.10. Stromal cells grown in Collagen I. Different z-planes (z1-z5) of fluorescence and phase-contrast images of BRL3A and MCF10A cells seeded into 2 mg/ml of GFR-matrigel at Day 2. Scale bar: 100 μm, between z-planes: 30 μm.

4.4. Invasion Assay

Metastatic dissemination of cancer cells starts with invasion and migration where cancer cells detach from their primary tumor sites and penetrate into the surrounding stromal microenvironment (Meirson, Gil-Henn, & Samson, 2020). Organ specific dissemination of cancer cells is considerably associated with cell-ECM and

cell-cell interactions between cancer cells and structural-cellular milieu of target site microenvironments (Emon, Bauer, Jain, Jung, & Saif, 2018; Esquivel-Velázquez et al., 2015). Therefore, the effects of different chemokines present in cell culture media and/or secreted from stromal cells in target tissue microenvironments, on the invasion of breast cancer cells were investigated. In that case, the invasion capacity of breast cancer cells towards cell-free hydrogels (Figure 4.11) or cell-laden hydrogels (Figure 4.12, 4.14, 4.15) was determined by IC-chips.

4.4.1. Cell-free Assays

Invasion of tumor cells in their primary site is mainly promoted by the factors present within target tissue microenvironments. These factors called as chemokines are the chemotactic cytokines and are essential regulators of cellular migration and directed movement of the cells (Méndez-García et al., 2019). The effects of serum that contains several growth factors and cytokines, on the invasion of MDAMB231 cells were investigated to demonstrate the use of IC-chip for invasion assays. Cell-free GFR-Matrigel was polymerized in HMC, while culture media with or without 10% FBS was loaded into MC2 channel of IC-chip. DsRed-labelled MDAMB231 cells were loaded into MC1 in serum-free media and the invasion was screened for 3 days (Figure 4.11a). In both condition, an increase in the invasion was observed from Day 1 to Day 3, consistent with the invasive characteristics of MDAMB231 cells (Figure 4.11b). Yet, MDAMB231 cells showed more invasion towards FBS-containing medium than to FBS-free medium which was also confirmed by the significant increase in mean and median distances invaded by the breast cancer cells towards FBS-containing condition (Figure 4.11c). Accordingly, IC-chip was able to exhibit the role of serum as a chemoattractant both visually and quantitatively (Figure 4.11) and demonstrate the invasion potential of breast cancer cells.

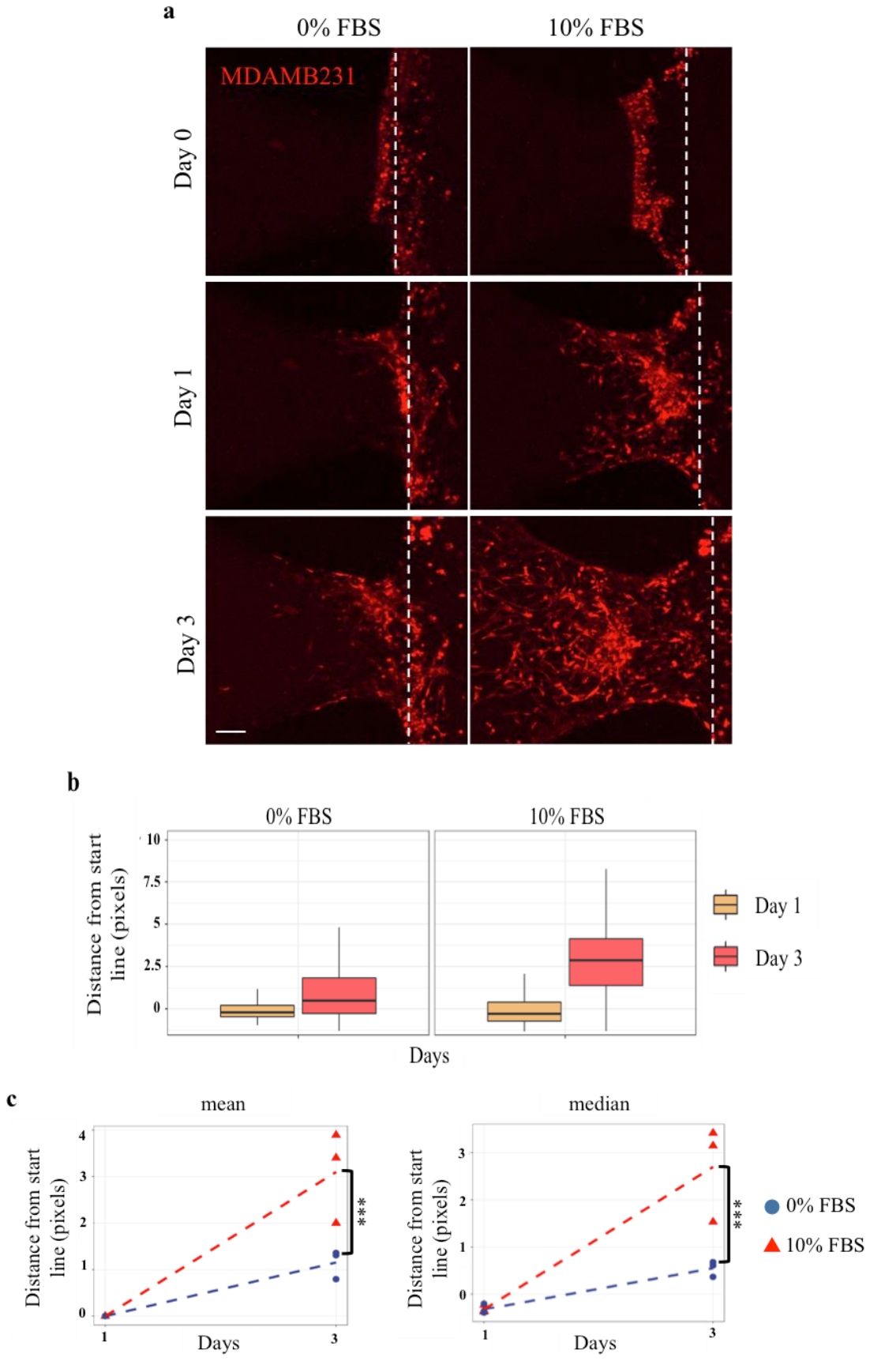
a
0% FBS
10% FBS
MDAMB231
Day 0
Day 1
Day 3
b
0% FBS
10% FBS
Distance from start line (pixels)
10
7.5
5
2.5
0
Day 1
Day 3
Days
c
mean
median
Distance from start line (pixels)
Days
***
0% FBS
10% FBS

Figure 4.11. Invasion of MDAMB231 cells towards empty matrigel in the presence or absence of serum. Representative Z-stack images showing invasion of MDAMB231 cells (red) towards a) empty matrigel in the absence (0%) or presence (10%) of serum (dashed line corresponds to the starting line for invasion) (Scale bar: 200 μm). b) The distance of each bright pixel to the starting line (dashed) was calculated after thresholding of Z-stack images. The data normalized to day 1 were plotted (n=3). c) Mean and median values of normalized distance distributions were plotted for day 1 and day 3 (n=3). *** $p \leq 0.005$. (FBS: fetal bovine serum).

4.4.2. Cell-laden Assays

The effects of homing stromal cells on the invasion of breast cancer cells were identified with different serum concentrations to optimize the invasion conditions towards different target site microenvironments.

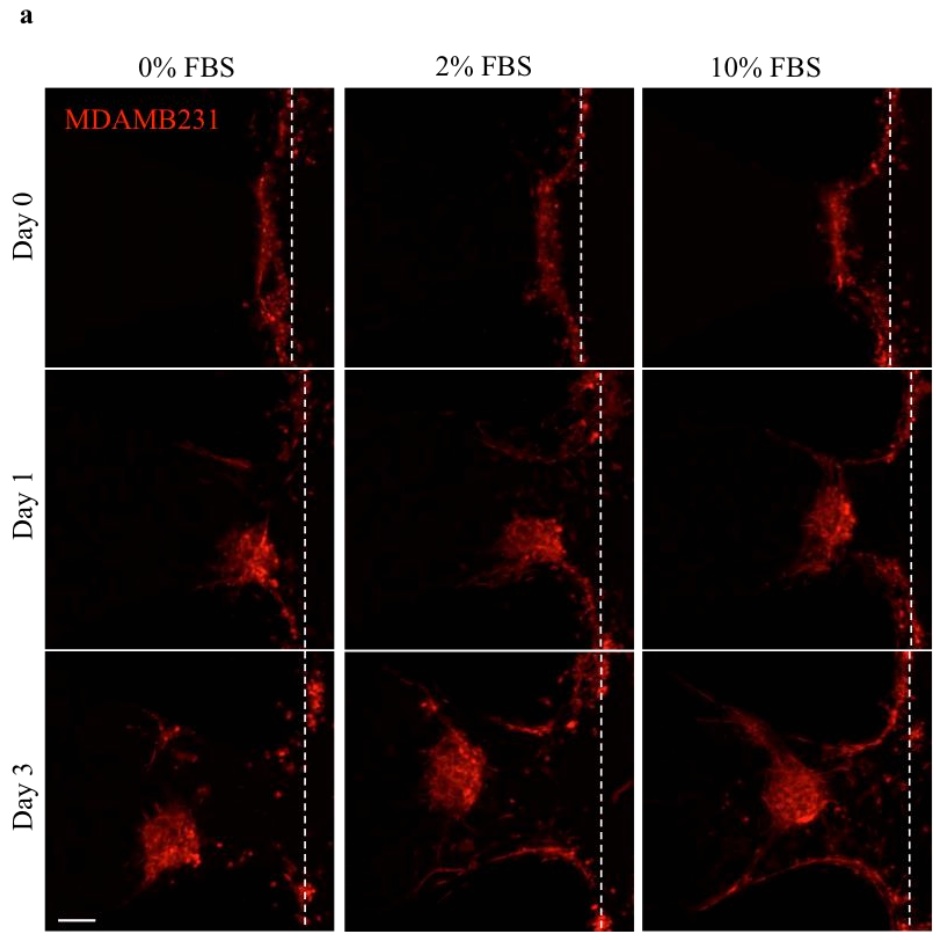

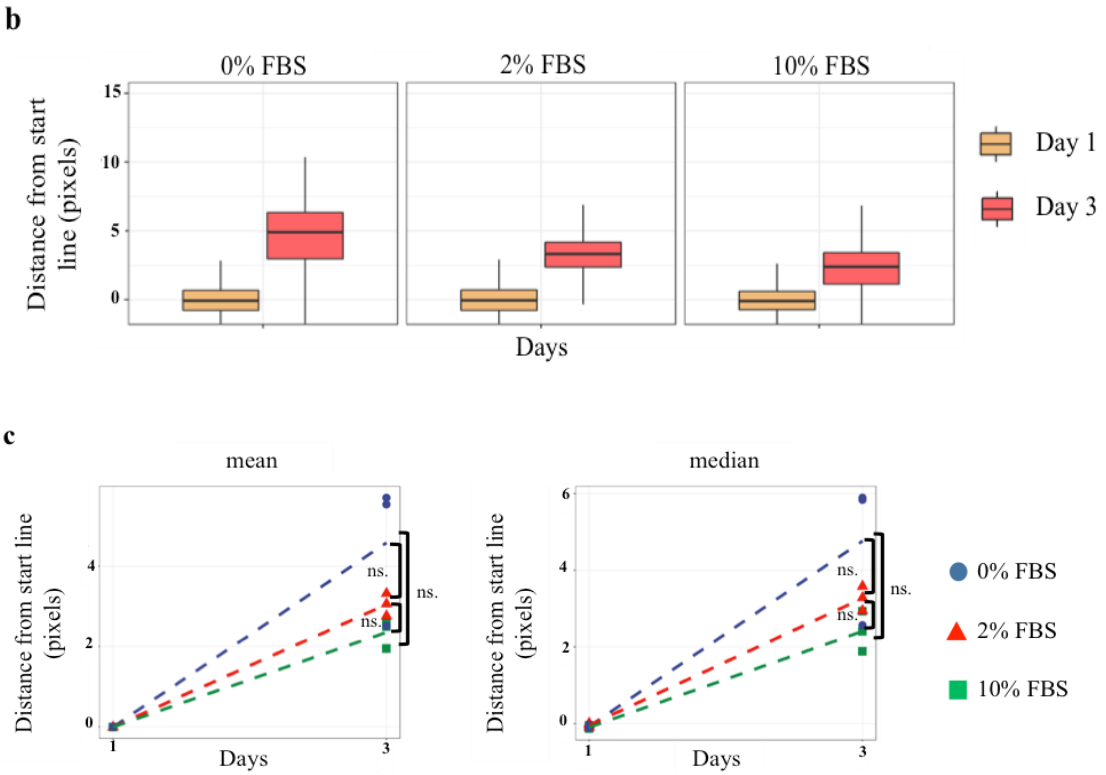

Figure 4.12. Invasion of MDAMB231 cells towards liver microenvironment in the presence or absence of serum. Representative Z-stack images showing invasion of MDAMB231 cells (red) towards a) liver environment generated by BRL3A with different serum concentrations (0, 2 and 10%) (dashed line corresponds to the starting line for invasion) (Scale bar: 200 µm). b) The distance of each bright pixel to the starting line (dashed) was calculated after thresholding of Z-stack images. The data normalized to day 1 were plotted (n=3). c) Mean and median values of normalized distance distributions were plotted for day 1 and day 3 (n=3). (FBS: fetal bovine serum).

BRL3A-laden GFR-Matrigel was formed in HMC and cell culture medium having 0%, 2% and 10% FBS was loaded into MC2. DsRed-labeled MDAMB231 cells were added into MC1 and their invasion towards generated liver microenvironment was observed for 3 days (Figure 4.12). An obvious increase in the invasion of MDAMB231 cells was shown by the quantitative analysis of fluorescence images for all three FBS concentrations from Day 1 to Day 3 (Figure 4.12a). Moreover, it was revealed that there were no significant differences in the invasion of MDAMB231 cells for different serum concentrations when homing cells were present in HMC (Figure 4.12b,c). There were also no significant differences in the mean and median distances invaded by

MDAMB231 cells in all three conditions (Figure 4.12c). Therefore, these results showed that the presence of homing cells, such as BRL3A in HMC, promoted invasion and chemotaxis of MDAMB231 cells towards modeled homing microenvironments.

In addition to invasion assay, the differences in the mRNA expression profiles of CXCL12, CCL5 and IGF1 chemokines were analyzed in homing stromal cells cultured in 3D with 0%, 2% and 10% FBS concentrations. BRL3A and WI38 cells were seeded into GFR-Matrigel with the concentrations of $1x10^7$ cells/ml and $5x10^6$ cells/ml, respectively. They were then isolated from the 3D environment at Day 3 and their mRNA levels were examined.

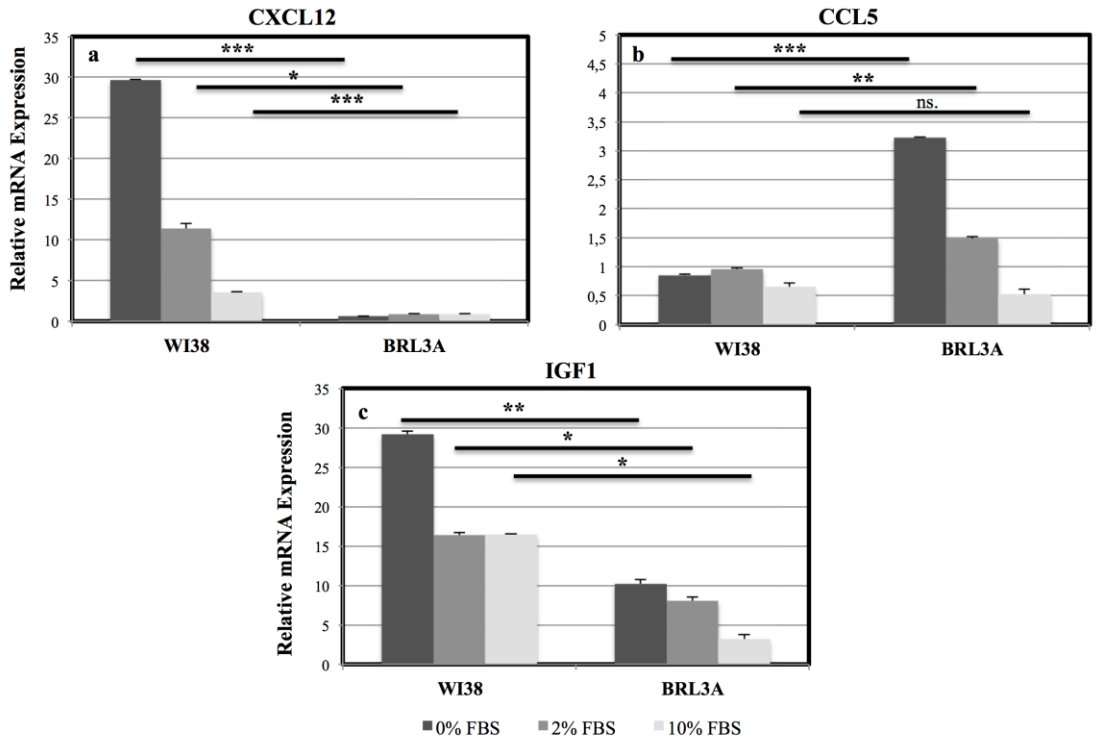

Figure 4.13. The effects of different serum concentrations on the expression of chemokines secreted from stromal cells in 3D culture. The mRNA expression patterns of a) CXCL12 , b) CCL5 and c) IGF1 in WI38 and BRL3A cell line. The relative expression levels show the mean ± standard deviation for three independent experiments. *$p \leq 0.05$; **$p \leq 0.01$; *** $p \leq 0.005$.

The expression levels of CXCL12 and IGF1 chemokines in WI38 cells and CCL5 chemokine in BRL3A cells were significantly higher when the cells cultured in serum-free conditions compared to those cultured in 2% and 10% serum concentrations (Figure 4.13).

Overall, serum-free DMEM media was determined to use in MC2 for further invasion and extravasation experiments with cell-laden hydrogels in HMC.

4.4.3. Invasion of Lung and Bone Metastatic Clones into Lung Microenvironment

The lungs are the most prevalent sites for the distant metastases of breast cancer especially for TNBC subtype of breast cancer. In recent years, 57-77% of breast cancer patients have been found to have lung metastases (Andy et al., 2005). Therefore, the invasive potential of MDAMB231 cells and its bone- and lung- specific (MDAMB231 BoM 1833 and MDAMB231 LM2, respectively) metastatic clones towards lung microenvironment generated in IC-chip, was investigated. WI38-laden GFR-Matrigel was formed in HMC and serum-free medium was loaded into MC2. DsRed-labeled parental MDAMB231, bone- or lung-specific metastatic clones were added to MC1 in serum-free medium. A remarkable increase in the invasion potentials of both parental and lung-specific (LM2) MDAMB231 cells was observed, while bone-specific (BoM 1833) cells invaded slightly towards generated lung microenvironment as expected (Figure 4.14a,b). The mean and median distances invaded by parental MDAMB231 cells and lung-specific metastatic LM2 cells were significantly higher compared to bone-specific metastatic BoM 1833 cells (Figure 4.14c), while there were no significant differences in the invasion of MDAMB231 and LM2 cells towards WI38-laden lung microenvironment. These data demonstrated that the *in vitro* lung microenvironment generated by WI38 lung fibroblasts embedded within GFR-Matrigel successfully mimicked the homing lung microenvironment to model *in vivo* behaviors of breast cancer cells.

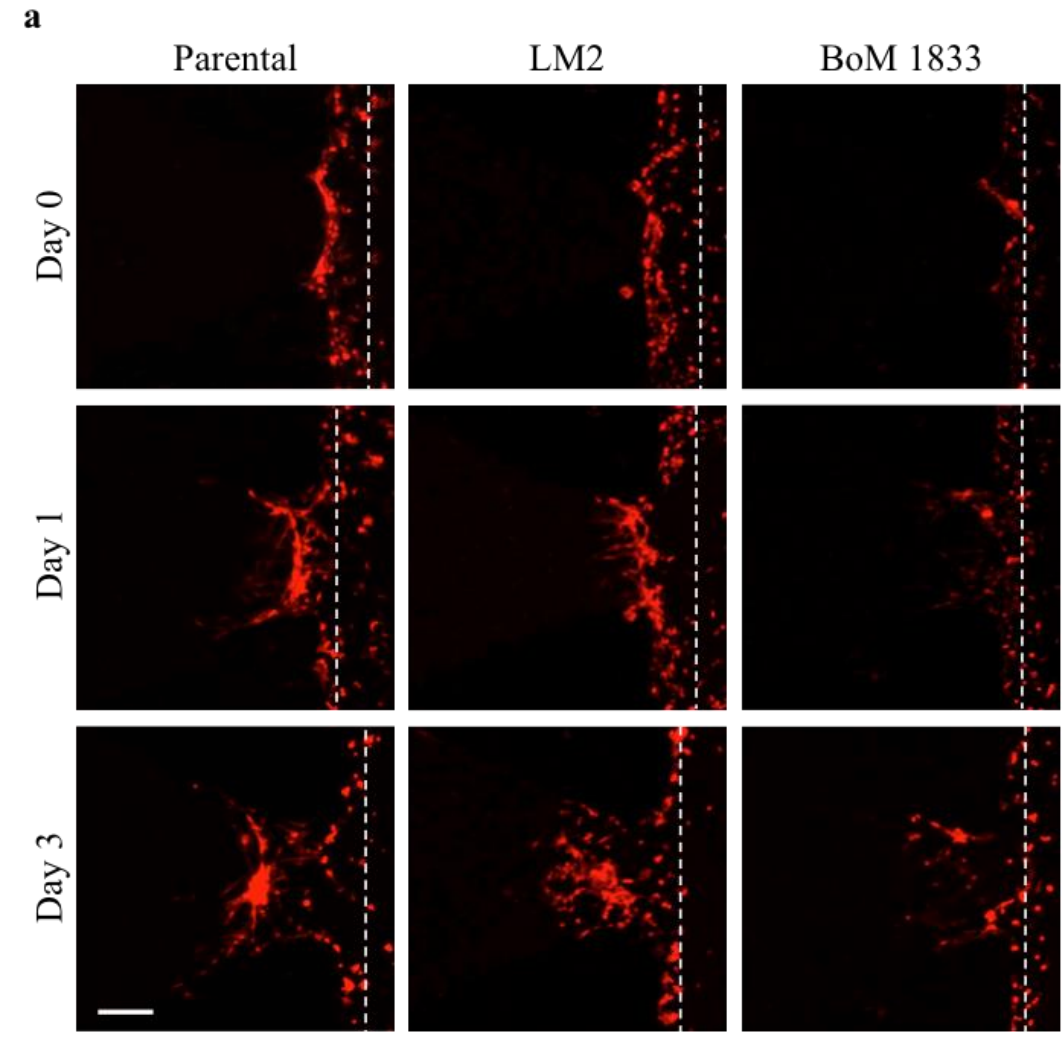
a
Parental
LM2
BoM 1833
Day 0
Day 1
Day 3
b
Parental
LM2
BoM 1833
Distance from start line (pixels)
4
2
0
Day 1
Day 3

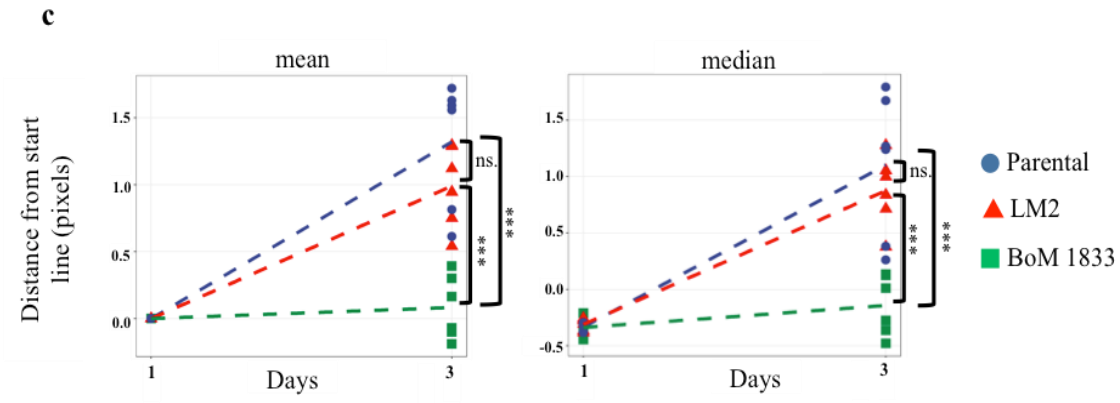

Figure 4.14. Invasion of lung-specific and bone-specific MDAMB231 clones towards the lung microenvironment. a) Representative Z-stack images showing invasion of parental, LM2 (lung-specific) and BoM 1833 (bone-specific) MDA-MB-231 cells (red) towards the lung microenvironment generated by WI38 cell line (dashed line corresponds to the starting line for invasion) (Scale bar: 200 μm). b) The distance of each bright pixel to the starting line (dashed) was calculated after thresholding of Z-stack images. The data normalized to day 1 were plotted (n=3). c) Mean and median values of normalized distance distributions were plotted for day 1 and day 3 (n=3). ***$p \leq 0.005$.

4.4.4. Invasion of Metastatic and Non-metastatic Breast Cancer Cells

Invasion capacity of metastatic MDAMB231 and non-metastatic MCF7 cells towards lung, liver, bone and breast microenvironments generated by WI38, BRL3A, HS5 and MCF10A cell lines embedded in GFR- matrigel in the HMC, respectively, was investigated. A clear increase in the mean and median distances invaded by MDAMB231 cells towards all microenvironments was observed from Day 1 to Day 3 (Figure 4.15c). The invasion potential of MDAMB231 cells towards lung and liver microenvironments was significantly higher compared to bone and breast microenvironments (Figure 4.15a-c) while MCF7 cells did not show a significant invasion to neither environment up to 3 days (Figure 4.15d-f) which was confirmed by the mean and median distances invaded by non-metastatic MCF7 breast cancer cells.

Altogether these results demonstrated that MDAMB231 breast cancer cells had a higher preference of invasion towards lung and liver microenvironments than the breast and bone microenvironments, expectedly whereas MCF7 breast cancer cells had no preference for different homing microenvironments. However, although bone-specific metastasis potential of MDAMB231 cells was determined in several studies, the invasion of MDAMB231 cells towards bone microenvironment generated by HS5 cells embedded in GFR-matrigel was quite limited (Figure 4.15a).

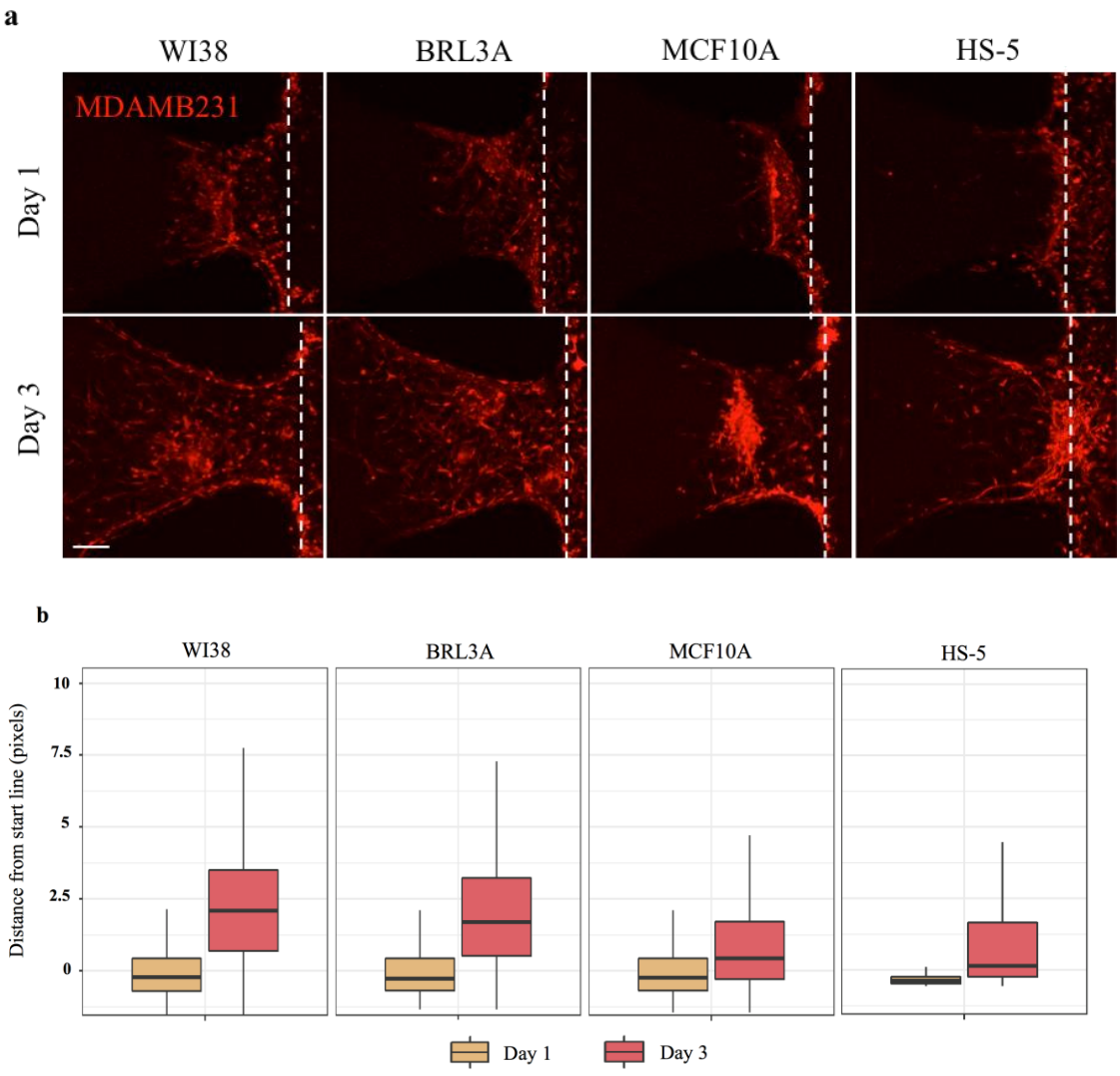

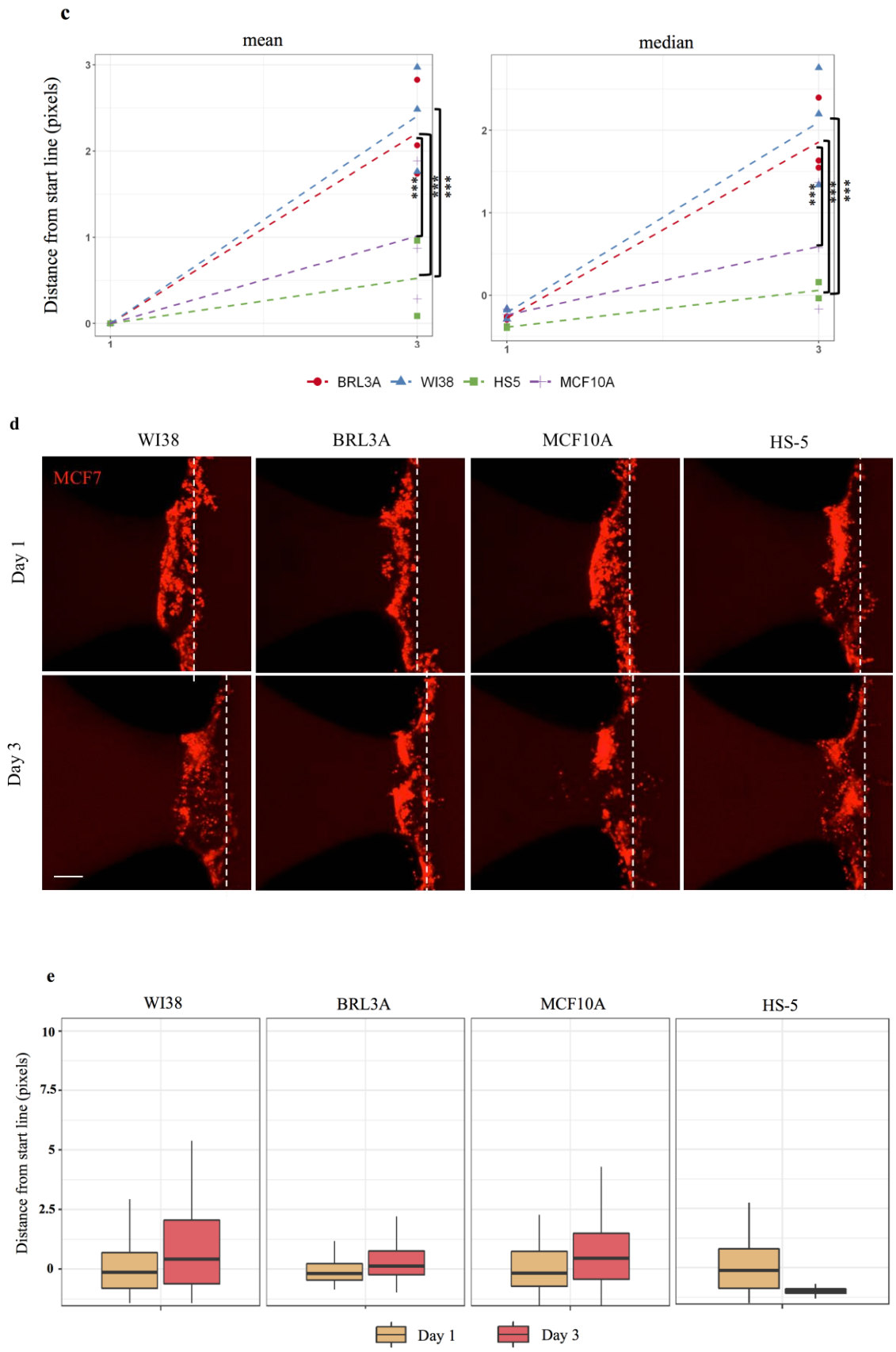
c
mean
median
Distance from start line (pixels)
***
BRL3A
WI38
HS5
MCF10A
d
WI38
BRL3A
MCF10A
HS-5
MCF7
Day 1
Day 3
e
WI38
BRL3A
MCF10A
HS-5
Distance from start line (pixels)
Day 1
Day 3

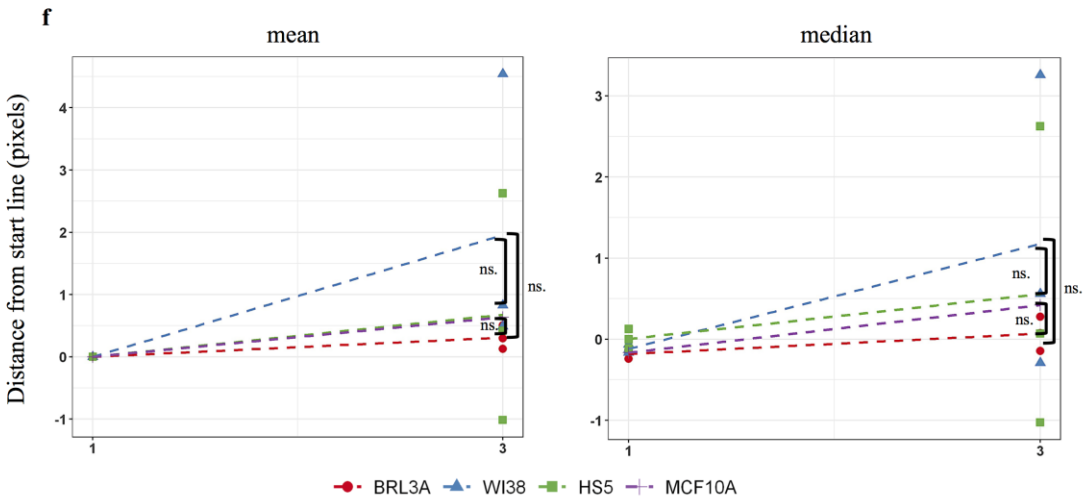

Figure 4.15. Invasion of metastatic (MDAMB231) and non- metastatic (MCF7) breast cancer cells towards lung, liver, breast and bone microenvironments. a, d) Representative Z-stack images showing invasion of MDAMB231 and MCF7 cells (red) towards lung, liver, breast and bone microenvironments generated by WI38, BRL3A, MCF10A and HS5 cell lines, respectively. (dashed line corresponds to the starting line for invasion) (Scale bar: 200 µm). b, e) The distance of each bright pixel to the starting line (dashed) was calculated after thresholding of Z-stack images. The data normalized to day 1 were plotted (n=9). c, f) Mean and median values of normalized distance distributions were plotted for day 1 and day 3 (n=9). ***p ≤ 0.005.

4.5. Optimization of Bone Microenvironment

4.5.1. Optimization of Cellular Milieu

The bone tissue includes various cell types, bone-specific cells (osteoblasts and osteoclasts), mesenchymal stem cells, immune cells and fibroblasts constituting the bone homeostasis together with the mechanical stimuli (stiffness and topography) (Buenrostro, Mulcrone, Owens, & Sterling, 2016) . That is why, cellular composition is one of the key regulators for generation more realistic 3D bone microenvironments. Therefore, different cell lines that represent *in vivo* bone cellular milieu were tested to simulate *in vivo* bone microenvironment conditions.

hFOB 1.19 is conditionally immortalized cell line with a temperature sensitive mutant of SV40 large T antigen gene. hFOB human-derived osteoblast cells proliferate rapidly at 33.5^0C while they differentiate into mature osteoblasts and exhibit osteoblast phenotype at 39^0C (Harris, Enger, Riggs, & Spelsberg, 1995). SaOs-2 cells, despite being osteosarcoma cell line, are commonly used in bone tissue engineering applications as they display osteoblastic properties (Bique, Kaivosoja, Mikkonen, & Paulasto-Kröckel, 2016). D1 ORL UVA is a mouse-derived bone marrow mesenchymal stem cell line that can differentiate into osteocytes with appropriate stimuli and commonly used for *in vitro* bone tissue engineering (Bertassoli et al., 2013). These three different cell lines together with HS-5 bone fibroblast cells were used to mimic bone microenvironment in HMC of IC-chips. Each cell line, individually or in combination, was seeded into HMC of LOC system and the invasion of MDAMB231 cells was examined towards the generated microenvironments.

The invasion of MDAMB231 cells was higher towards hFOB-laden bone microenvironment compared to other bone microenvironments generated by HS-5, SaOs-2 or D1 cells (Figure 4.16a) which was also confirmed by the significant increase in the mean and median distances invaded by MDAMB231 cells towards hFOB-laden microenvironment. In addition to individual cell seeding into GFR-Matrigel, the combinations of cells were used for bone microenvironment generation. As the cancer cell invasion was higher towards hFOB-laden environment, the co-culture of hFOB cells with D1, Saos-2 and HS5 cells was performed and the effects of these co-culturing on the invasiveness of MDAMB231, were assessed. Although the presence of hFOB cells increased the invasion of MDAMB231 cells towards hydrogels formed by co-cultures, there were no significant differences between hFOB-laden and co-culture-laden hydrogels (Figure 4.16b), while more significant increase in the invasion of MDAMB231 breast cancer cells was observed towards hFOB+HS5-laden bone microenvironment.

Altogether, these results revealed that the invasion of MDAMB231 cells was evidently affected by different homing microenvironments formed by a variety of cell lines even though they are originated from the same biological tissue. Therefore, hFOB osteoblast cells were decided to use for bone microenvironment generation together with HS5 fibroblast cells.

Besides osteoblast cells, osteoclast cells are also important to maintain the homeostasis of bone tissue through reformation and resorption processes, respectively. The origin of osteoclasts is known to be hematopoietic cells from the mononuclear lineage and their differentiation into osteoclasts is mainly dependent on growth factors secreted from osteoblasts (Borciani et al., 2020). Therefore, to mimic the cellular milieu of native bone microenvironment, human monocytic cell line, U937, which serves as a osteoclast precursor cell source (Sieberath et al., 2020), was used together with hFOB and HS5 osteoblast and fibroblast cell lines.

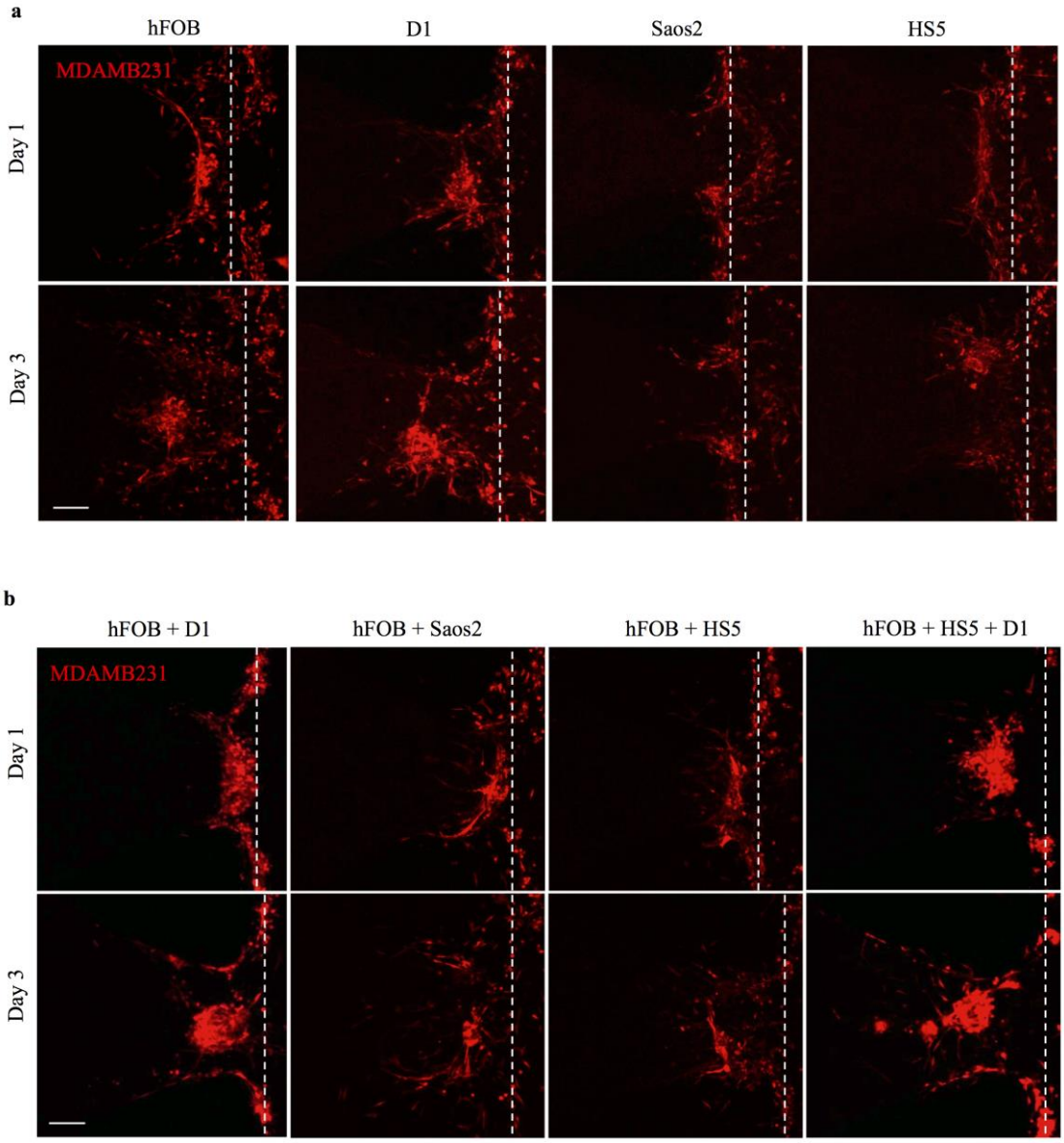

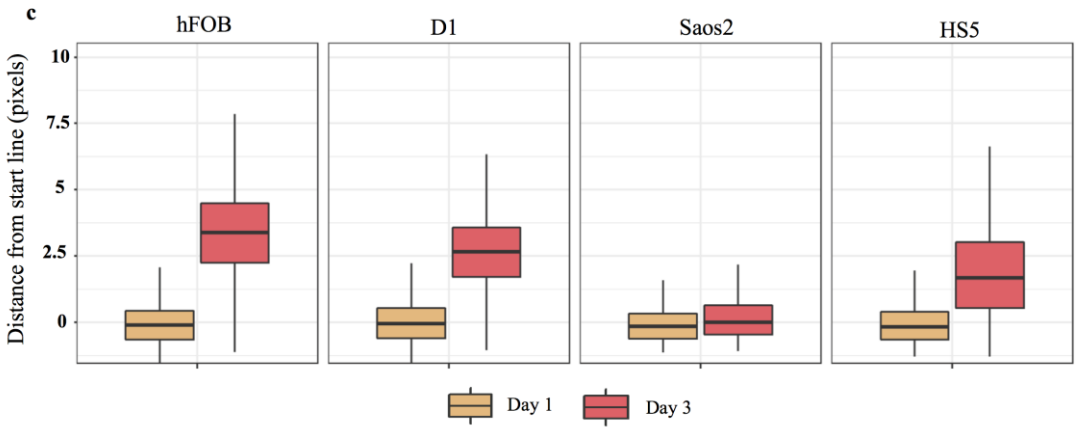
c
hFOB
D1
Saos2
HS5
Distance from start line (pixels)
10
7.5
5
2.5
0
Day 1
Day 3

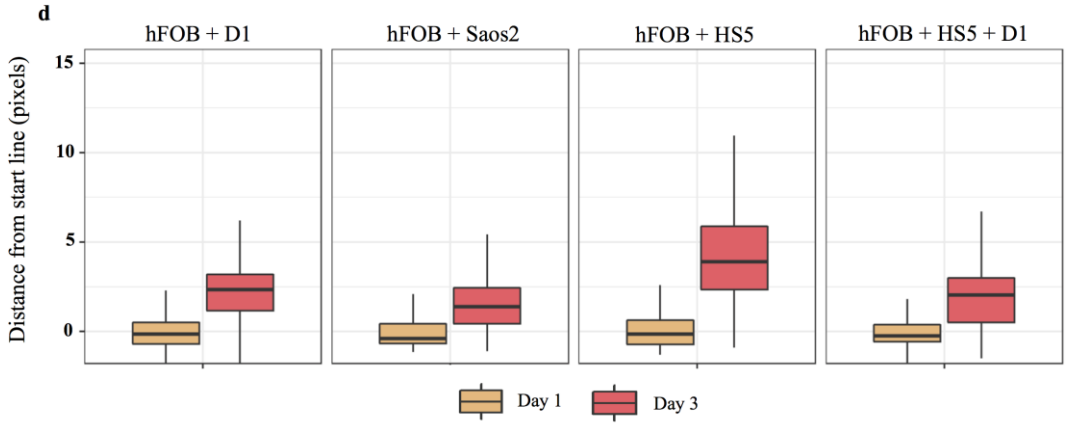
d
hFOB + D1
hFOB + Saos2
hFOB + HS5
hFOB + HS5 + D1
Distance from start line (pixels)
15
10
5
0
Day 1
Day 3

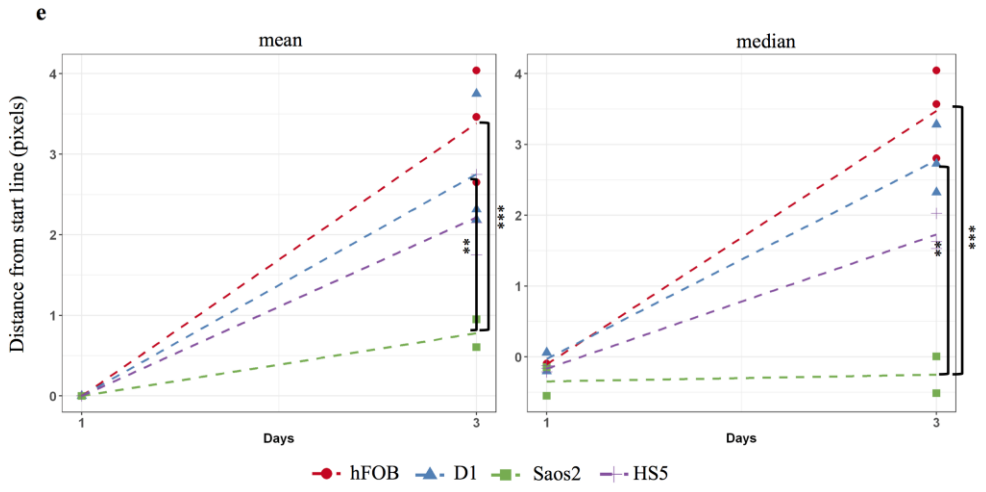
e
mean
median
Distance from start line (pixels)
Days
Days
***
**
hFOB
D1
Saos2
HS5

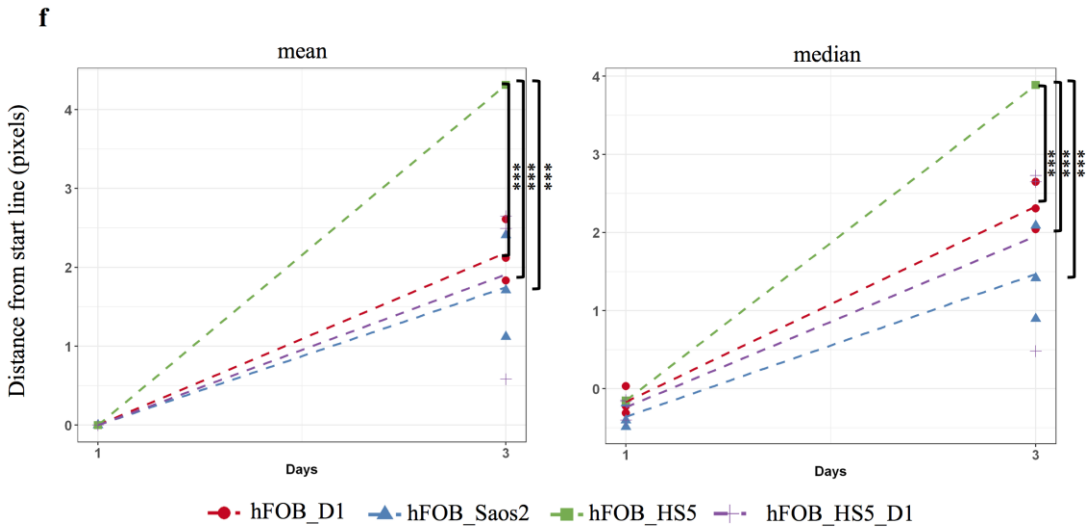

Figure 4.16. The invasion capacity of MDAMB231 cells towards the bone microenvironment. a) Representative Z-stack images showing invasion of MDAMB231 cells (red) towards the bone microenvironment towards HS5, hFOB, Saos2 and D1-laden GFR-Matrigel a) individually and b) in combination (dashed line corresponds to the starting line for invasion). (Scale bar: 100 μm) b) The distance of each bright pixel to the starting line (dashed) was calculated after thresholding of Z-stack images. The data normalized to day 1 were plotted (n=3). c) Mean and median values of normalized distance distributions were plotted for day 1 and day 3 (n=3). **p≤ 0.01, ***p ≤ 0.005.

4.5.2. Optimization of ECM Component

In 3D *in vitro* bone microenvironment modeling, it is crucial to have the engineered extracellular matrix (ECM) structure to be similar to that of native bone tissue microenvironment. The toughness, tensile stiffness and elastic properties of bone ECM are mainly supported by the organic matrix that is mostly composed of collagen I molecules (Deville & Cordes, 2019). That is why, the generation of ideal bone microenvironment scaffold requires the presence of type I collagen to provide the adequate mechanical properties (Dawei Zhang, Wu, Chen, & Lin, 2018) .

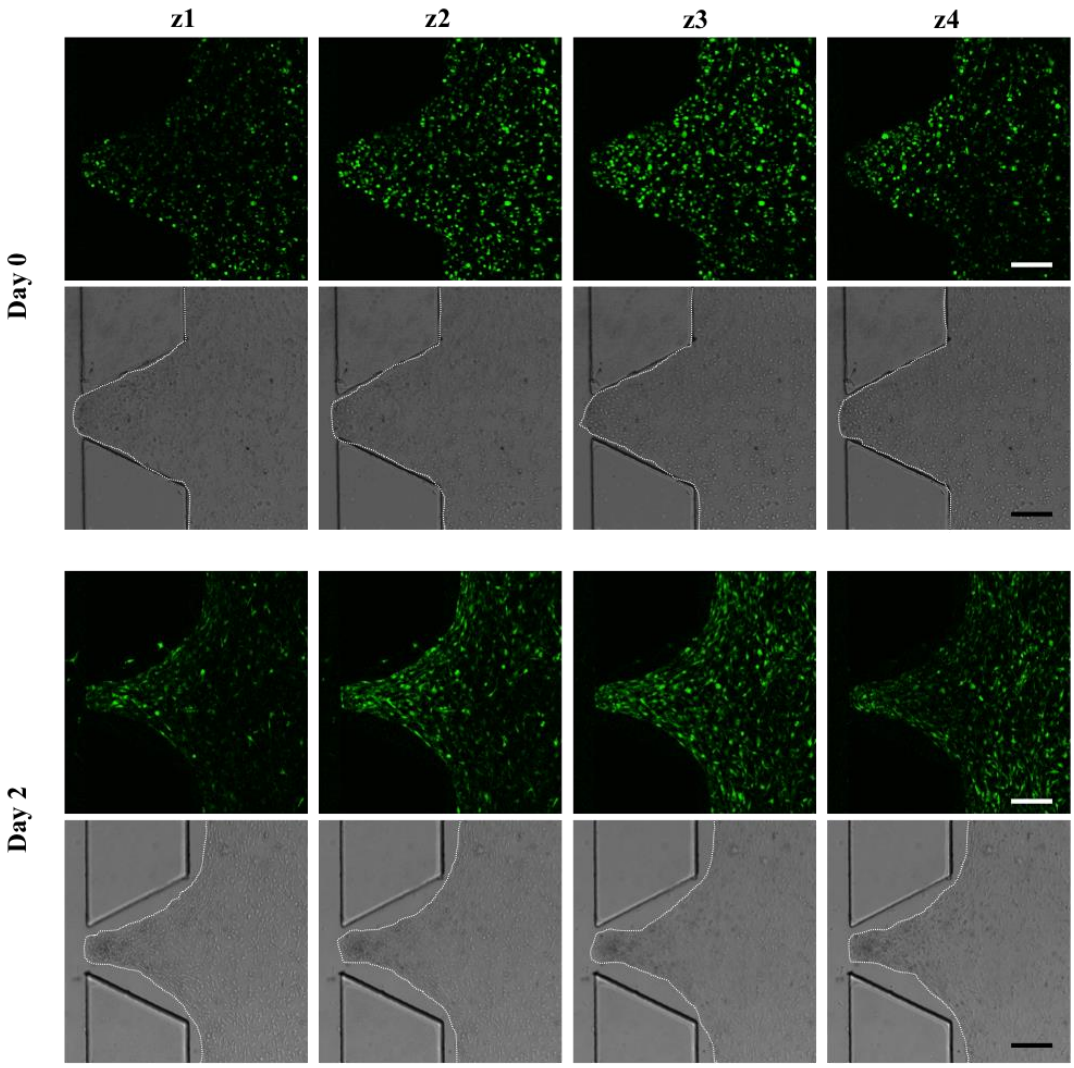

Figure 4.17. Different Z planes (z1- z4) of fluorescence and phase-contrast images of HS5 cells seeded into 2mg/ml of collagen I solution at Day 0 and Day 2. White dashed lines are representing the borders of collagen I hydrogel. Scale bar: 200 μm and between planes: 30 μm.

Bone fibroblast cell line, HS5 was seeded into 2 mg/ml of collagen I and the polymerization was performed at 37°C in a humidified incubator with 5% CO_2. 2 days after the seeding of cell-laden collagen I hydrogel into HMC of IC-chips, collagen gel contraction was observed (Figure 4.17). Although collagen gel contraction is commonly studied to identify cell-induced reorganization of ECM (T. Zhang et al., 2019), it is a limiting factor for collagen-based hydrogels in tissue remodeling experiments.

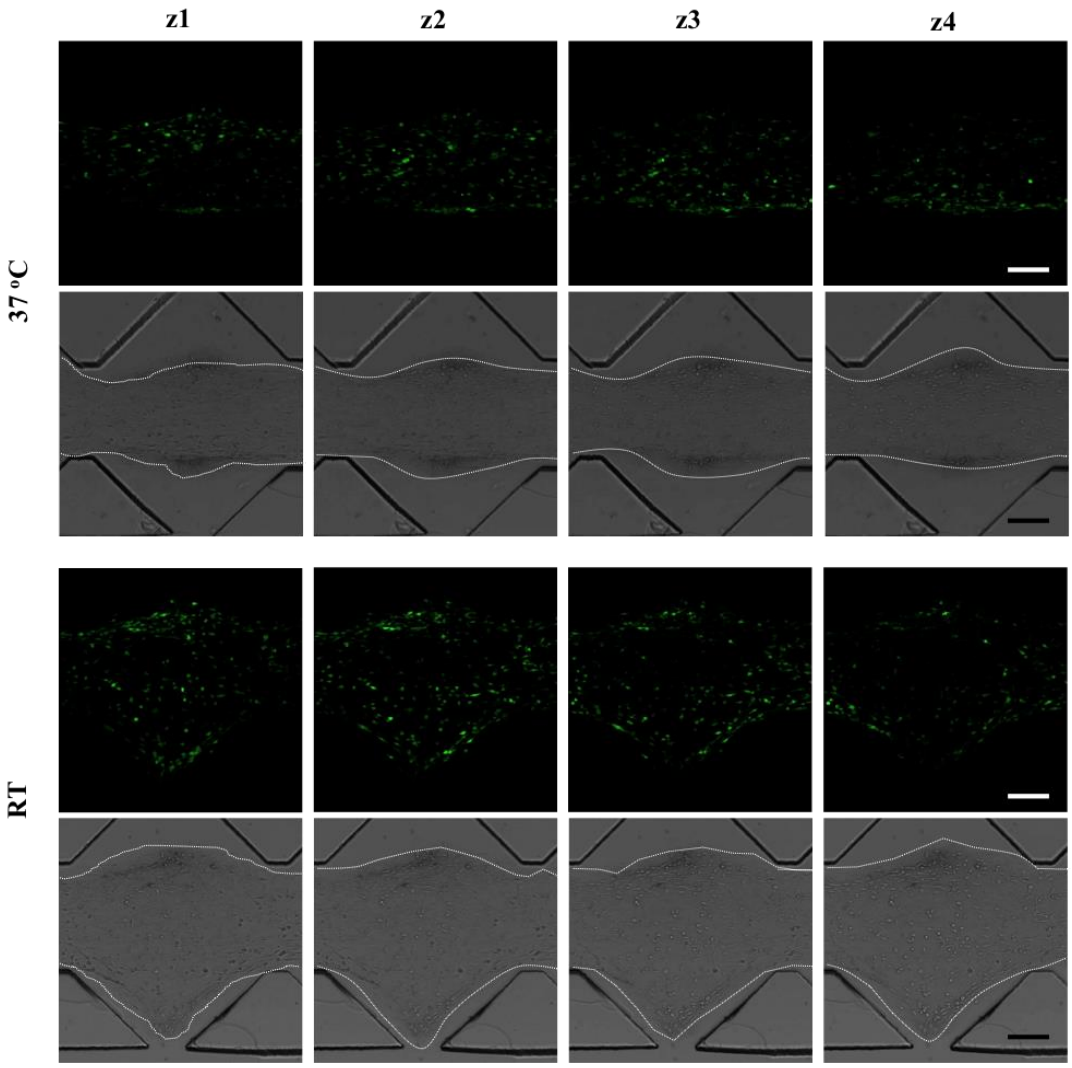

Figure 4.18. Different Z planes (z1- z4) of fluorescence and phase-contrast images of HS5 cells seeded into 2mg/ml of collagen I solution and polymerized either at 37^0C or RT at Day 2. White dashed lines are representing the borders of collagen I hydrogel. Scale bar: 200 μm and between planes: 30 μm.

The collagen gel contraction observed at Day 2, restricted the interaction of cancer cells with the stromal cells which might affect the invasiveness of cancer cells towards generated bone microenvironment. Thus, to prevent the formation of collagen gel contraction, the polymerization was also performed at RT in laminar flow cabin with the same collagen I concentration. The gel contraction was again detected at Day 2 after the first seeding, but in contrast to polymerization at 37°C, it was slightly less (Figure 4.18).

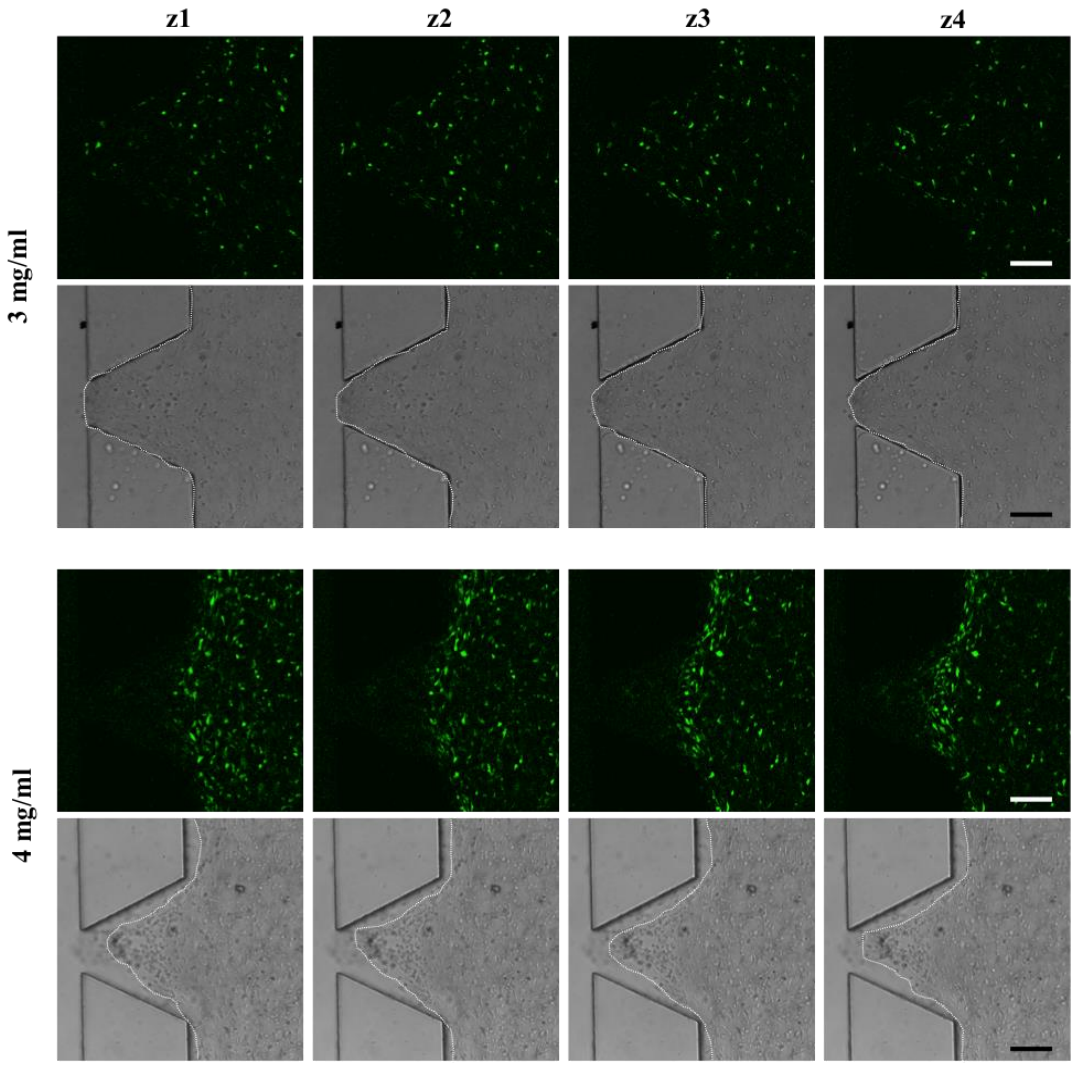

Figure 4.19. Different Z planes (z1- z4) of fluorescence and phase-contrast images of HS5 cells seeded either into 3mg/ml or 4mg/ml of collagen I solution and polymerized at RT at Day 2. White dashed lines are representing the borders of collagen I hydrogel. Scale bar: 200 μm and between planes: 30 μm.

In addition to polymerization temperature, different concentrations of collagen I was tested to evaluate the effect of concentration on the gel contraction. 3mg/ml and 4mg/ml of collagen I solution was used and polymerization was performed at RT. As nicely observed in Figure 4.18, there was no gel contraction of the hydrogel formed by 3mg/ml collagen I, while a compressed cell-laden collagen gel was evidently seen with 4mg/ml collagen I (Figure 4.19).

Overall, these results showed that both polymerization temperature and collagen I concentration are contributing to the gel contraction. As a result, 3mg/ml of collagen I and RT polymerization were determined to be used for the formation of cell-laden collagen I hydrogels for further experiments.

Beside protein-based scaffolds, polymer-based scaffolds from non-mammalian origin are widely used in 3D *in vitro* bone microenvironment modeling (Turnbull et al., 2018). Agarose is one of these polymers being frequently used for the formation of polymer-based scaffolds with its tunable mechanical properties from a few Pa to 100 kPa. Importantly, the biocompatibility and recently reported strain-stiffening properties suggest that their mechanical properties are suitable for 3D cell culture (Bertula et al., 2019). That is why, agarose with combination of collagen type I, was tested to reach the adequate tensile stiffness in the generated 3D bone microenvironments.

First, the viability of hFOB and HS5 cell lines was analyzed within agarose gels. The cells were seeded into 2 different concentrations of agarose (2% w/v (20mg/ml) and 1% w/v (10mg/ml)) and their viability was quantified for 4 days. It was revealed that there was a decline in the growth rate of both cell lines compared to their 2D culture controls, although they were still viable when seeded within agarose hydrogels (Figure 4.20). During the culture of viability tests, it was observed that the cells formed spheroids within agarose hydrogels as opposed to anticipated elongated fibroblast-like morphology. Thus, the effects of increasing agarose concentrations in the presence of collagen I on the morphology of bone stromal cells were tested. The cells were seeded within only collagen I (3mg/ml) and collagen I-agarose hydrogels (2.5, 5 and 10 mg/ml agarose concentration). In 2.5mg/ml agarose containing collagen I hydrogels, the morphology of the cells was similar when they were within collagen I only (Figure 4.21) However, the cells started to form spheroids within 5mg/ml and 10mg/ml agarose containing collagen I hydrogels similar to the previous observations with the agarose hydrogels that did not contain collagen I (Figure 4.21). It can be clearly stated that with increasing agarose concentration, the invasive behaviors of the cells were restricted. The most likely cause of spheroid formation may be the transition of the cells from mesenchymal to amoeboid stage within high agarose concentration thereby limiting the interaction of the cells with the matrices they are residing in.

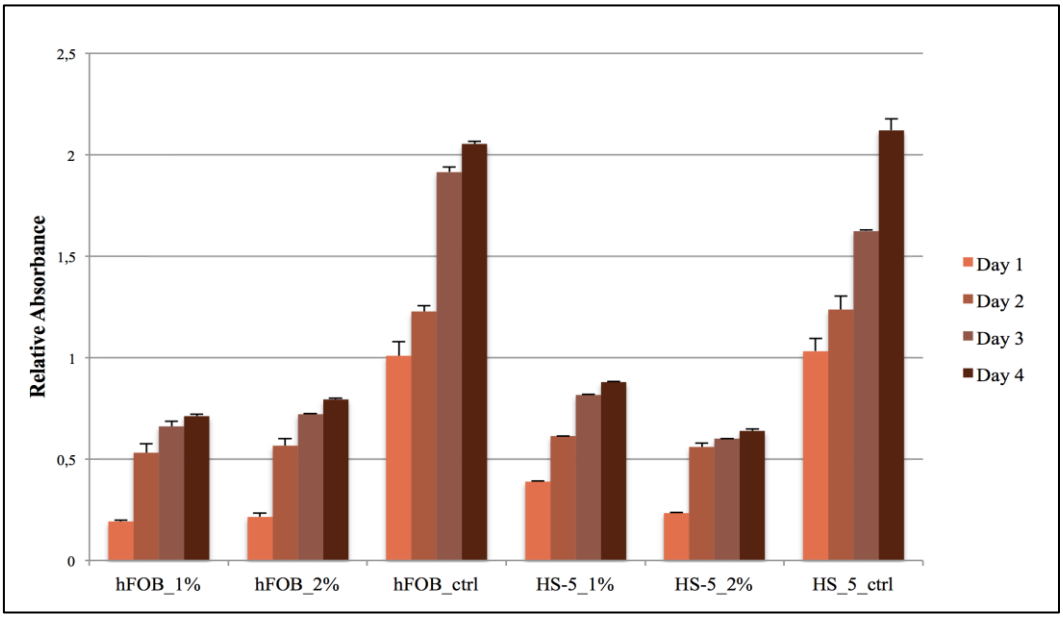

Figure 4.20. CCK8 assay for the viability of bone stromal cells in 20mg/ml (2% w/v) and 10mg/ml (1% w/v) of agarose hydrogels and for 4 days. Their 2D cell culture conditions were used as a control. The relative absorbance values show the mean ± standard deviation for three independent experiments.

As a result, the viability test and 3D culture demonstrated that 2.5mg/ml agarose as the final concentration is the maximal amount that can be used for cell-laden agarose hydrogels formation. Altogether, 3mg/ml collagen I and 2.5mg/ml agarose concentrations were determined for further generation of 3D bone microenvironments within LOC platforms.

Recent studies have revealed that matrix stiffness is a strong regulator of a variety of cellular processes including cell growth, adhesion, migration and cell fate (G. Chen, Dong, Yang, & Lv, 2015). The degree of matrix stiffness has important impacts on the diffusion of nutrients among the cells and the activation of intracellular signaling pathways via mechanotransduction mechanism (Matellan & Armando, 2019). Therefore, modulation of gel stiffness must be considered besides ECM components and cellular composition and density to obtain a more physiologically relevant 3D bone microenvironment.

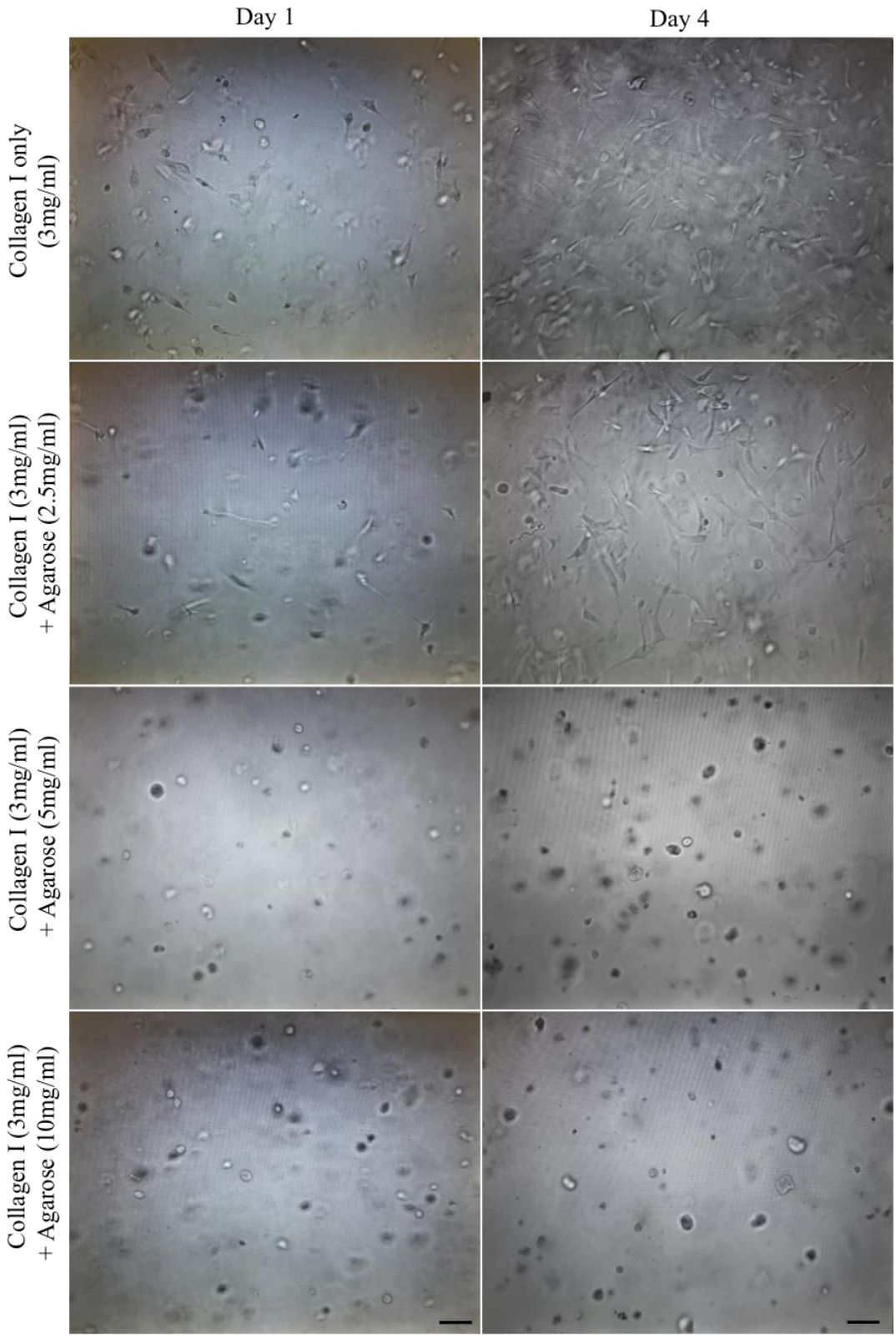

Figure 4.21. The phase-contrast images of bone fibroblast cells seeded into collagen I only (3mg/ml) and collagen I (3mg/ml) and agarose (2.5, 5 and 10 mg/ml) hydrogels at Day 1 and Day 4. Scale bar: 100 μm.

The mechanical behavior of gels is often studied using oscillatory rheological measurements. Accordingly, here the stiffness of the hydrogels having 3mg/ml collagen I, 2.5 mg/ml agarose and their combinations with or without fibroblast cells was determined at 37 ^{o}C. Strain stiffening was observed as an increase of storage modulus (*G′*) in all combinations. The stiffness of the gels having both collagen I and agarose was higher compared with hydrogels containing either only agarose or only collagen I. Furthermore, the stiffness was much higher when the cells were present within the gels compared to native gels. The average values for stiffness of the gels were 102.05 Pa and 46.2 Pa for collagen I and agarose, respectively. In the presence of cell, the stiffness values were 174.05 Pa and 73.85 Pa, respectively for collagen I and agarose. The collagen I and agarose combination displayed stiffness values of 254.5 Pa and 261.2 Pa without and with cells, respectively. Figure 4.22 shows the time sweep rheological measurement of the gels without (Figure 4.22a) and with cells (Figure 4.22b). All compositions show storage modulus (G′) is higher than loss modulus (G′′) suggesting their gel like behavior. More importantly, the gels remained stable through the experimental conditions.

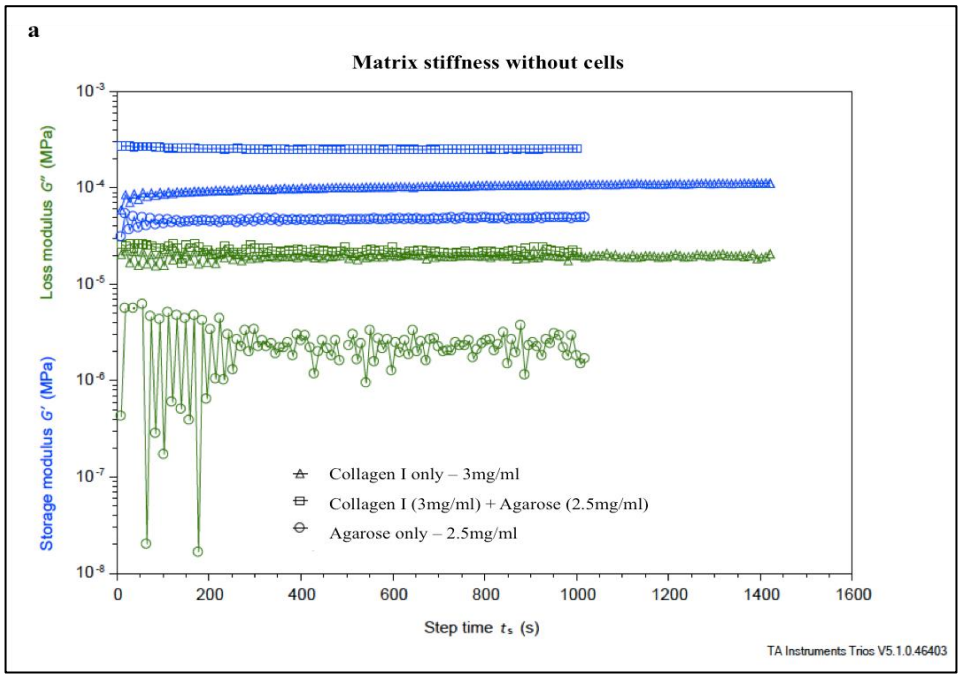

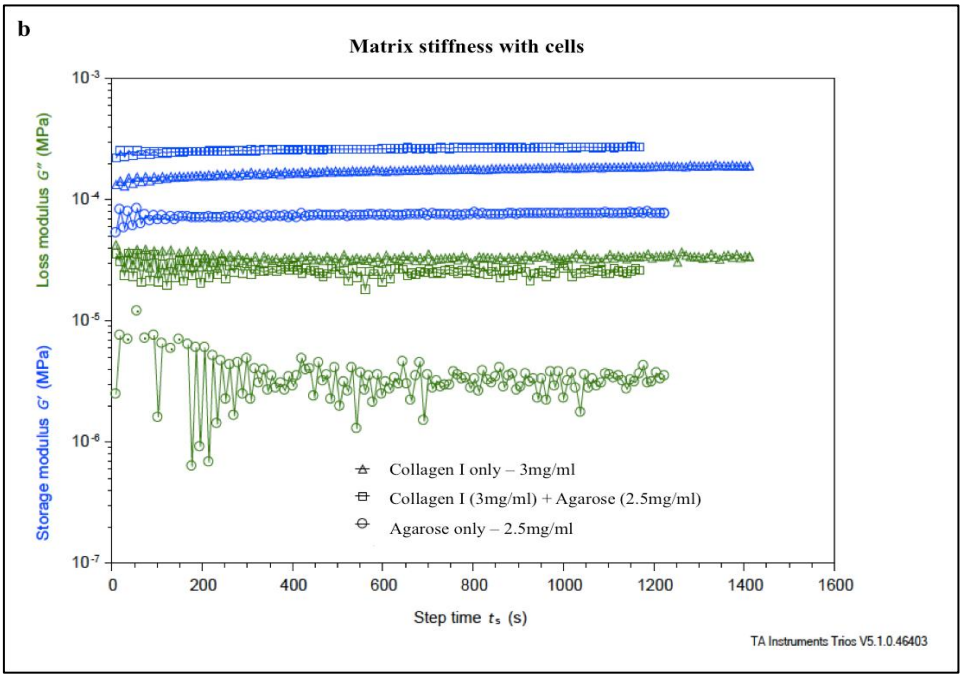

Figure 4.22. Time sweep oscillatory rheology measurements of hydrogels having only agarose (2.5mg/ml), only collagen I (3mg/ml) and agarose+collagen I (2.5mg/ml + 3mg/ml) combinations (a) without cells and (b) with cells.

The stiffness, which is expressed as the storage moduli, of native bone structures can vary from 0.1 kPa to 40-50 kPa depending on the amount of mineralization as well as cellular and matrix compositions (Pellowe & Gonzalez, 2016; M. Sun et al., 2018). Therefore, being as a polymer-based scaffold from non-mammalian origin, chitosan is also a widely used polysaccharide applied to several applications especially in bone remodeling and regeneration (Rodríguez-Vázquez, Vega-Ruiz, Ramos-Zúñiga, Saldaña-Koppel, & Quiñones-Olvera, 2015). That is why, to increase the stiffness of the generated 3D bone microenvironment, chitosan polysaccharide together within collagen type I was used.

Initially, the morphology of the hFOB cells was visualized to observe whether they form spheroids when cultured within chitosan. The hFOB cells with the concentration of $5x10^6$ cells/ml were seeded in collagen I only and collagen I + chitosan hydrogels and the morphology of the cells were visualized on Day 1 and Day 4. Unlike agarose, even the high concentration of chitosan did not cause spheroid formation by hFOB cells (Figure 4.23).

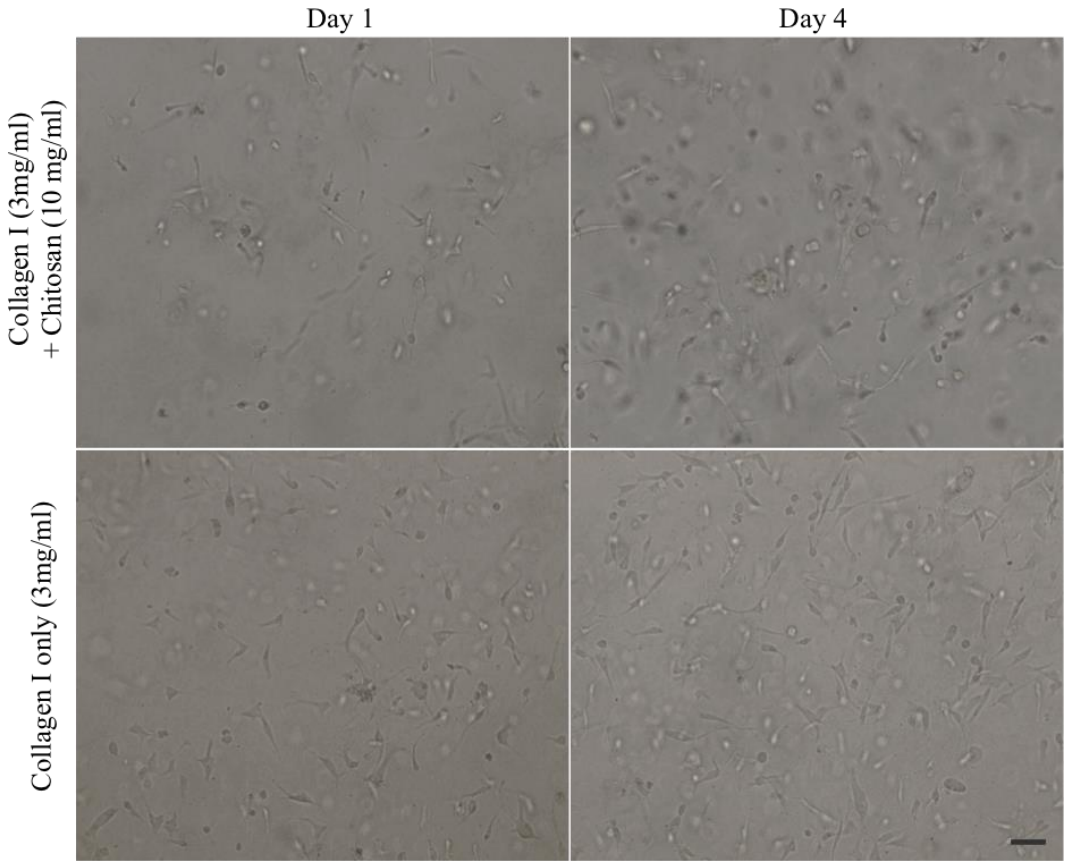

Figure 4.23. The phase-contrast images of osteoblast cells (hFOB) seeded into collagen I only (3mg/ml) and collagen I (3mg/ml) and chitosan (10 mg/ml) hydrogels on Day 1 and Day 4. Scale bar: 100 μm.

The viability of U937 and hFOB cell lines was then analyzed within chitosan (10mg/ml) and agarose (2.5mg/ml) hydrogels combined with collagen I (3mg/ml) for 4 days. It was observed that the growth rate of the cells seeded into different hydrogels was largely lower compared to those cultured in 2D (Figure 4.24). However, the growth trend of each cell line was similar in every hydrogel condition. The lower values obtained from hydrogel conditions might be caused by a diffusion problem of MTT dye into the hydrogels. Therefore, to obtain a more reasonable result for the viability of the cells, LiveDead assay was conducted for the same hydrogel conditions as for MTT assay.

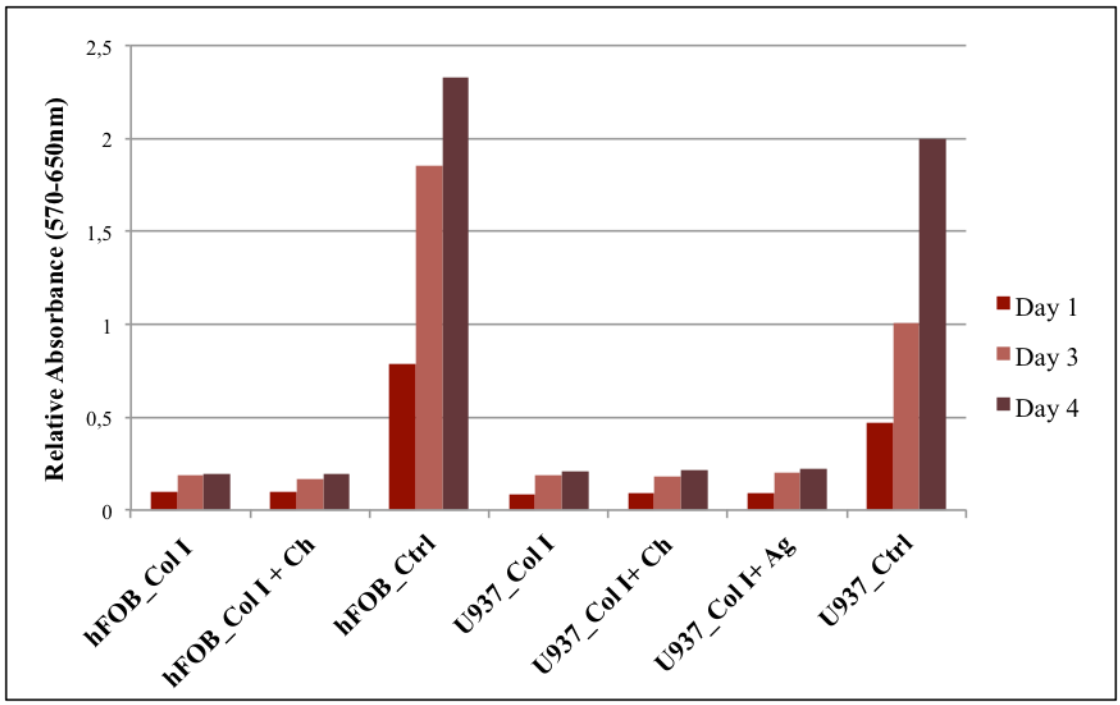

Figure 4.24. MTT assay was performed to detect the viability of hFOB and U937 cell lines within different hydrogels. The viability of hFOB cells within collagen I only and collagen I+chitosan hydrogels and U937 cells within collagen I only, collagen I+agarose and collagen I+chitosan hydrogels for 4 days.

Nuclei of all the cells (blue) and nuclei of the dead cells (green) were visualized by confocal microscope and the viability of the cells was then calculated as the percentage of viable cells (Figure 4.25). It was revealed both by 3D images and their quantification, the viability of both cells were evidently lower when the cells were within collagen I+agarose hydrogels. The viability of U937 cells was 78.8% in collagen I+agarose hydrogel, while it was 93.9% and 95.2% in collagen I+chitosan and collagen I only hydrogels respectively. The similar decrease was observed in the viability of hFOB cells cultured in collagen I+agarose hydrogels in comparison of other hydrogel conditions. The viability of hFOB cells was 65.4% in collagen I+agarose hydrogel, 79.4% in collagen I+chitosan hydrogel and 82.7% in collagen I only hydrogels (Figure 4.26).

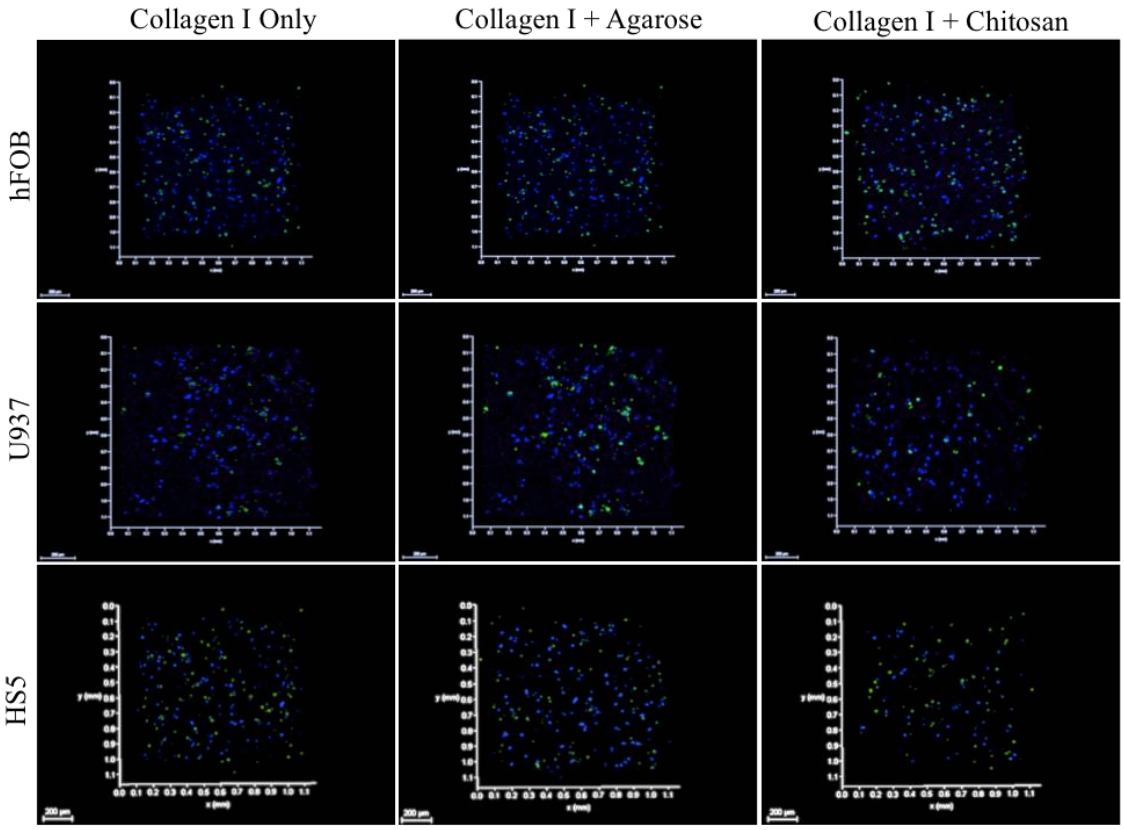

Figure 4.25. 3D merge images of hFOB, U937 and HS5 cell lines within collagen I only, collagen I+agarose and collagen I+chitosan hydrogels on Day 3. Blue: Live reagent showing the staining for nuclei of all cells, Green: Dead reagent, showing the staining for nuclei of dead cells. Scale bar: 200 μm.

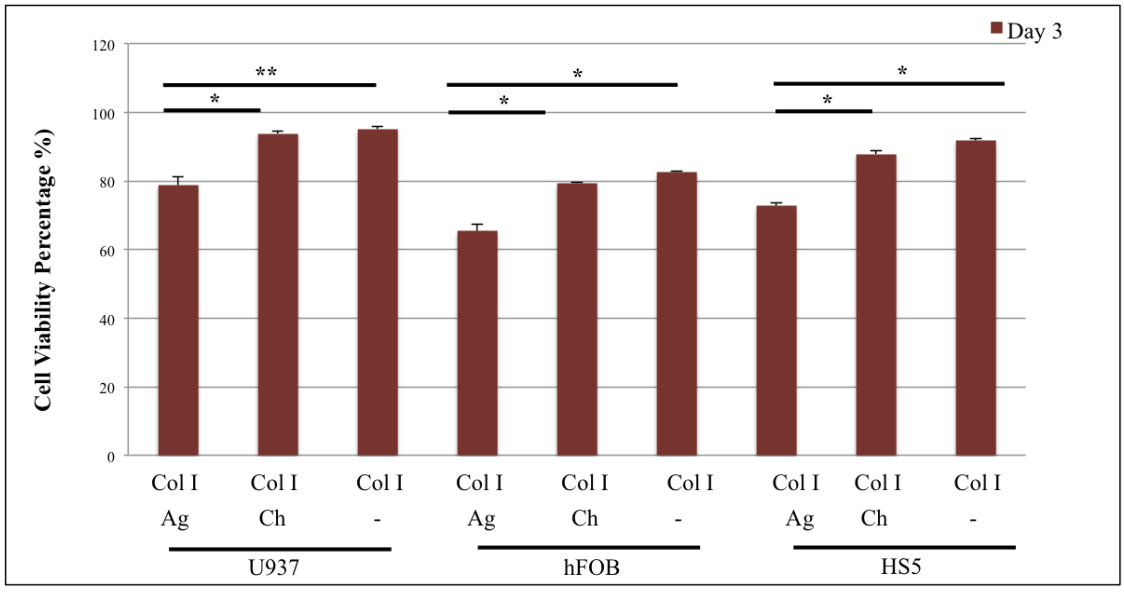

Figure 4.26. Quantification of LiveDead Assay showing the viability of hFOB and U937 cell lines in collagen I only, collagen I+agarose and collagen I+chitosan hydrogels on Day 3.

Following the viability test of the cells within collagen I, collagen I + agarose and collagen I + chitosan hydrogels, the invasion capacity of bone- specific (MDAMB231 BoM 1833) and lung-specific (MDAMB231 LM2) metastasizing cells towards hFOB, HS5 and U937-laden hydrogels was analyzed (Figure 4.27). The invasion of MDAMB231 BoM 1833 cells towards cell-laden collagen I only and collagen I + chitosan hydrogels was significantly higher than cell-laden collagen I + agarose hydrogels as was demonstrated by the mean and median distances invaded by the cells (Figure 4.27c). A limited invasion was observed by MDAMB231 LM2 cells towards each hydrogel as expected, confirming that *in vitro* bone microenvironment generated by osteoblasts, fibroblasts and monocytes within collagen I individually or in combination with chitosan mimicked the homing properties of *in vivo* bone tissue and attracted breast cancer cells towards their sites.

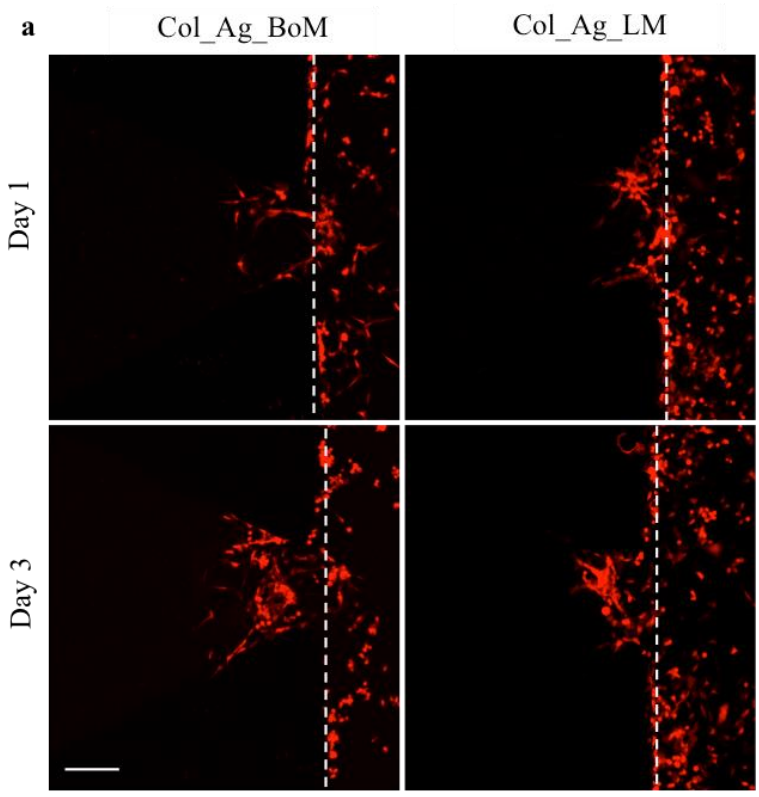

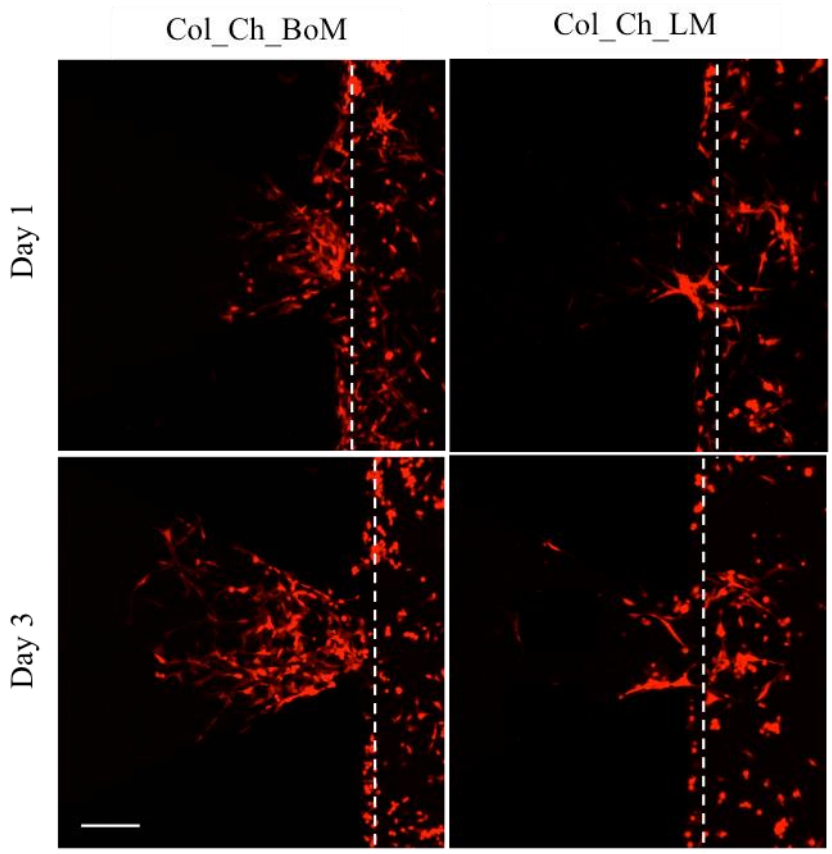
Col_Ch_BoM
Col_Ch_LM
Day 1
Day 3

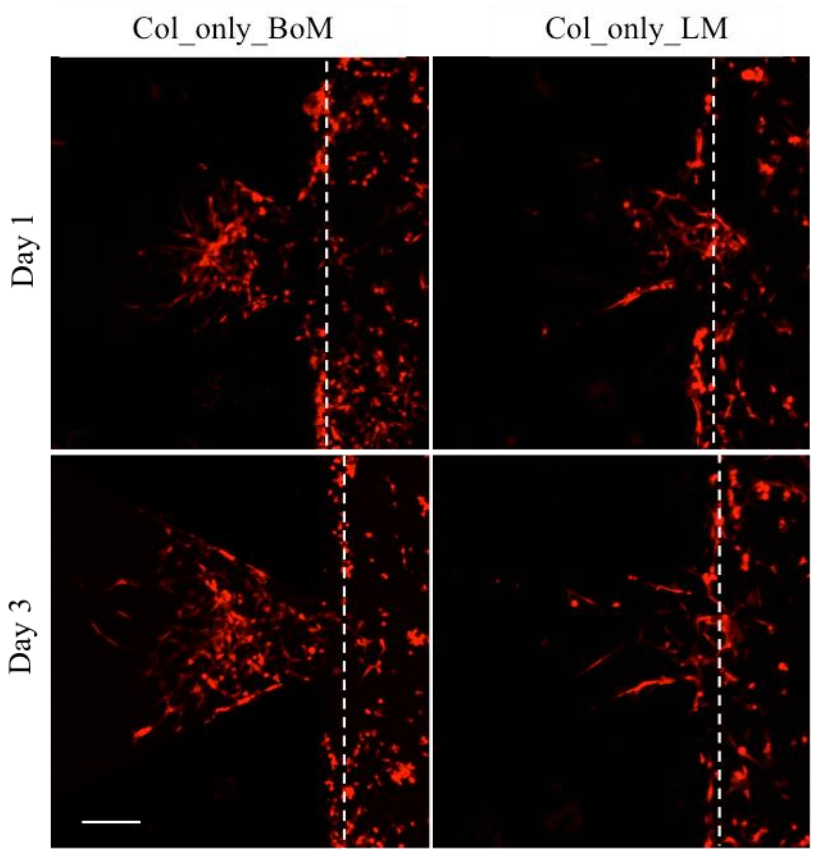
Col_only_BoM
Col_only_LM
Day 1
Day 3

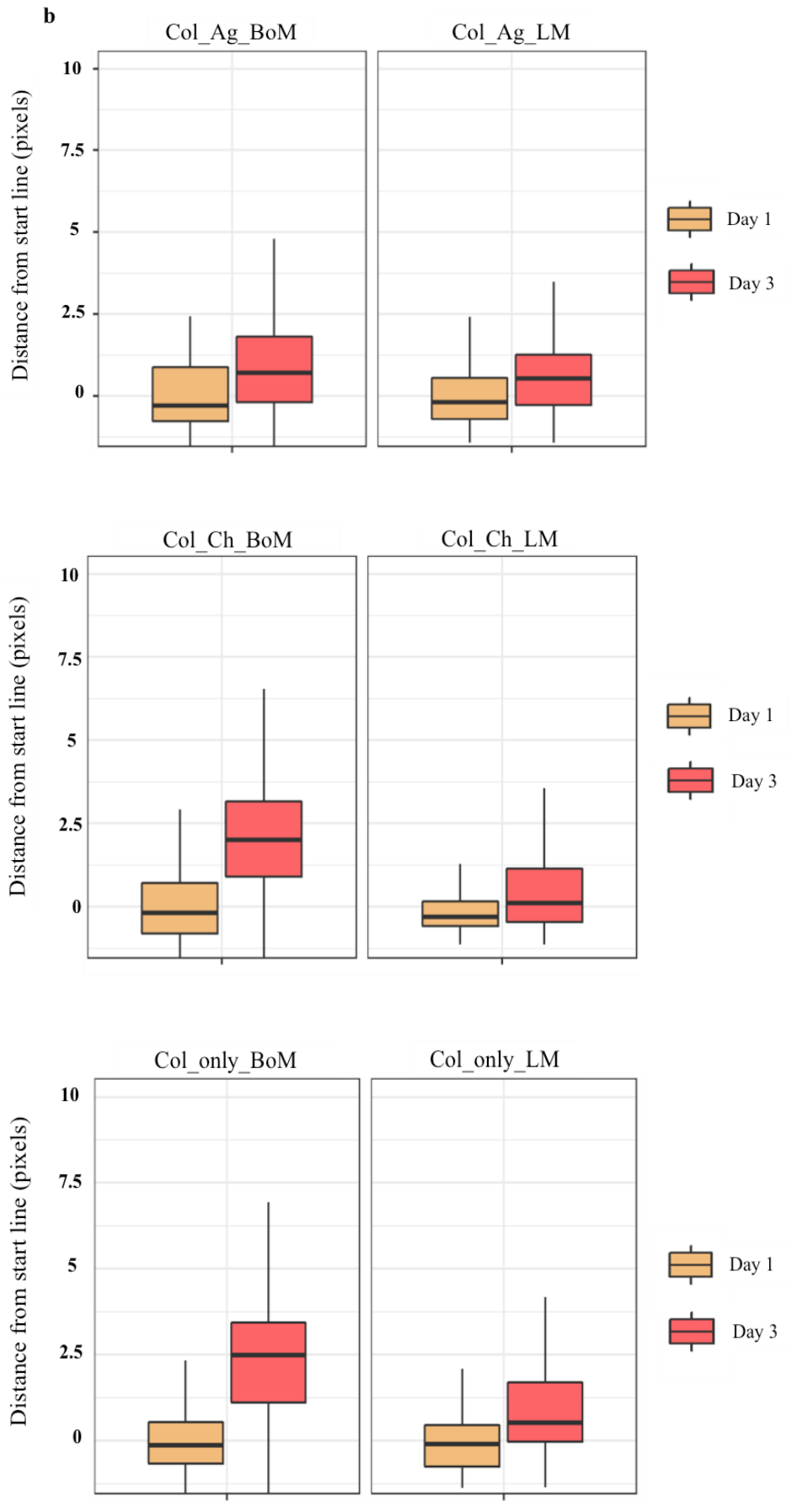
b
Col_Ag_BoM
Col_Ag_LM
Col_Ch_BoM
Col_Ch_LM
Col_only_BoM
Col_only_LM
Distance from start line (pixels)
10
7.5
5
2.5
0
Day 1
Day 3

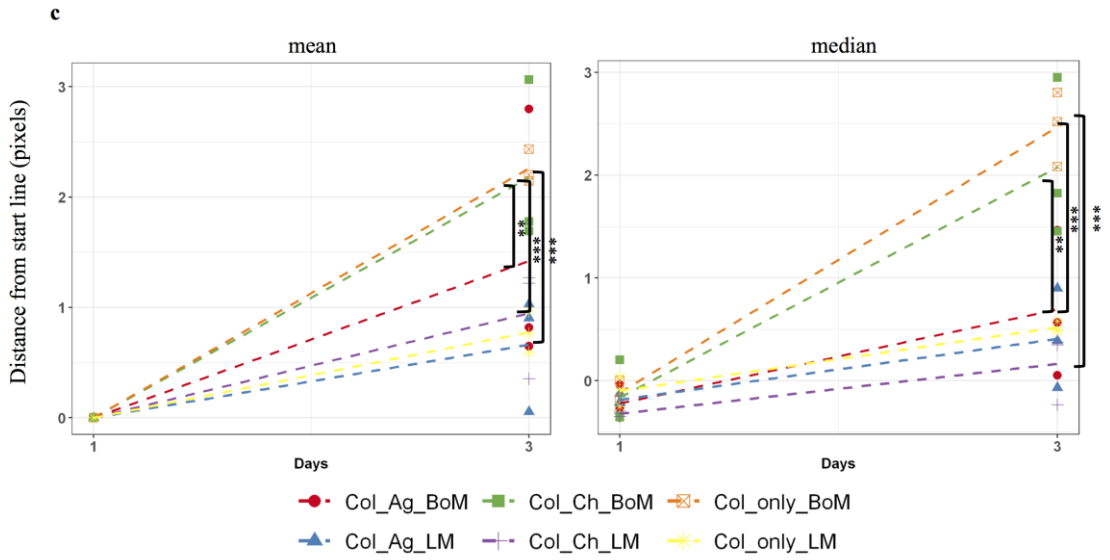

Figure 4.27. The invasion capacity of MDAMB231 cell line clones towards the bone microenvironment. a) Representative Z-stack images showing invasion of MDAMB231 BoM 1833 and MDAMB231 LM2 cells (red) towards the bone microenvironment towards HS5, hFOB and U937-laden collagen I only, collagen I + chitosan or collagen + agarose hydrogels (dashed line corresponds to the starting line for invasion). (Scale bar: 100 μm) b) The distance of each bright pixel to the starting line (dashed) was calculated after thresholding of Z-stack images. The data normalized to day 1 were plotted (n=6). c) Mean and median values of normalized distance distributions were plotted for day 1 and day 3 (n=6). **p≤ 0.01, ***p ≤ 0.005.

4.6. Extravasation Assay

4.6.1. Formation of Endothelial Monolayer

Modeling of extravasation process in metastatic dissemination requires the presence of an intact endothelial monolayer. Since the homogeneous distribution of endothelial cells is essential for a monolayer formation in EMC, HUVEC-C cells were resuspended in 8% dextran containing culture medium to inhibit cellular cluster formation.

The hydrophobicity of PDMS restricts the adhesion of endothelial cells on the interior of PDMS surfaces (Akther, Yakob, Nguyen, & Ta, 2020). Therefore, the interior surfaces of EX-chips were modified to increase the hydrophilicity, which promote the adhesion of endothelial cells for the formation of an intact endohelial monolayer. 3-Aminopropyl triethoxysilane (APTES) which is a coupling agent used for immobilization of biomolecules, was coated to functionalize the inner surfaces of EX-chips. APTES pre-coated EX-chips were then coated with laminin to ensure a natural moiety for the adhesion and survival of endothelial cells (Akther et al., 2020).

HUVEC-C cells were used to form an intact endothelial monolayer in EMC following the seeding of stromal cells to generate the homing microenvironments in HMC of EX-chips. It was nicely observed in representative images of the formed endothelial monolayer that HUVEC-C cells could form a vessel-like structure towards homing microenvironments in which the endothelial cells closed only the end of the structure as a monolayer (Figure 4.28).

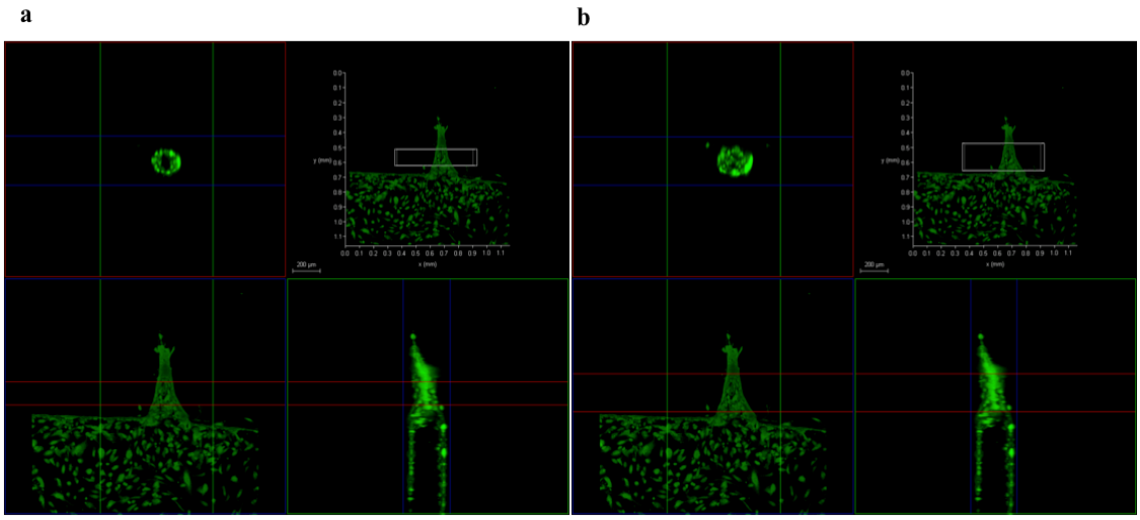

Figure 4.28. Representative 3D confocal images of an intact endothelial monolayer formation. The formation of a vessel-like structure by HUVEC-C (green) cells a) the middle of the channel, b) the end of the channel. Scale bar: 200 μm.

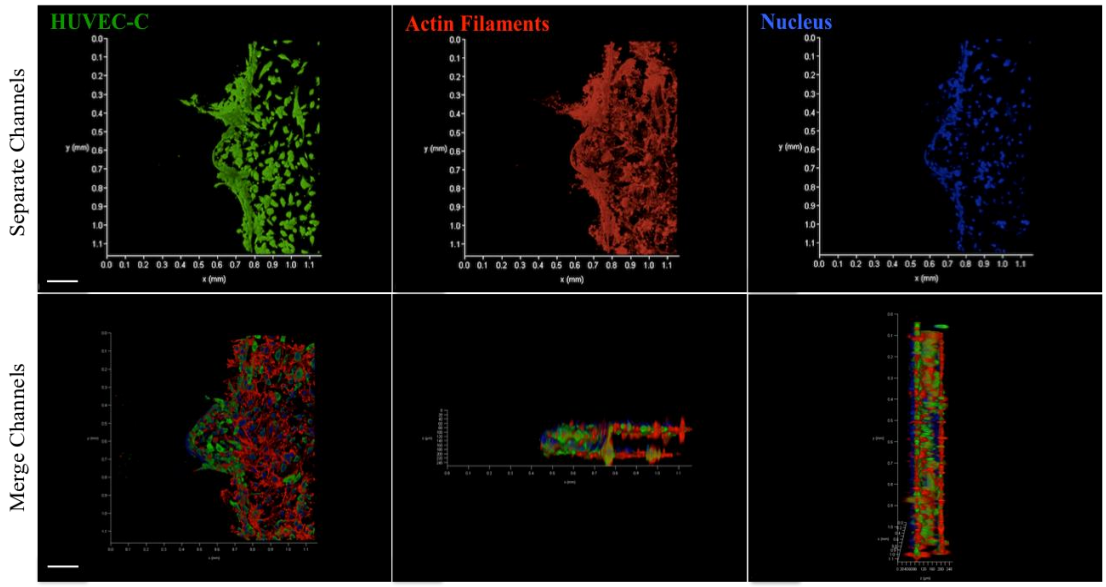

Figure 4.29. Formation of endothelial monolayer was confirmed by actin staining. Confocal images showing HUVEC-C (cell tracker), actin (phalloidin) and nuclei (DAPI) with separate and merge channels in red, blue and green, respectively from different views in APTES-laminin coated EX-chip. Scale bar: 200 μm.

The formation of an intact endothelial monolayer was confirmed by actin filament staining (Figure 4.29). It was revealed by the staining that the endothelial cells were confluent enough to form a monolayer although the green flourescence signal coming from HUVEC-C cells was rare due to Green Cell Tracker labeling. This result demonstrated that the green fluorescence signal acquired by transient labeling of HUVEC-C cells might not show the degree of endothelial cell coverage on the surfaces of EMC of EX-chips.

4.6.2. Extravasation Assay without Flow

The homing choices of extravasating breast cancer cells were examined towards lung, liver, breast and bone microenvironments generated in HMC through an intact endothelial monolayer formed in EMC of the EX-chips. Cancer cells were considered as extravasated when they entirely passed through the endothelial monolayer and as

associated when they were still connected to and detected within endothelial monolayer (Figure 3.7) (Figure 4.30a,b). The number of extravasated breast cancer cells was significantly higher towards lung, which was followed by liver, bone and breast microenvironments (Figure 4.30c,d). Associated breast cancer cell numbers were higher where the bone and breast microenvironments were present in HMC (Figure 4.30c,d). The number of extravasated and associated breast cancer cells was determined by counting the cells in every side of 3D confocal images.

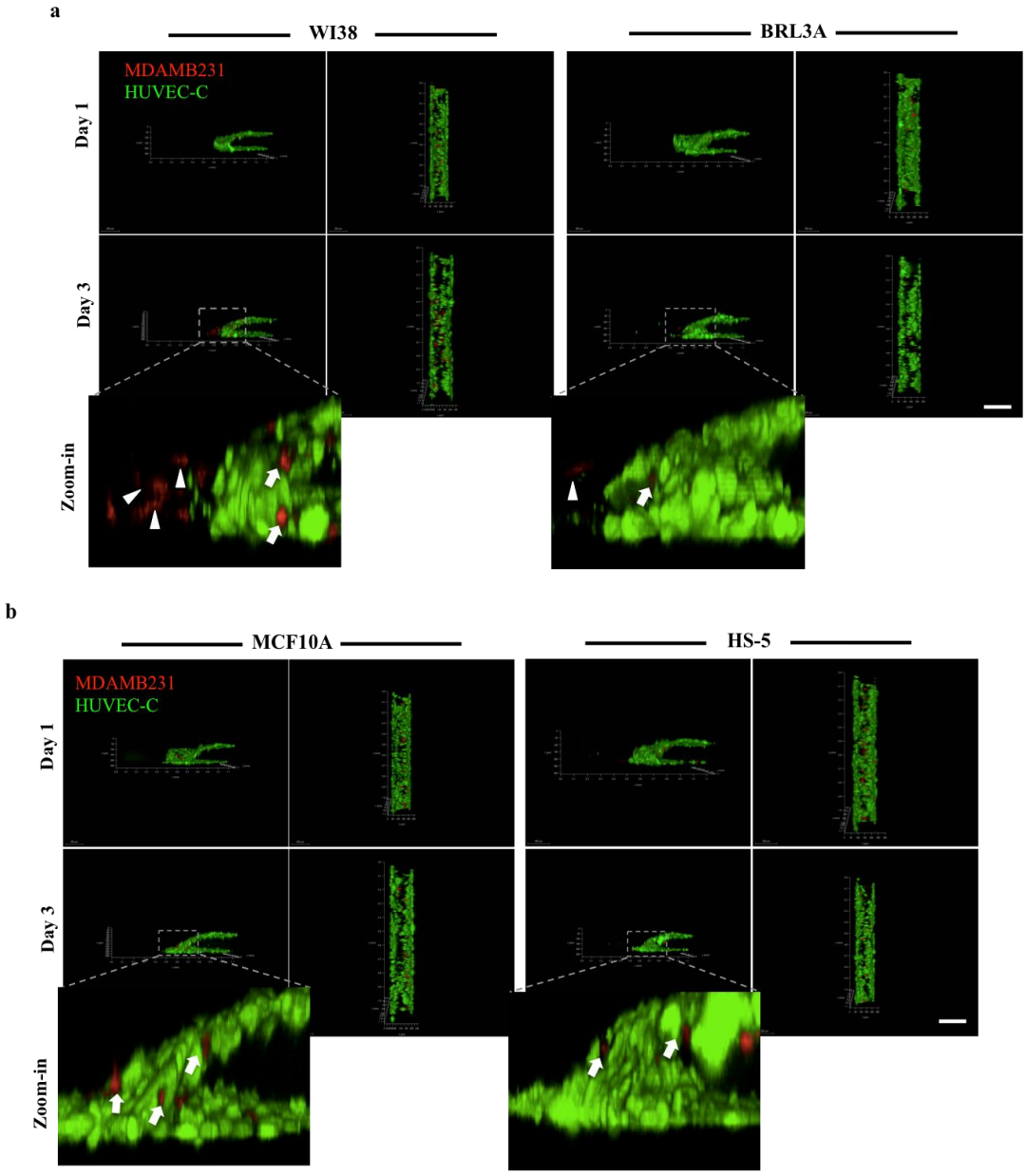

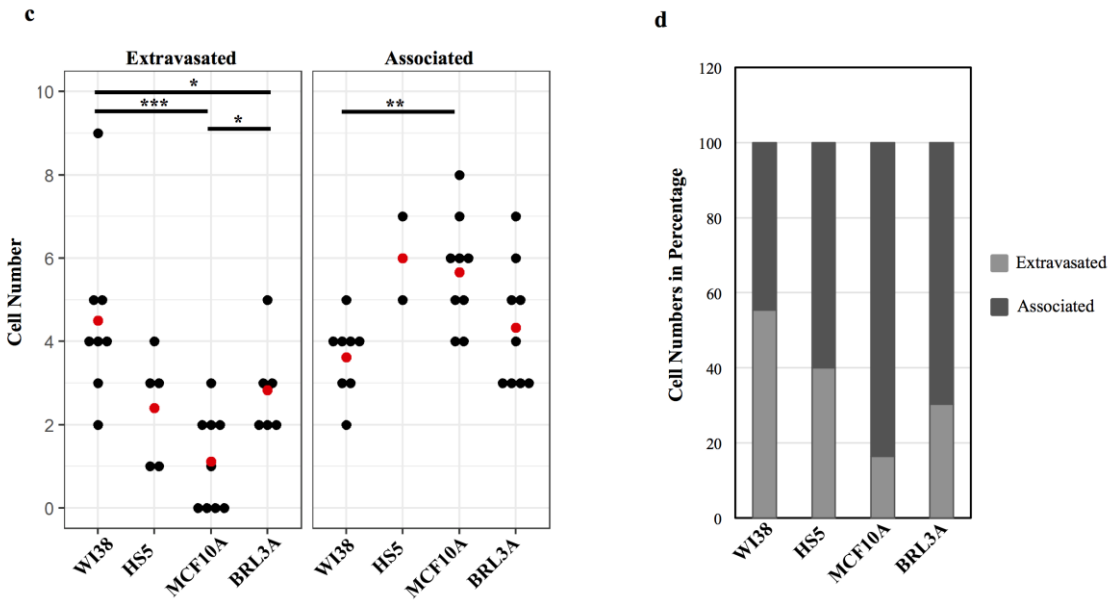

Figure 4.30. Extravasation of metastatic breast cancer cells into lung, liver, breast and bone homing microenvironments without flow conditions. Representative Z-stack images showing different side views of endothelial monolayer formation by HUVEC-C cells (green) and extravasated (arrow head) or associated (arrow) MDAMB231 cells (red) into a) lung and liver generated by WI38 and BRL3A cells lines or b) breast and bone microenvironments generated by MCF10A and HS5 cell lines, respectively. Scale bar: 200 µm. c) The number of extravasated and associated MDAMB231 cells. Each black dot represents the cell number for one post gap within the EX-chip, while the red dot is the average number of cells for each condition (n=9), d) the number of extravasated and associated MDAMB231 cells in percentages. *$p \leq 0.05$; **$p \leq 0.01$; *** $p \leq 0.005$.

In addition, the homing choices of bone- (MDAMB231 BoM 1833) and lung-specific (MDAMB231 LM2) extravasating breast cancer cells towards 3D bone microenvironment generated either by collagen type I only, collagen I and agarose or collagen I and chitosan scaffolds and by HS5, hFOB and U937 cell lines, were analyzed (Figure 4.31). The number of extravasated bone-specific metastasizing cells towards collagen I only and collagen I/chitosan conditions was evidently higher compared to lung-specific metastasizing ones (Figure 4.31d). Expectedly, the lung-specific metastasizing cells preferred to stay associated rather than being extravasated towards every conditions.

Altogether, hFOB, HS5 and U937 cell lines embedded within collagen I only or collagen I/chitosan scaffolds were sufficient to simulate *in vivo* conditions of bone microenvironment as bone-specific metastasizing cells significantly invaded and extravasated towards these sites.

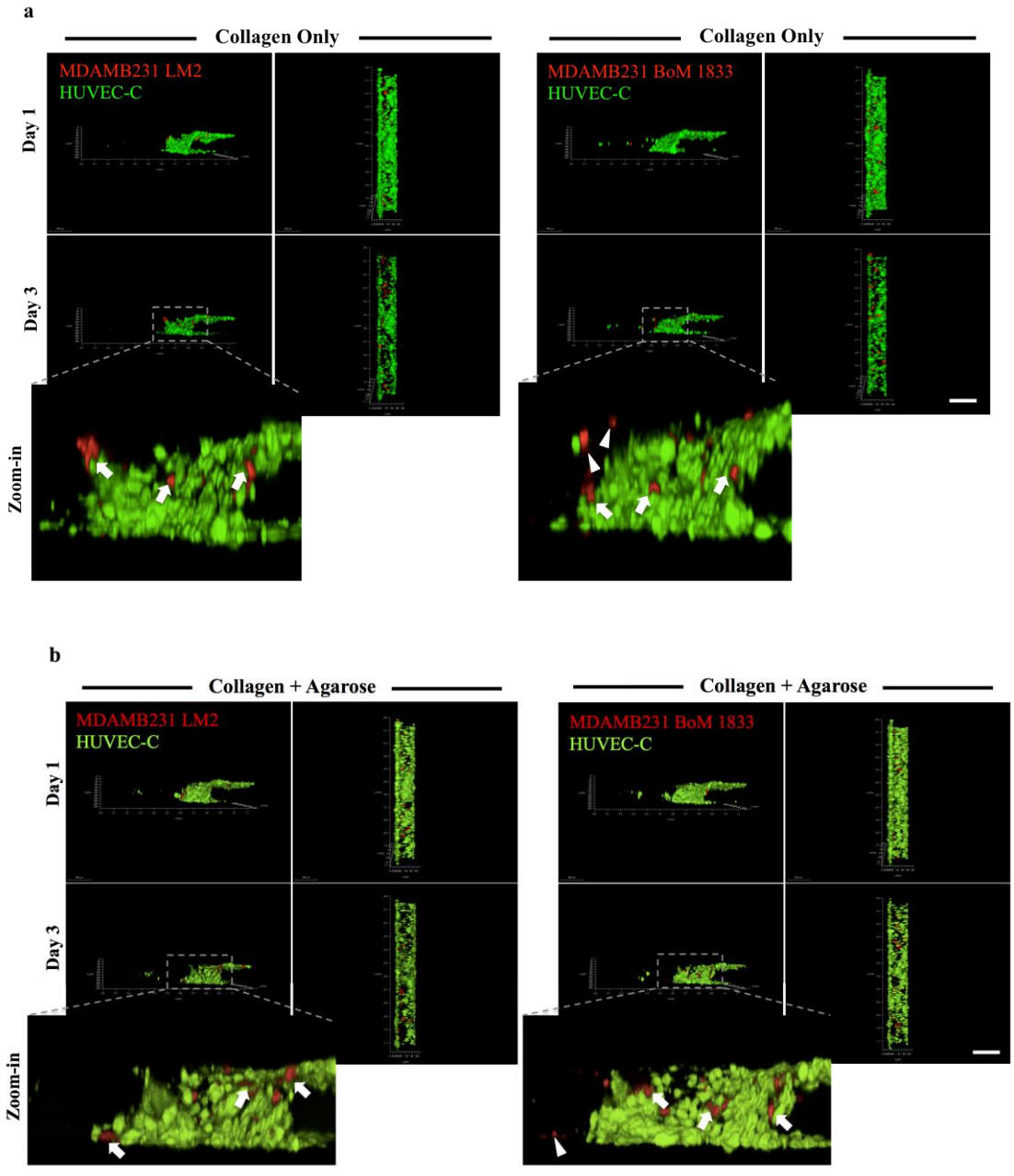

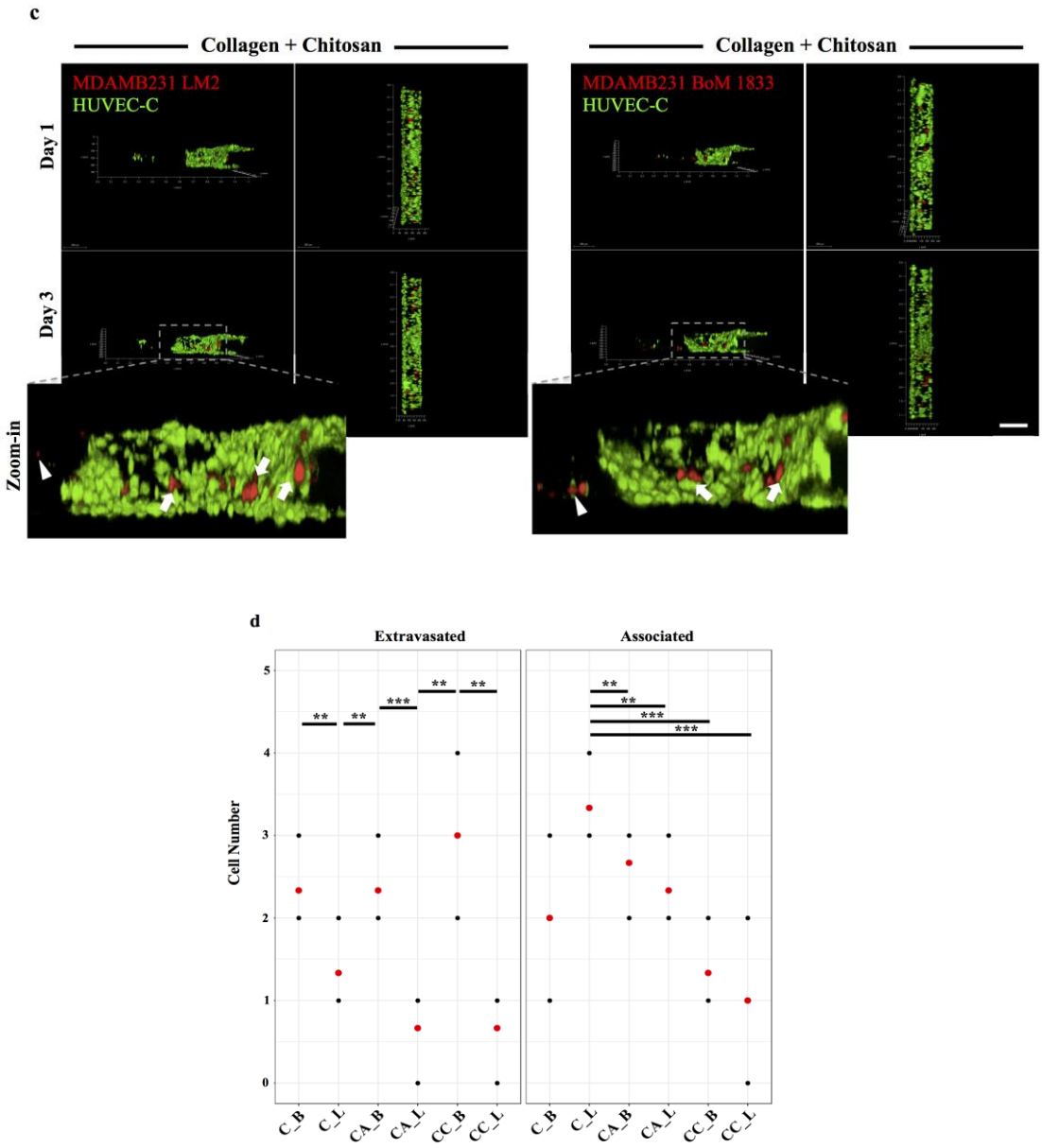

Figure 4.31. Extravasation of bone- and lung- specific metastasizing breast cancer cells into bone homing microenvironments generated by hFOB, HS5 and U937-laden collagen I only, collagen I + agarose or collagen I + chitosan hydrogels without flow conditions. Representative Z-stack images showing different side views of endothelial monolayer formation by HUVEC-C cells (green) and extravasated (arrow head) or associated (arrow) MDAMB231 subclones (red) into a) hFOB, HS5 and U937-laden collagen I only hydrogels, b) hFOB, HS5 and U937-laden collagen I + agarose hydrogels, c) hFOB, HS5 and U937-laden collagen I + chitosan hydrogels. Scale bar: 200 μm. d) The number of extravasated and associated MDAMB231 subclones. Each black dot represents the cell number for one post gap within the EX-chip, while the red dot is the average number of cells for each condition (n=3). **p ≤ 0.01; *** p ≤ 0.005.

4.6.3. Extravasation Assay under Flow

Circulation of breast cancer cells in the bloodstream is one of the crucial events for cancer dissemination especially for extravasation phase, during which the cells are subject to hemodynamic shear stress (S. Ma, Fu, Chiew, & Luo, 2017). The shear stress within blood circulation was shown to promote migration and extravasation of breast cancer cells (S. Ma et al., 2017). Therefore, shear stress was applied to breast cancer cells to mimic *in vivo* physiological conditions for cancer cell extravasation.

4.6.3.1. Viability of Cells under Flow

The MDAMB231 cells, which were selected as the metastatic cancer model in the thesis project, are adherent cells and have a limited lifetime under suspension conditions. Therefore, it was important to maintain the viability of MDAMB231 cells for the success of the extravasation experiments under flow conditions. It was aimed to investigate how many days MDAMB231 cells might maintain their viability and to understand whether cell density can have any effects on the cellular viability under flow conditions.

MDAMB231 cells with concentrations of $5x10^4$ cells/ml and $7.5x10^4$ cells/ml to mimic the concentration of circulating tumor cells (CTCs) in native blood circulation, were subject to flow at 0.75 dyne/cm^2 shear stress that was calculated due to height and width of the EX-chips as well as the viscosity and flow rate of fluid in circulation, for 2 days. The viability of the cells under flow conditions was determined both by MTT assay and through cell counter machine (Figure 4.32). MTT assay result revealed that around 50% of MDAMB231 cells died at the end of the first 24 hours, while it was around 70% at Day 2 (Figure 4.32a). A similar decrease trend was observed in both concentrations of MDAMB231 cells indicating that the concentration did not affect the viability of the cells under flow conditions (Figure 4.32). Therefore, the viability of MDAMB231 cells with a concentration of $5x10^4$ cells/ml was analyzed within the first 24 hours in 4-hour intervals to determine the optimal flow time.

The viability of MDAMB231 cells was 92% at the beginning of the flow, which then decreased to 73% at the end of the first 4 hours. The viability was detected as 47% and 40% at the end of 8 hours and 12 hours, respectively (Figure 4.32b).

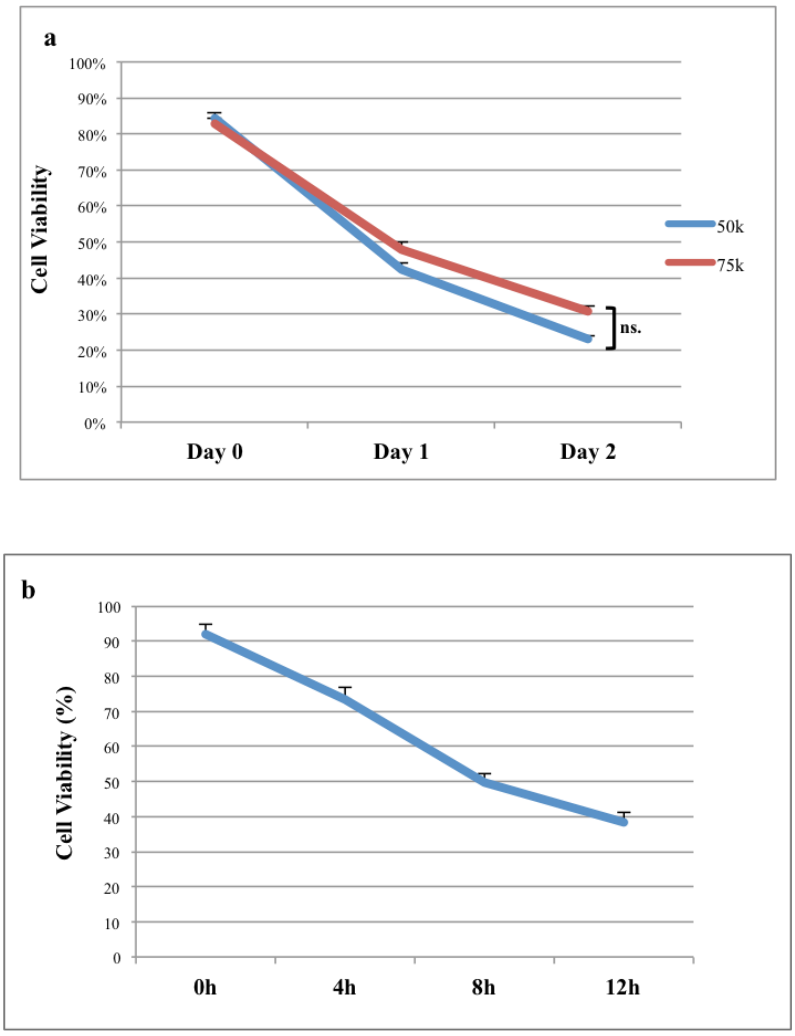

Figure 4.32. The viability of MDAMB231 cells under flow conditions. a) MTT assay showing the viability of two different MDAMB231 concentrations for 2 days, b) cell viability percentages of MDAMB231 cells in 4-hour intervals. The relative absorbance levels show the mean ± standard deviation for three independent experiments.

In addition MTT assay, colony formation assay was also performed to investigate the ability of single MDAMB231 cells to form colonies as an indicator of the survival of cells. The cell suspensions were collected from bubble trap under flow

conditions, seeded into 6 cm culture plates, cultured for 10 days and stained with crystal violet. It was clearly observed that the colony densities formed by MDAMB231 cells decreased from Day 0 to Day 3 (Figure 4.33).

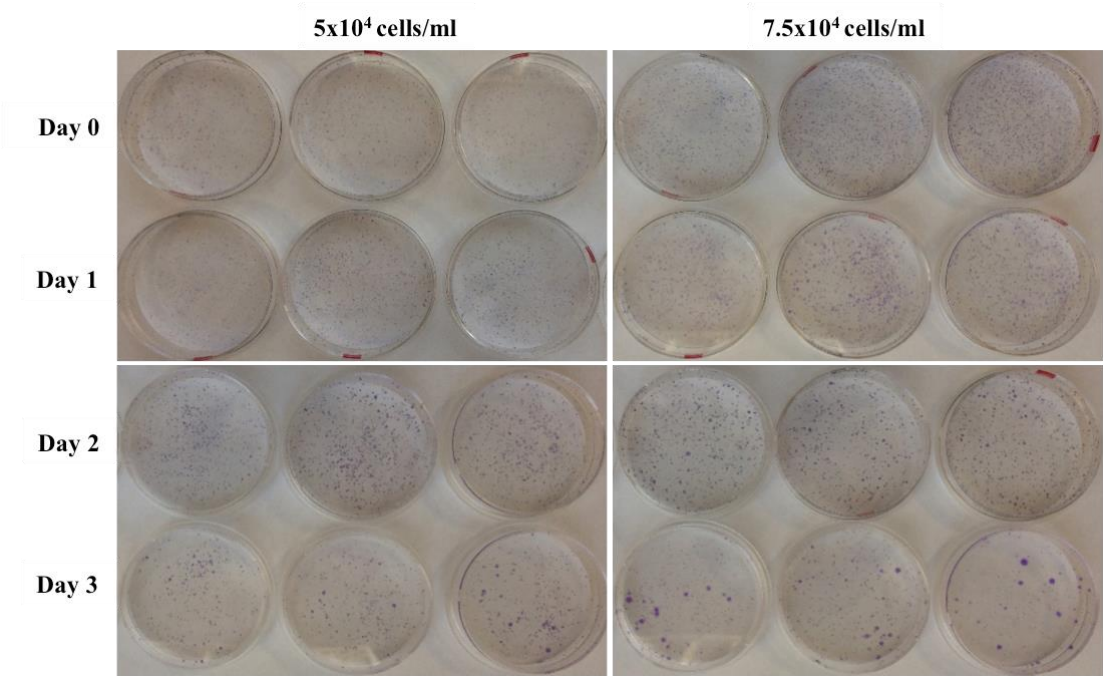

Figure 4.33. Colony formation assay of MDAMB231 cells kept in suspension conditions. The colony formation capacity of MDAMB231 cells taken from flow conditions, was investigated by crystal violet staining.

Altogether, depending on the viability and survival analyses of MDAMB231 cells under flow conditions, the flow time was determined as 4 hours.

The homing choices of extravasating breast cancer cells were examined towards lung, liver, breast and bone microenvironments generated in HMC through an intact endothelial monolayer formed in EMC of the EX-chips under a shear stress of 0,75 dyne/cm^2 (20 rpm) and with a flow time of 4 hours. MDAMB231 cells which were collected from bubble trap after 4 hours of flow, were seeded into EMC of EX-chips and the extravasation capacities of them towards generated 3D microenvironments were investigated for 3 days through confocal microscope.

The breast cancer cells preferred to stay associated with the endothelial monolayer rather than being extravasated in each condition when they were subject to shear stress and flow (Figure 4.34). The number of associated cancer cells was higher when lung and breast microenvironments were present in HMC of EX-chips.

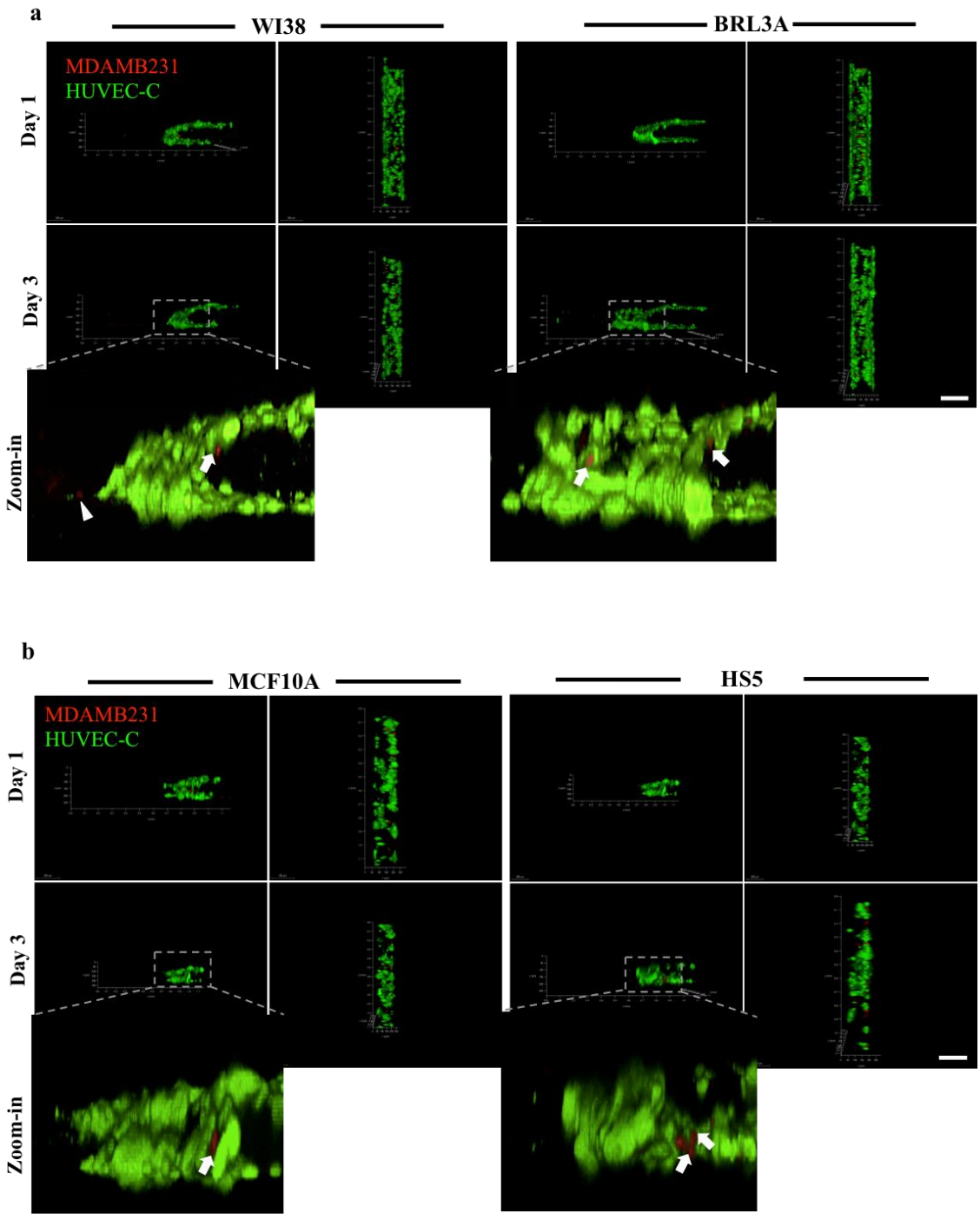

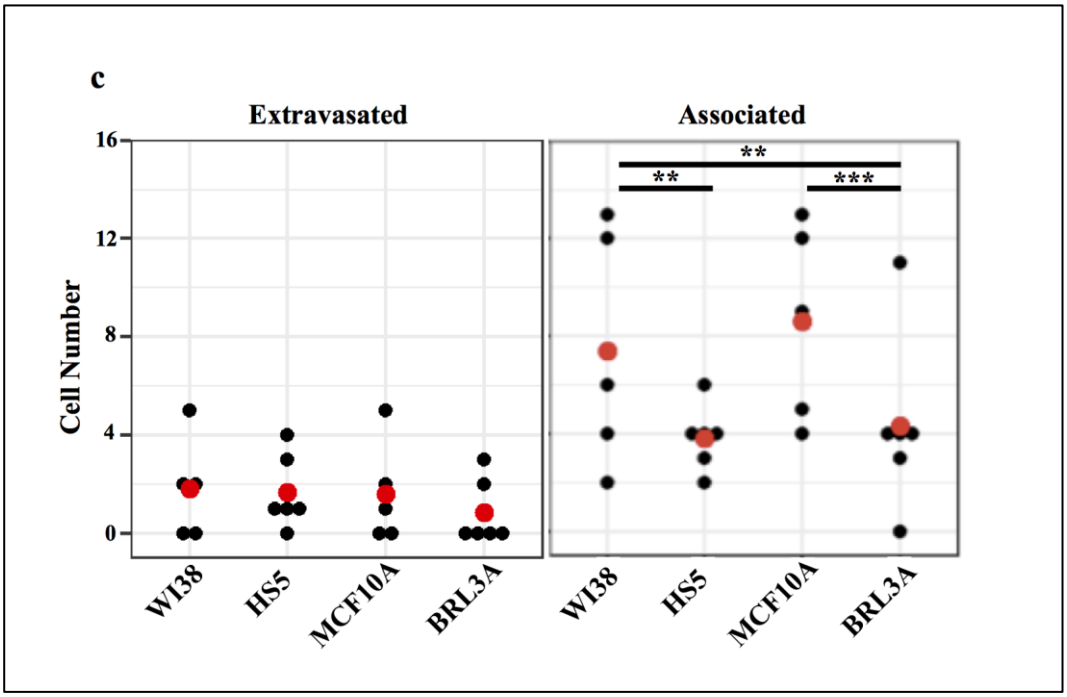

Figure 4.34. Extravasation of metastatic breast cancer cells into lung, liver, breast and bone homing microenvironments under flow. Representative Z-stack images showing different side views of endothelial monolayer formation by HUVEC-C cells (green) and extravasated (arrow head) or associated (arrow) MDAMB231 cells (red) into a) lung and liver generated by WI38 and BRL3A cells lines or b) breast and bone microenvironments generated by MCF10A and HS5 cell lines, respectively. Scale bar: 200 μm. c) The number of extravasated and associated MDAMB231 cells. Each black dot represents the cell number for one post gap within the EX-chip, while the red dot is the average number of cells for each condition (n=3). *$p \leq 0.05$; **$p \leq 0.01$; *** $p \leq 0.005$.

CHAPTER 5

CONCLUSION & DISCUSSION

In this study, we used two different LOC platforms, which are invasion (IC-chip) and extravasation chips (EX-chips) to investigate the homing site preferences of breast cancer cell lines. We demonstrated the *in vivo* behaviors of breast cancer cells with *in vitro* cell line models towards generated lung, bone, liver and breast microenvironments.

The use of multiple cell lines is a common approach for modeling experiments. Thus, it is important to generate an environment with minimal interference from external factors that can affect the outcome of the approaches. Therefore, to compare the effects of cell line models independent of culture conditions and to eliminate any effect on the invasiveness of breast cancer cell lines due to cell culture media differences, the same cell culture media was employed to each cell type used in an individual LOC platform. When the cells were cultured with serum-free DMEM-based culture media, they continued to grow and express chemokines in a similar profile to their own culture media. The use of serum-free DMEM-based cell culture media for the entire LOC platform was essential to evaluate the results based on only the cells, secreted factors and ECM components within the homing sites. Furthermore, the advantages of three-dimensional (3D) culture over two-dimensional (2D) culture were also demonstrated by CXCL12, CCL5 and IGF1 chemokines gene expression patterns. All three chemokines was expressed when the cells were cultured in 3D, but not all chemokine expression was detected in 2D culture. The differential expression of the chemokines in 2D and 3D cultures revealed that the 3D cell culture portrayed the *in vivo* conditions better, which enables greater clinical relevance compared to 2D cell culture.

Breast cancer mostly metastasized to bone, lung and liver. Consistent with the clinical data, triple-negative breast cancer cell line, MDAMB231 showed higher invasion and extravasation towards lung and liver compared to breast microenvironments while non-metastatic MCF7 cell showed no preference to either site. The invasion pattern towards different homing sites displayed differences. Mostly single cells were observed during the invasion of MDAMB231 cells to the lung and

liver microenvironments, while coordinated collective migration was observed when they invaded towards breast microenvironment. The variations in the movement of MDAMB231 cells towards generated tissue microenvironments can be caused by the cell type, tissue stiffness, strength in the adhesion and communication between cancer cells (De Pascalis & Etienne-Manneville, 2017).

The potency of lung homing site was further tested with lung-specific metastasizing MDAMB231 LM2 cells. The lung- and bone-specific metastatic subclones were generated through the *in vivo* selection of MDAMB231 metastatic subpopulations and each subclone indicates the organs, which they were isolated from (Bos et al., 2009; Kang et al., 2005; Minn et al., 2005). The MDAMB231 LM2 clone invaded better compared to MDAMB231 BoM subclone towards lung microenvironment explaining the *in vitro* system we generated can demonstrate *in vivo* metastatic preferences of metastatic cells. Furthermore, a similar invasion potential was observed between MDAMB231 LM2 clone and parental MDAMB231 cells. A slight difference between the invasion rate of parental and LM2 cells might be related to the heterogeneity of the parental MDAMB231 cell line in which lung-specific metastasizing cells could be more populated.

The *in vivo* tissue preferences of breast cancer cells were further demonstrated by *in vitro* extravasation assay towards bone, lung, liver and breast microenvironments through endothelial monolayer with or without flow. However, in contrast the invasion results, the higher number of extravasated cells towards lung but not liver microenvironment was observed in static extravasation condition. Furthermore, breast cancer cells preferred to stay associated with endothelial monolayer rather than being extravasated where breast microenvironment was the homing site. These observations might be explained by the VCAM-1 expression on both tumor cells and endothelial cells that can promote extravasation but not invasion of breast cancer cells towards lung microenvironment (Q. Chen & Massagué, 2012). On the other hand, the breast cancer cells preferred to be associated with endothelial monolayer regardless of the different homing tissue sites when they were subjected to flow.

Consistent with the literature, the gene expression profiles of CXCL12, CCL5 and IGF1 chemokines from both lung and liver stromal cells, but not from breast stromal cells, were correlated with both invasion and extravasation patterns of MDAMB231 cells that are positive for the receptors, CXCR4, CCR5 and IGFR1. These secreted factors can be considered as the leading factors for the regulation of invasion

and extravasation of MDAMB231 cells towards generated microenvironments. These observations suggest that the LOC platforms we generated could be used for chemokine-receptor interaction studies and drug testing approaches.

Although our results were consistent with the clinical studies, the microenvironments we generated have the disadvantage of depending on a single cell line to represent a multicellular tissue environment. The model requires to be improved by addition of mesenchymal stem cells (MSC), myoepithelial cells, bone marrow derived cells (BMDCs) including macrophages and neutrophils to generate a more physiologically relevant environments that mimic the cellular milieu of native lung, liver and breast tissues.

In order to mimic bone tissue microenvironment, HS5 fibroblast cell line was first used in GFR-Matrigel, which is composed of laminin, collagen IV and heparan sulfate proteoglycan. However, although the breast cancer cell line, MDAMB231 is more prone to metastasize to bone tissue, an intensive invasion or extravasation towards the *in vitro* generated model by HS5 cells was not observed. The lack of a potential homing mechanism for the attraction of breast cancer cells to bone microenvironment model can be explained by the absence of adequate cellular and structural content as well as the poor mechanical properties exhibited by GFR-Matrigel. In addition to that, BMP9 (bone morphogenetic protein) secretion from HS5 cells, was previously shown to inhibit the invasion of MDAMB231 cells through inhibiting AKT signaling pathway (Wan et al., 2014), which might block the invasion of MDAMB231 cells in our case as well. To overcome these limitations and to model a microenvironment that can mimic bone tissue better, both protein-based (by collagen type I) and polymer-based scaffolds (by agarose or chitosan) were generated. Collagen type I was chosen as being the most abundant ECM component in bone stroma, whereas agarose and chitosan polymers were selected to modify the stiffness of bone matrices. Furthermore, to model the bone tissue complexity, different cell lines representing osteoblasts, monocytes and fibroblasts were used to have more native-like bone microenvironment models. U937 monocytes were shown to differentiate into osteoclast-like cells when they are cultured with osteoblast cells and commonly considered in the first steps of bone tissue model development (Sieberath et al., 2020). Therefore, to maintain a bone microenvironment with a similar bone homeostasis observed in *in vivo* conditions, U937 cells together with hFOB osteoblast cells and HS5 fibroblast cells were used.

The representative 3D bone microenvironments generated by collagen I, agarose and/or chitosan together with HS5, hFOB and U937 cell lines to mimic *in vivo* conditions were tested with bone-specific metastatic clone, MDAMB231 BoM 1833. More intensive invasion of bone-specific subclone was observed towards both collagen I only and collagen I and chitosan containing scaffolds, while the invasion of lung-specific metastatic clone, MDAMB231 LM2 was limited towards both scaffolds. This data confirmed that MDAMB231 BoM 1833 clones preferred the scaffolds, which were physiologically more comparable to the *in vivo* conditions of bone tissue, consistent with the previous *in vivo* studies (Kang et al., 2005). These results highlight the adequacy of the matrix components, collagen I individually or in combination with chitosan, as well as the cellular content of the generated scaffolds to mimic 3D bone microenvironment and to attract bone-specific cells towards their sites. This *in vitro* model we generated demonstrates the *in vivo* behaviors of MDAMB231 BoM 1833 cells whose bone specificity was previously established *in vivo* (Kang et al., 2005).

In recent years, a variety of studies had investigated the role matrix stiffness on tumor cell invasion especially by regulating cell-to-cell communication within the matrices and promoting cellular differentiation (Berger et al., 2020). Stiff scaffolds were shown to have a low rate of nutrient diffusion into the cells, thereby affecting the viability, proliferation, migration ad invasion of cells negatively compared to softer scaffolds (J. Zhang et al., 2020). Similar to that, higher calcium content was observed in osteoblast cells seeded in 3D hydrogels with low stiffness (0.58 kPa) than those observed in hydrogels with high stiffness (1.5 kPa) hydrogels (Mc Garrigle, Mullen, Haugh, Voisin, & McNamara, 2016). Besides, less stiff collagen scaffolds were shown to better promote osteogenic differentiation compared to scaffolds with intermediate or high stiffness (Duarte Campos et al., 2016). Therefore, consistent with these findings, the less stiff scaffolds observed in collagen I individually or in combination with polymers were sufficient to promote the invasion and extravasation of breast cancer cells. In addition to that, regardless of the gel stiffness, the breast cancer cells preferred to invade and extravasate towards collagen I/chitosan scaffolds rather than collagen I/ agarose scaffolds. The amino functional groups present on the surface of the chitosan polymers enable them to interact with collagen I and the stromal cells both physically and chemically (Nurunnabi, Revuri, Huh, & Lee, 2017) which can provide more physiological environment compared to agarose-based scaffolds for the invasion and extravasation of bone-specific metastasizing MDAMB231 cells.Altogether, our results

revealed the importance of IC-chip and EX-chips for determination of invasion and extravasation potentials of breast cancer cells both qualitatively and quantitatively. Similar to clinical data, *in vivo* metastatic behaviors of breast cancer cells were simulated towards *in vitro* generated 3D homing microenvironments considering the roles ECM components, cellular milieu and secreted chemokines. Here, we showed that LOC platforms with *in vitro* generated 3D microenvironments, can demonstrate the *in vivo* metastatic behaviors and tissue preferences of breast cancer cells. These platforms can be further developed as a diagnostic kit after being tested with patient samples. The roles of downstream signaling pathways together with the receptor-ligand interactions can be further investigated to obtain detailed information underlying the metastatic preference of breast cancer cells, which will enable to develop more reliable and promising therapeutic approaches.

REFERENCES

Akekawatchai, C., Holland, J. D., Kochetkova, M., Wallace, J. C., & McColl, S. R. (2005). Transactivation of CXCR4 by the insulin-like growth factor-1 receptor (IGF-1R) in human MDA-MB-231 breast cancer epithelial cells. *Journal of Biological Chemistry, 280*(48), 39701-39708.

Akther, F., Yakob, S. B., Nguyen, N.-T., & Ta, H. T. (2020). Surface Modification Techniques for Endothelial Cell Seeding in PDMS Microfluidic Devices. *Biosensors, 10*(11), 182.

Andy, J., Gaorav, P., Peter, M., Paula, D., Weiping, S., Dilip, D., . . . Joan, M. (2005). Genes that mediate breast cancer metastasis to lung. *Nature, 436*, 518-524.

Arora, M. (2013). Cell culture media: a review. *Mater methods, 3*(175), 24.

Baenke, F. (2013). *Metabolic dependencies of breast cancer cells.* UCL (University College London),

Bai, H., Weng, Y., Bai, S., Jiang, Y., Li, B., He, F., . . . Wang, J. (2014). CCL5 secreted from bone marrow stromal cells stimulates the migration and invasion of Huh7 hepatocellular carcinoma cells via the PI3K-Akt pathway. *International journal of oncology, 45*(1), 333-343.

Berger, A. J., Renner, C. M., Hale, I., Yang, X., Ponik, S. M., Weisman, P. S., . . . Kreeger, P. K. (2020). Scaffold stiffness influences breast cancer cell invasion via EGFR-linked Mena upregulation and matrix remodeling. *Matrix Biology, 85*, 80-93.

Bersini, S., Jeon, J. S., Dubini, G., Arrigoni, C., Chung, S., Charest, J. L., . . . Kamm, R. D. (2014). A microfluidic 3D in vitro model for specificity of breast cancer metastasis to bone. *Biomaterials, 35*(8), 2454-2461.

Bertassoli, B. M., Assis Neto, A. C. d., Oliveira, F. D. d., Arroyo, M. A. M., Ferrão, J. S. P., Silva, J. B. d., . . . Braga, P. B. (2013). Mesenchymal stem cells: emphasis in adipose tissue. *Brazilian Archives of Biology and Technology, 56*(4), 607-617.

Bertula, K., Martikainen, L., Munne, P., Hietala, S., Klefström, J., Ikkala, O., & Nonappa. (2019). Strain-stiffening of agarose gels. *Acs macro letters, 8*(6), 670-675.

Bique, A.-M., Kaivosoja, E., Mikkonen, M., & Paulasto-Kröckel, M. (2016). Choice of osteoblast model critical for studying the effects of electromagnetic stimulation on osteogenesis in vitro. *Electromagnetic biology and medicine, 35*(4), 353-364.

Borciani, G., Montalbano, G., Baldini, N., Cerqueni, G., Vitale-Brovarone, C., & Ciapetti, G. (2020). Co–culture systems of osteoblasts and osteoclasts: Simulating in vitro bone remodeling in regenerative approaches. *Acta Biomaterialia, 108*, 22-45.

Bos, P. D., Zhang, X. H.-F., Nadal, C., Shu, W., Gomis, R. R., Nguyen, D. X., . . . Foekens, J. A. (2009). Genes that mediate breast cancer metastasis to the brain. *Nature, 459*(7249), 1005-1009.

Bray, F., Ferlay, J., Soerjomataram, I., Siegel, R. L., Torre, L. A., & Jemal, A. (2018). Global cancer statistics 2018: GLOBOCAN estimates of incidence and mortality worldwide for 36 cancers in 185 countries. *CA: a cancer journal for clinicians, 68*(6), 394-424.

Broxmeyer, H. E., Orschell, C. M., Clapp, D. W., Hangoc, G., Cooper, S., Plett, P. A., . . . Campbell, T. B. (2005). Rapid mobilization of murine and human hematopoietic stem and progenitor cells with AMD3100, a CXCR4 antagonist. *The Journal of experimental medicine, 201*(8), 1307-1318.

Buenrostro, D., Mulcrone, P. L., Owens, P., & Sterling, J. A. (2016). The bone microenvironment: a fertile soil for tumor growth. *Current osteoporosis reports, 14*(4), 151-158.

Chatterjee, S., Azad, B. B., & Nimmagadda, S. (2014). The intricate role of CXCR4 in cancer. *Advances in cancer research, 124*, 31-82.

Chen, G., Dong, C., Yang, L., & Lv, Y. (2015). 3D scaffolds with different stiffness but the same microstructure for bone tissue engineering. *ACS applied materials & interfaces, 7*(29), 15790-15802.

Chen, Q., & Massagué, J. (2012). Molecular pathways: VCAM-1 as a potential therapeutic target in metastasis. *Clinical Cancer Research, 18*(20), 5520-5525.

Chen, W., Hoffmann, A. D., Liu, H., & Liu, X. (2018). Organotropism: new insights into molecular mechanisms of breast cancer metastasis. *NPJ precision oncology, 2*(1), 1-12.

Chow, M. T., & Luster, A. D. (2014). Chemokines in cancer. *Cancer immunology research, 2*(12), 1125-1131.

Dai, X., Cheng, H., Bai, Z., & Li, J. (2017). Breast cancer cell line classification and its relevance with breast tumor subtyping. *Journal of Cancer, 8*(16), 3131.

De Pascalis, C., & Etienne-Manneville, S. (2017). Single and collective cell migration: the mechanics of adhesions. *Molecular biology of the cell, 28*(14), 1833-1846.

Deville, S. S., & Cordes, N. (2019). The extracellular, cellular and nuclear stiffness, a trinity in the cancer resistome–A review. *Frontiers in Oncology, 9*, 1376.

Duarte Campos, D. F., Blaeser, A., Buellesbach, K., Sen, K. S., Xun, W., Tillmann, W., & Fischer, H. (2016). Bioprinting organotypic hydrogels with improved mesenchymal stem cell remodeling and mineralization properties for bone tissue engineering. *Advanced healthcare materials, 5*(11), 1336-1345.

Emon, B., Bauer, J., Jain, Y., Jung, B., & Saif, T. (2018). Biophysics of tumor microenvironment and cancer metastasis-a mini review. *Computational and structural biotechnology journal, 16*, 279-287.

Esquivel-Velázquez, M., Ostoa-Saloma, P., Palacios-Arreola, M. I., Nava-Castro, K. E., Castro, J. I., & Morales-Montor, J. (2015). The role of cytokines in breast cancer development and progression. *Journal of Interferon & Cytokine Research, 35*(1), 1-16.

Fares, J., Fares, M. Y., Khachfe, H. H., Salhab, H. A., & Fares, Y. (2020). Molecular principles of metastasis: a hallmark of cancer revisited. *Signal transduction and targeted therapy, 5*(1), 1-17.

Ferlay, J., Colombet, M., Soerjomataram, I., Mathers, C., Parkin, D., Piñeros, M., . . . Bray, F. (2019). Estimating the global cancer incidence and mortality in 2018: GLOBOCAN sources and methods. *International journal of cancer, 144*(8), 1941-1953.

Gao, Y., Bado, I., Wang, H., Zhang, W., Rosen, J. M., & Zhang, X. H.-F. (2019). Metastasis organotropism: redefining the congenial soil. *Developmental cell, 49*(3), 375-391.

Guo, F., Wang, Y., Liu, J., Mok, S., Xue, F., & Zhang, W. (2016). CXCL12/CXCR4: a symbiotic bridge linking cancer cells and their stromal neighbors in oncogenic communication networks. *Oncogene, 35*(7), 816-826.

Harris, S. A., Enger, R. J., Riggs, L. B., & Spelsberg, T. C. (1995). Development and characterization of a conditionally immortalized human fetal osteoblastic cell line. *Journal of Bone and Mineral Research, 10*(2), 178-186.

Heng, B. C., Bezerra, P. P., Preiser, P. R., Alex Law, S., Xia, Y., Boey, F., & Venkatraman, S. S. (2011). Effect of cell-seeding density on the proliferation and gene expression profile of human umbilical vein endothelial cells within ex vivo culture. *Cytotherapy, 13*(5), 606-617.

Hiraga, T., Myoui, A., Hashimoto, N., Sasaki, A., Hata, K., Morita, Y., . . . Yoneda, T. (2012). Bone-derived IGF mediates crosstalk between bone and breast cancer cells in bony metastases. *Cancer research, 72*(16), 4238-4249.

Hughes, C. S., Postovit, L. M., & Lajoie, G. A. (2010). Matrigel: a complex protein mixture required for optimal growth of cell culture. *Proteomics, 10*(9), 1886-1890.

Ilhan, M., Kucukkose, C., Efe, E., Gunyuz, Z. E., Firatligil, B., Dogan, H., . . . Yalcin-Ozuysal, O. (2020). Pro-metastatic functions of Notch signaling is mediated by CYR61 in breast cells. *European Journal of Cell Biology*, 151070.

Javed, A., & Lteif, A. (2013). *Development of the human breast.* Paper presented at the Seminars in plastic surgery.

Jeon, J. S., Zervantonakis, I. K., Chung, S., Kamm, R. D., & Charest, J. L. (2013). In vitro model of tumor cell extravasation. *PloS one, 8*(2), e56910.

Kang, Y., He, W., Tulley, S., Gupta, G. P., Serganova, I., Chen, C.-R., . . . Massagué, J. (2005). Breast cancer bone metastasis mediated by the Smad tumor suppressor pathway. *Proceedings of the National Academy of Sciences, 102*(39), 13909-13914.

Karnoub, A. E., Dash, A. B., Vo, A. P., Sullivan, A., Brooks, M. W., Bell, G. W., . . . Weinberg, R. A. (2007). Mesenchymal stem cells within tumour stroma promote breast cancer metastasis. *Nature, 449*(7162), 557-563.

Karnoub, A. E., & Weinberg, R. A. (2007). Chemokine networks and breast cancer metastasis. *Breast disease, 26*(1), 75-85.

Kennecke, H., Yerushalmi, R., Woods, R., Cheang, M. C. U., Voduc, D., Speers, C. H., . . . Gelmon, K. (2010). Metastatic behavior of breast cancer subtypes. *Journal of clinical oncology, 28*(20), 3271-3277.

Kimbung, S., Loman, N., & Hedenfalk, I. (2015). *Clinical and molecular complexity of breast cancer metastases.* Paper presented at the Seminars in cancer biology.

Lu, X., & Kang, Y. (2007). Organotropism of breast cancer metastasis. *Journal of mammary gland biology and neoplasia, 12*(2-3), 153.

Ma, R., Feng, Y., Lin, S., Chen, J., Lin, H., Liang, X., . . . Cai, X. (2015). Mechanisms involved in breast cancer liver metastasis. *Journal of translational medicine, 13*(1), 1-10.

Ma, S., Fu, A., Chiew, G. G. Y., & Luo, K. Q. (2017). Hemodynamic shear stress stimulates migration and extravasation of tumor cells by elevating cellular oxidative level. *Cancer letters, 388*, 239-248.

Maia, F. R., Lourenço, A. H., Granja, P. L., Gonçalves, R. M., & Barrias, C. C. (2014). Effect of cell density on mesenchymal stem cells aggregation in RGD-alginate 3D matrices under osteoinductive conditions. *Macromolecular bioscience, 14*(6), 759-771.

Makki, J. (2015). Diversity of breast carcinoma: histological subtypes and clinical relevance. *Clinical Medicine Insights: Pathology, 8*, CPath. S31563.

Malhotra, G. K., Zhao, X., Band, H., & Band, V. (2010). Histological, molecular and functional subtypes of breast cancers. *Cancer Biology & Therapy, 10*(10), 955-960.

Matellan, C., & Armando, E. (2019). Engineering the cellular mechanical microenvironment–from bulk mechanics to the nanoscale. *Journal of cell science, 132*(9).

Mc Garrigle, M., Mullen, C. A., Haugh, M. G., Voisin, M. C., & McNamara, L. M. (2016). Osteocyte differentiation and the formation of an interconnected cellular network in vitro. *Eur Cell Mater, 31*, 323-340.

Meirson, T., Gil-Henn, H., & Samson, A. O. (2020). Invasion and metastasis: the elusive hallmark of cancer. *Oncogene, 39*(9), 2024-2026.

Méndez-García, L. A., Nava-Castro, K. E., Ochoa-Mercado, T. d. L., Palacios-Arreola, M. I., Ruiz-Manzano, R. A., Segovia-Mendoza, M., . . . Morales-Montor, J. (2019). Breast cancer metastasis: are cytokines important players during its development and progression? *Journal of Interferon & Cytokine Research, 39*(1), 39-55.

Minn, A. J., Gupta, G. P., Siegel, P. M., Bos, P. D., Shu, W., Giri, D. D., . . . Massagué, J. (2005). Genes that mediate breast cancer metastasis to lung. *Nature, 436*(7050), 518-524.

Monteiro, C. F., Custódio, C. A., & Mano, J. F. (2019). Three-Dimensional Osteosarcoma Models for Advancing Drug Discovery and Development. *Advanced Therapeutics, 2*(3), 1800108.

Müller, A., Homey, B., Soto, H., Ge, N., Catron, D., Buchanan, M. E., . . . Wagner, S. N. (2001). Involvement of chemokine receptors in breast cancer metastasis. *Nature, 410*(6824), 50-56.

Nurunnabi, M., Revuri, V., Huh, K. M., & Lee, Y.-k. (2017). Polysaccharide based nano/microformulation: an effective and versatile oral drug delivery system. In *Nanostructures for Oral Medicine* (pp. 409-433): Elsevier.

Ohira, S., Sasaki, M., Harada, K., Sato, Y., Zen, Y., Isse, K., . . . Nimura, Y. (2006). Possible regulation of migration of intrahepatic cholangiocarcinoma cells by interaction of CXCR4 expressed in carcinoma cells with tumor necrosis factor-α and stromal-derived factor-1 released in stroma. *The American journal of pathology, 168*(4), 1155-1168.

Park, S. H., Eber, M. R., Widner, D. B., & Shiozawa, Y. (2018). Role of the bone microenvironment in the development of painful complications of skeletal metastases. *Cancers, 10*(5), 141.

Patel, L. R., Camacho, D. F., Shiozawa, Y., Pienta, K. J., & Taichman, R. S. (2011). Mechanisms of cancer cell metastasis to the bone: a multistep process. *Future oncology, 7*(11), 1285-1297.

Pellowe, A. S., & Gonzalez, A. L. (2016). Extracellular matrix biomimicry for the creation of investigational and therapeutic devices. *Wiley Interdisciplinary Reviews: Nanomedicine and Nanobiotechnology, 8*(1), 5-22.

Piaseczny, M. M., & Allan, A. L. (2014). Why does breast cancer often spread to the lung? *Women's Health, 10*(6), 561-564.

Pommier, R. M., Sanlaville, A., Tonon, L., Kielbassa, J., Thomas, E., Ferrari, A., . . . Tissier, A. (2020). Comprehensive characterization of claudin-low breast tumors reflects the impact of the cell-of-origin on cancer evolution. *Nature communications, 11*(1), 1-12.

Rodríguez-Vázquez, M., Vega-Ruiz, B., Ramos-Zúñiga, R., Saldaña-Koppel, D. A., & Quiñones-Olvera, L. F. (2015). Chitosan and its potential use as a scaffold for tissue engineering in regenerative medicine. *BioMed research international, 2015*.

Sachdev, D., Hartell, J. S., Lee, A. V., Zhang, X., & Yee, D. (2004). A dominant negative type I insulin-like growth factor receptor inhibits metastasis of human cancer cells. *Journal of Biological Chemistry, 279*(6), 5017-5024.

Samani, A. A., Yakar, S., LeRoith, D., & Brodt, P. (2007). The role of the IGF system in cancer growth and metastasis: overview and recent insights. *Endocrine reviews, 28*(1), 20-47.

Sarvaiya, P. J., Guo, D., Ulasov, I., Gabikian, P., & Lesniak, M. S. (2013). Chemokines in tumor progression and metastasis. *Oncotarget, 4*(12), 2171.

Sieberath, A., Della Bella, E., Ferreira, A. M., Gentile, P., Eglin, D., & Dalgarno, K. (2020). A comparison of osteoblast and osteoclast in vitro co-culture models and their translation for preclinical drug testing applications. *International journal of molecular sciences, 21*(3), 912.

Soria, G., & Ben-Baruch, A. (2008). The inflammatory chemokines CCL2 and CCL5 in breast cancer. *Cancer letters, 267*(2), 271-285.

Stormes, K. A., Lemken, C. A., Lepre, J. V., Marinucci, M. N., & Kurt, R. A. (2005). Inhibition of metastasis by inhibition of tumor-derived CCL5. *Breast cancer research and treatment, 89*(2), 209-212.

Sun, D., Lu, J., Chen, Z., Yu, Y., & Li, Y. (2014). A novel three-dimensional microfluidic platform for on chip multicellular tumor spheroid formation and culture. *Microfluidics and nanofluidics, 17*(5), 831-842.

Sun, M., Chi, G., Li, P., Lv, S., Xu, J., Xu, Z., . . . Li, L. (2018). Effects of matrix stiffness on the morphology, adhesion, proliferation and osteogenic differentiation of mesenchymal stem cells. *International journal of medical sciences, 15*(3), 257.

Sun, X., Cheng, G., Hao, M., Zheng, J., Zhou, X., Zhang, J., . . . Wang, J. (2010). CXCL12/CXCR4/CXCR7 chemokine axis and cancer progression. *Cancer and Metastasis Reviews, 29*(4), 709-722.

Truong, D., Puleo, J., Llave, A., Mouneimne, G., Kamm, R. D., & Nikkhah, M. (2016). Breast Cancer Cell Invasion into a Three Dimensional Tumor-Stroma Microenvironment.

Turnbull, G., Clarke, J., Picard, F., Riches, P., Jia, L., Han, F., . . . Shu, W. (2018). 3D bioactive composite scaffolds for bone tissue engineering. *Bioactive materials, 3*(3), 278-314.

Vickerman, V., & Kamm, R. D. (2012). Mechanism of a flow-gated angiogenesis switch: early signaling events at cell–matrix and cell–cell junctions. *Integrative Biology, 4*(8), 863-874.

Wan, S., Liu, Y., Weng, Y., Wang, W., Ren, W., Fei, C., . . . Wang, J. (2014). BMP9 regulates cross-talk between breast cancer cells and bone marrow-derived mesenchymal stem cells. *Cellular Oncology, 37*(5), 363-375.

Weber, L., Kirsch, E., Müller, P., & Krieg, T. (1984). Collagen type distribution and macromolecular organization of connective tissue in different layers of human skin. *Journal of investigative dermatology, 82*(2), 156-160.

Wirtz, D., Konstantopoulos, K., & Searson, P. C. (2011). The physics of cancer: the role of physical interactions and mechanical forces in metastasis. *Nature Reviews Cancer, 11*(7), 512-522.

Wu, Q., Li, J., Zhu, S., Wu, J., Chen, C., Liu, Q., . . . Sun, S. (2017). Breast cancer subtypes predict the preferential site of distant metastases: a SEER based study. *Oncotarget, 8*(17), 27990.

Xian, L., Wu, X., Pang, L., Lou, M., Rosen, C. J., Qiu, T., . . . Rodriguez, J. P. (2012). Matrix IGF-1 maintains bone mass by activation of mTOR in mesenchymal stem cells. *Nature medicine, 18*(7), 1095.

Yin, J. J., Pollock, C. B., & Kelly, K. (2005). Mechanisms of cancer metastasis to the bone. *Cell research, 15*(1), 57-62.

Yousefi, M., Nosrati, R., Salmaninejad, A., Dehghani, S., Shahryari, A., & Saberi, A. (2018). Organ-specific metastasis of breast cancer: molecular and cellular mechanisms underlying lung metastasis. *Cellular Oncology, 41*(2), 123-140.

Zervantonakis, I. K., Hughes-Alford, S. K., Charest, J. L., Condeelis, J. S., Gertler, F. B., & Kamm, R. D. (2012). Three-dimensional microfluidic model for tumor cell intravasation and endothelial barrier function. *Proceedings of the National Academy of Sciences, 109*(34), 13515-13520.

Zhang, D., Bar-Eli, M., Meloche, S., & Brodt, P. (2004). Dual regulation of MMP-2 expression by the type 1 insulin-like growth factor receptor: the phosphatidylinositol 3-kinase/Akt and Raf/ERK pathways transmit opposing signals. *Journal of Biological Chemistry, 279*(19), 19683-19690.

Zhang, D., Wu, X., Chen, J., & Lin, K. (2018). The development of collagen based composite scaffolds for bone regeneration. *Bioactive materials, 3*(1), 129-138.

Zhang, J., Wehrle, E., Adamek, P., Paul, G. R., Qin, X.-H., Rubert, M., & Müller, R. (2020). Optimization of mechanical stiffness and cell density of 3D bioprinted cell-laden scaffolds improves extracellular matrix mineralization and cellular organization for bone tissue engineering. *Acta Biomaterialia, 114*, 307-322.

Zhang, T., Day, J. H., Su, X., Guadarrama, A. G., Sandbo, N. K., Esnault, S., . . . Theberge, A. B. (2019). Investigating fibroblast-induced collagen gel contraction using a dynamic microscale platform. *Frontiers in bioengineering and biotechnology, 7*, 196.